

Leptonic and semileptonic decays of B mesons

Jochen Dingfelder

Physikalisches Institut, Universität Bonn, Nußallee 12, 53115 Bonn, Germany

Thomas Mannel

Theoretische Physik I, Universität Siegen, Walter-Flex-Strasse 3, 57068 Siegen, Germany

(published 21 September 2016)

Semileptonic decays are ideally suited to study the weak interaction as well as strong interaction effects in B -meson decays. In the last decade, precision studies of semileptonic B decays have been made possible by the large samples of B mesons collected at the B factories KEKB in Japan and PEP-II in the USA. Measurements of the charged-current semileptonic transitions $b \rightarrow q\ell\nu$ ($q = u, c$) allow for a determination of the magnitude of the Cabibbo-Kobayashi-Maskawa matrix elements V_{cb} and V_{ub} and the masses of the b and c quarks, which are fundamental parameters of the standard model of particle physics. The values of $|V_{cb}|$ and $|V_{ub}|$ are determined from measurements of inclusive B decays in combination with calculations of partial decay rates or from exclusive decays combined with theoretical predictions of hadronic form factors. Purely leptonic B decays $B \rightarrow \ell\nu$ ($\ell = e, \mu, \tau$) also provide access to $|V_{ub}|$. They are theoretically simpler, but the available signal samples are still small. Decays involving a τ lepton, $B \rightarrow \tau\nu$ and $B \rightarrow D^{(*)}\tau\nu$, are sensitive to new physics, in particular, to charged Higgs bosons in models with an extended Higgs sector, and provide a window to the physics of the third generation. In this article, the measurements and theoretical descriptions of charged-current leptonic and semileptonic B decays and the status of $|V_{cb}|$ and $|V_{ub}|$ determinations are reviewed. An overview of the theoretical approaches and the experimental techniques used in the study of these decays is also provided.

DOI: [10.1103/RevModPhys.88.035008](https://doi.org/10.1103/RevModPhys.88.035008)

CONTENTS

I. Introduction	2	A. Theory	20
II. Theoretical Overview	3	B. Measurements	22
A. Semileptonic decays in the standard model	3	1. Measurements of moments of inclusive spectra	22
B. Decay kinematics of leptonic and semileptonic B decays	3	2. Determination of $ V_{cb} $, b -quark mass, and HQE parameters	24
C. Decay constants and form factors	5	VI. Inclusive Charmless Semileptonic B Decays	25
D. Heavy-quark methods	5	A. Theory	26
E. Lattice QCD	7	B. Measurements	28
F. Other methods: Sum rules and quark models	8	1. Measurement of partial branching fractions	28
III. Experimental Overview	9	2. Determination of $ V_{ub} $	29
A. Accelerators and detectors	9	VII. Exclusive Semileptonic B Decays to Charm Mesons	31
1. B -meson production at colliders	9	A. Theory	31
2. Detectors	9	1. $B \rightarrow D\ell\nu$ and $B \rightarrow D^*\ell\nu$	31
B. Reconstruction of leptonic and semileptonic B decays	11	2. Semileptonic B decays to excited charm mesons	32
1. Lepton identification	11	B. Measurements	33
2. Hadron reconstruction	11	1. $B \rightarrow D\ell\nu$	33
3. Neutrino reconstruction	12	2. $B \rightarrow D^*\ell\nu$	34
C. Background suppression and experimental techniques	12	3. Determination of $ V_{cb} $	36
1. Continuum background suppression	13	4. $B \rightarrow D^{**}\ell\nu$	36
2. Combinatorial background suppression	13	5. Putting it all together	37
3. B tagging	14	VIII. Exclusive Charmless Semileptonic B Decays	37
D. Branching fraction measurement	15	A. Theory	38
IV. Leptonic B Decays	16	1. $B \rightarrow \pi\ell\nu$	38
A. Theory	16	2. Other charmless semileptonic modes	39
B. Measurements	17	B. Measurements	39
1. $B \rightarrow \ell\nu$ ($\ell = e, \mu$)	17	1. $B \rightarrow \pi\ell\nu$	39
2. $B \rightarrow \tau\nu$	18	2. $B \rightarrow \pi$ form factor shape	40
3. Interpretation of $B \rightarrow \tau\nu$ results: $ V_{ub} $, f_B , and new physics	20	3. Determination of $ V_{ub} $ from $B \rightarrow \pi\ell\nu$	42
V. Inclusive Semileptonic B Decays to Charm Mesons	20	4. Other charmless semileptonic B decays	43
		5. $\Lambda_b \rightarrow p\mu\nu$	44
		6. Status of $ V_{ub} $ from exclusive decays	44

7. New physics in $b \rightarrow u\ell\nu$	44
IX. Semileptonic B Decays with a τ Lepton	45
A. Theory	45
B. Measurements	46
C. Charged Higgs and new physics interpretation	48
X. Isospin and Flavor Symmetry	50
A. Isospin symmetry	50
B. Weak annihilation	50
C. Semileptonic B_s decays and flavor symmetry	50
XI. Conclusions and Outlook	51
Acknowledgments	53
References	53

$$V_{\text{CKM}} = \begin{pmatrix} V_{ud} & V_{us} & V_{ub} \\ V_{cd} & V_{cs} & V_{cb} \\ V_{td} & V_{ts} & V_{tb} \end{pmatrix}. \quad (1)$$

I. INTRODUCTION

The standard model (SM) of particle physics is a very successful theory which describes all phenomena observed at particle colliders and other terrestrial experiments, ranging from the smallest energy scales up to the scale of several TeV set by the center-of-mass energy of the Large Hadron Collider (LHC) at CERN. With the recent discovery of the Higgs boson, the particle content of the SM corresponds to a renormalizable theory and is in this sense complete. On the other hand, the SM has some shortcomings. First, its particle content seems to describe only a small fraction of the matter and energy density needed to explain cosmological observations. Based on general relativity and the standard model of cosmology it can be concluded that we understand only about 5% of the energy density in the Universe, the remainder is “dark matter” and “dark energy.” However, it is currently completely unclear if this question has an answer within particle physics. In addition, there are a few more problems which are mainly theoretical issues, related to the stabilization of the electroweak symmetry breaking scale. The question why all particles appear in three copies, which differ only by their mass, is among the most intriguing outstanding questions in contemporary physics. Overall, the SM has a sizable number of parameters, most of which emerge from the parametrization of its flavor structure. While this parametrization is phenomenologically very successful, the origin of the parameters remains obscure. In particular, the origin of the hierarchical structure of the parameters in the flavor sector (masses and mixing angles) is presumably nontrivial.

The SM is the product of almost a century of investigations which relied on close collaboration between experiment and theory. Often the developments were not straightforward and in many cases experimental puzzles created new theoretical ideas which are nowadays considered common knowledge. The historical developments that led to the SM are, for example, gathered in the textbook of Siegmund Brandt (Brandt, 2009). The study of weak decays, in particular, those of hadrons, played a prominent role in these developments due to its extensive phenomenology. These processes are interpreted within the SM as transitions between quarks of different flavors. The relative strengths of these transitions are parametrized in terms of the Cabibbo-Kobayashi-Maskawa (CKM) matrix

The CKM matrix is unitary in the SM, since it corresponds to a basis transformation from the states generated in weak interactions and the mass eigenstates. Details of the flavor sector of the SM can be found in many textbooks, e.g., in Quigg (2013).

From the experimental side, a significant effort has been made to study the flavor structure of the SM. During the last 15 years, the B factories KEKB in Tsukuba, Japan and PEP-II at SLAC in the USA have made major contributions to the advancement of our knowledge of the flavor sector through studies of B mesons produced in electron-positron collisions. The violation of CP symmetry in the B -meson system was observed for the first time in 2001 by the Belle and BABAR experiments at KEKB and PEP-II, respectively. Since then, numerous measurements of B decays have been performed which have led to an advanced understanding of the weak interaction of b quarks and the mechanism for CP violation in the SM. The CP violation measured in B decays has been found to be well described by the CKM matrix. Hints for physics beyond the SM have been looked for by checking the consistency of many complementary measurements to test the unitarity of the CKM matrix and by studying rare B decays. Sensitivity to new physics is limited by both the experimental precision of the measurements and the uncertainties involved in the theoretical calculations of B decays.

The BABAR and Belle experiments stopped operation in 2008 and 2010, respectively. Nevertheless, many analyses are still ongoing to exploit the full data samples collected by these experiments. Several key measurements involving B , B_s , and other b -hadron decays have also been performed at hadron colliders, by the Tevatron experiments at Fermilab and more recently by the LHC experiments at CERN, in particular, the dedicated B -physics experiment LHCb.

In this article, we review the status of charged-current leptonic and semileptonic B decays. In particular, we discuss their impact on the determination of SM flavor parameters. A salient feature of these decays is the presence of a charged lepton and a neutrino in the final state. Experimentally, the charged lepton is a signature that can be well identified and reconstructed, while the neutrino cannot be directly detected and thus complicates the reconstruction of the decay kinematics. Among the weak processes of quarks, the leptonic and semileptonic processes are of particular relevance as they are much simpler to calculate than fully hadronic processes. This is mainly due to the fact that leptons do not interact strongly and hence the part of the decay related to the quarks is easier to describe. The leptonic processes are mainly governed by a single parameter, the decay constants of the meson, while the semileptonic processes are governed by form factors, which are defined as scalar functions of the momentum transfer to the leptons. Leptonic and semileptonic decays constitute the “backbone” of precision determinations of the flavor parameters of the SM, in particular, the magnitudes of CKM matrix elements.

The review is organized in the following way. In Sec. II, we give an overview of the theoretical input to the calculation of leptonic and semileptonic B decays, such as the effective Hamiltonian, the kinematics, and the theoretical methods. The production and detection of B mesons at particle colliders are discussed in Sec. III. We also present the experimental techniques used in their measurements. Here and in the discussion of experimental results, we put a focus on the B -factory experiments Belle and BABAR, which currently provide the most precise measurements of charged-current leptonic and semileptonic B decays. In Sec. IV, we present the searches for purely leptonic decays $B \rightarrow \ell \nu$ ($\ell = e, \mu, \tau$). A review of inclusive and exclusive measurements of semileptonic decays with charm and charmless final states, $B \rightarrow X_c \ell \nu$ and $B \rightarrow X_u \ell \nu$, is given in Secs. V–X. Each section contains a brief theoretical introduction, followed by a discussion of the measurements, the experimental results, and the extraction of the corresponding CKM matrix element. Section X is dedicated to semileptonic B decays with τ leptons and their special sensitivity to new physics. In Sec. XI, the results of the previous sections are revisited in view of isospin and flavor symmetry. The article concludes with a summary of the status of $|V_{ub}|$ and $|V_{cb}|$ determinations and gives a brief outlook of further developments in the area of leptonic and semileptonic B decays in the future.

II. THEORETICAL OVERVIEW

In this section, we give a compact overview of the theoretical methods used to compute the hadronic matrix elements needed for a quantitative analysis of semileptonic decays. Many of these methods make use of the fact that the mass of the bottom quark is large compared to the typical hadronic scale Λ_{QCD} that determines the running of the QCD coupling constant $\alpha_s(\mu)$. In this way, QCD-based methods have been developed which in many cases make model assumptions obsolete.

In the next section, we briefly introduce the kinematics of leptonic and semileptonic B decays, which we use in Sec. II.C to write down the general matrix elements needed for the decays under consideration. The remainder of this section is devoted to a short description of heavy-quark methods (Sec. II.D), lattice QCD calculations (Sec. II.E), and other methods that are frequently used (Sec. II.F).

A. Semileptonic decays in the standard model

Within the SM, charged-current leptonic and semileptonic processes at the quark level are mediated by an exchange of a charged weak boson W_μ^\pm between a quark and a lepton current. The quark current can be written as

$$J_\mu = (\bar{U}_L \gamma_\mu V_{\text{CKM}} \mathcal{D}_L), \quad (2)$$

where we use the notation

$$U_L = \begin{bmatrix} u_L \\ c_L \\ t_L \end{bmatrix}, \quad \mathcal{D}_L = \begin{bmatrix} d_L \\ s_L \\ b_L \end{bmatrix} \quad (3)$$

involving the left-handed up- and down-type quarks. The lepton current is given by

$$j_\mu = (\bar{e}_L \gamma_\mu \bar{\nu}_{e,L} + \bar{\mu}_L \gamma_\mu \bar{\nu}_{\mu,L} + \bar{\tau}_L \gamma_\mu \bar{\nu}_{\tau,L}). \quad (4)$$

Here we do not discuss lepton mixing, which would occur as a unitary rotation among the three neutrinos but is irrelevant for our purposes since we do not identify the neutrino flavors.

All the quarks with the exception of the top quark are light compared to the mass of the W^\pm . On the other hand, the top quark does not form hadrons, so when considering weak decays of hadrons, we may consider the W_μ^\pm to be infinitely heavy, leaving us with a local effective Hamiltonian of the form

$$H_{\text{eff}}^{(st)} = \frac{4G_F}{\sqrt{2}} (\bar{U}_L \gamma_\mu V_{\text{CKM}} \mathcal{D}_L) \times (\bar{e}_L \gamma_\mu \bar{\nu}_{e,L} + \bar{\mu}_L \gamma_\mu \bar{\nu}_{\mu,L} + \bar{\tau}_L \gamma_\mu \bar{\nu}_{\tau,L}) + \text{H.c.}, \quad (5)$$

where U_L does not contain the top quark anymore,

$$U_L = \begin{bmatrix} u_L \\ c_L \\ 0 \end{bmatrix}, \quad (6)$$

and

$$G_F = \frac{g^2}{4\sqrt{2}M_W^2} \quad (7)$$

is the Fermi coupling constant obtained from comparing to the full SM calculation. From this form of the effective Hamiltonian it becomes clear that all CKM matrix elements except the ones involving the top quark (V_{tq}) are accessible in leptonic and semileptonic decays.

B. Decay kinematics of leptonic and semileptonic B decays

The kinematics of purely leptonic decays [see Fig. 1(a)] are simple, since the final state consists of only a charged lepton $\ell = e, \mu, \tau$, and a neutrino. Denoting the momentum of the decaying B meson as p_B , the momentum of the charged lepton as p_ℓ , and the one of the neutrino as p_ν , we have for the purely leptonic case

$$p_B = p_\ell + p_\nu, \quad p_B^2 = m_B^2, \quad p_\ell^2 = m_\ell^2, \quad p_\nu^2 = 0, \quad (8)$$

assuming a massless neutrino. Since this is a two-particle decay, all kinematic quantities are fixed, e.g., the energy E_ℓ of the outgoing charged lepton in the rest frame of the B meson is

$$E_\ell = \frac{p_B p_\ell}{m_B} = \frac{m_B^2 - m_\ell^2}{2m_B}. \quad (9)$$

For the semileptonic decays [see Fig. 1(b)] we have in addition one or more hadrons in the final state. Denoting the hadronic momentum as p_X , we have

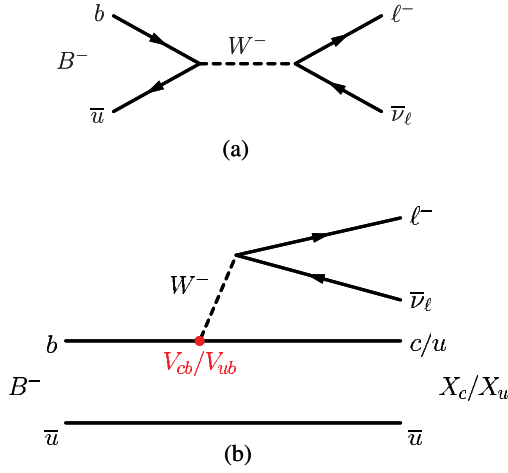


FIG. 1. (a) A leptonic B decay ($B \rightarrow \ell \nu$), and (b) a semileptonic B decay ($B \rightarrow X \ell \nu$).

$$p_B = p_X + p_\ell + p_\nu, \\ p_B^2 = m_B^2, \quad p_X^2 = m_X^2, \quad p_\ell^2 = m_\ell^2, \quad p_\nu^2 = 0, \quad (10)$$

where m_X is the mass of the final-state hadronic system.

Semileptonic decays for a fixed mass m_X are described by two kinematic quantities, which can be chosen to be the four-momentum transfer squared q^2 and the energy of the charged lepton E_ℓ :

$$q^2 = (p_\ell + p_\nu)^2 = (p_B - p_X)^2, \quad m_\ell^2 \leq q^2 \leq (m_B - m_X)^2, \\ E_\ell = \frac{p_B p_\ell}{m_B}, \quad m_\ell \leq E_\ell \leq \frac{1}{2m_B} (m_B^2 - m_X^2 + m_\ell^2). \quad (11)$$

The two variables are not independent; Fig. 2 shows the boundaries of the allowed region in the q^2 - E_ℓ plane for the specific case of a $B \rightarrow D^* \ell \bar{\nu}$ decay.

The various semileptonic B decay modes have spectra with different end points. Figure 3 shows the lepton momentum spectra for the different $B \rightarrow X_c \ell \nu$ and $B \rightarrow X_u \ell \nu$ decays, where X_c and X_u denote hadronic final states containing a charm quark and an up quark, respectively.

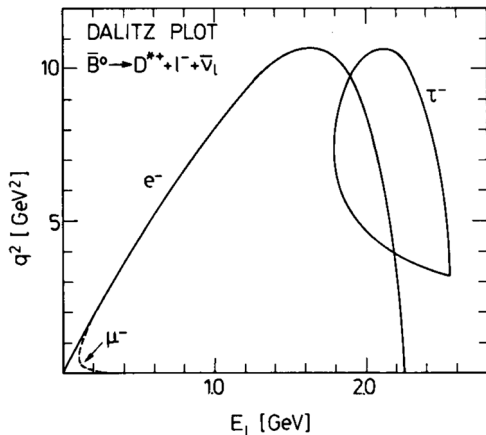


FIG. 2. Allowed kinematic region in the q^2 - E_ℓ plane for $B \rightarrow D^* \ell \bar{\nu}$ decays. From Korner and Schuler, 1990.

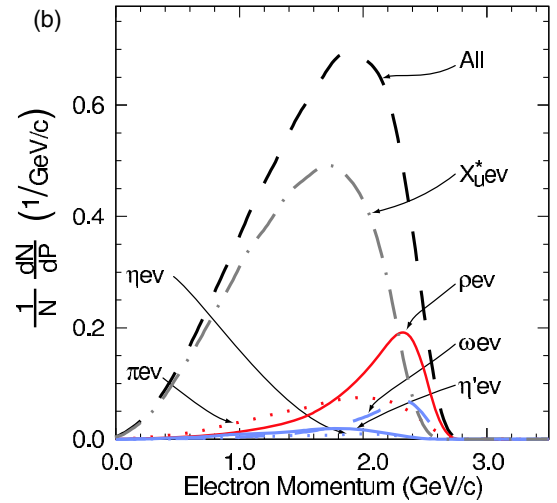
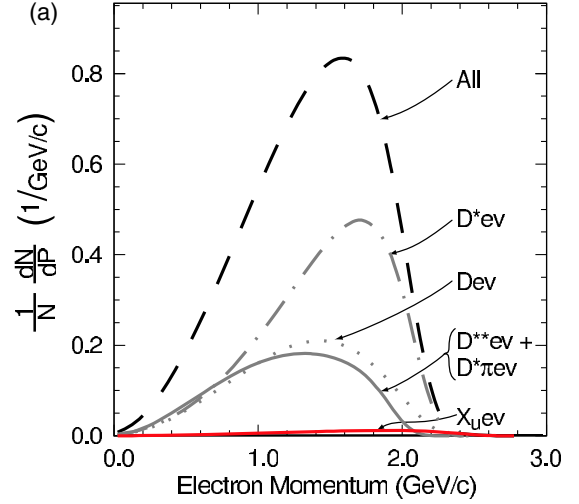


FIG. 3. Lepton momentum distributions for semileptonic B decays: (a) $B \rightarrow X_c \ell \nu$ and (b) $B \rightarrow X_u \ell \nu$. From Aubert *et al.*, 2006c.

In the context of the heavy-quark expansion (see Sec. II.D) it is convenient to introduce velocities instead of momenta. For the case of heavy mesons like B and $D^{(*)}$ mesons we define

$$v_B = \frac{p_B}{m_B}, \quad v_{D^{(*)}} = \frac{p_{D^{(*)}}}{m_{D^{(*)}}}, \quad w = v_B v_{D^{(*)}}, \quad (12)$$

and the scalar product w of the two velocities is used instead of the momentum transfer $q^2 = m_B^2 + m_{D^{(*)}}^2 - 2m_B m_{D^{(*)}} w$. The point $w = 1$ corresponds to the maximum momentum transfer to the leptons $q_{\max}^2 = (m_B - m_{D^{(*)}})^2$, while $q^2 = 0$ yields the maximum value of w , thus

$$1 \leq w \leq \frac{m_B^2 + m_{D^{(*)}}^2}{2m_B m_{D^{(*)}}}. \quad (13)$$

Finally, for heavy-to-light transitions it is useful to define light-cone components of the momenta. For a decay with the kinematics given in Eq. (10), it is convenient to define

$$P_- = E_X + |\vec{p}_X|, \quad P_+ = E_X - |\vec{p}_X|, \quad (14)$$

where E_X and \vec{p}_X are the energy and the momentum of the final state X in the rest frame of the B meson. The product $P^2 = P_+ P_-$ can be close to zero in the case of a heavy-to-light transition but either P_+ or P_- can still be large, corresponding to a situation where a light particle or a jet with a small invariant mass has a large energy in the rest frame of the B meson. The phase space for these variables is given by

$$\frac{m_X^2}{P_-} \leq P_+ \leq P_- \leq m_B. \quad (15)$$

C. Decay constants and form factors

In this section, we give the general parametrizations of decay constants and form factors for exclusive leptonic and semileptonic decays.

The simplest case is the purely leptonic decay $B \rightarrow \ell \nu$. The necessary matrix elements of a pseudoscalar ground state B meson with valence-quark content $q\bar{b}$ are given in terms of a single parameter

$$\langle 0 | \bar{q} \gamma^\mu \gamma_5 b | B(p_B) \rangle = p_B^\mu f_B, \quad (16)$$

where f_B is the so-called decay constant of the B meson. If the quark fields are written without argument, they are given for the space-time point $x = 0$. For the SM prediction, only the matrix element in Eq. (16) is needed, but a possible contribution beyond the standard model could involve also other currents such as a pseudoscalar current. However, all other nonvanishing matrix elements can be expressed in terms of f_B by using the equations of motion of the quark fields

$$(i\cancel{D} - m_q)q = 0 \quad \text{and} \quad (i\cancel{D} - m_b)b = 0. \quad (17)$$

Thus the pseudoscalar density is given by

$$\langle 0 | \bar{q} \gamma_5 b | B(p_B) \rangle = \frac{m_B^2}{m_b + m_q} f_B, \quad (18)$$

where m_B is the mass of the B meson.

Exclusive semileptonic decays are described in terms of form factors, which are functions of the leptonic momentum transfer q^2 . Looking first at the SM contributions only, we need to parametrize the matrix elements of the vector and the axial-vector currents. For the decays into the ground-state pseudoscalar meson only the vector current can contribute, which is parametrized in terms of two form factors:

$$\begin{aligned} \langle P(p_P) | \bar{q} \gamma^\mu b | B(p_B) \rangle &= f_+(q^2) \left(p_B^\mu + p_P^\mu - \frac{m_B^2 - m_P^2}{q^2} q^\mu \right) \\ &+ f_0(q^2) \frac{m_B^2 - m_P^2}{q^2} q^\mu. \end{aligned} \quad (19)$$

For a vector final state V , both the vector and axial currents contribute, and one obtains

$$\langle V(p_V, \epsilon) | \bar{q} \gamma^\mu b | B(p_B) \rangle = V(q^2) \epsilon^{\mu\sigma} \epsilon_\nu^* \frac{2p_B^\nu p_V^\rho}{m_B + m_V}, \quad (20)$$

$$\begin{aligned} \langle V(p_V, \epsilon) | \bar{q} \gamma^\mu \gamma^5 b | B(p_B) \rangle \\ = i\epsilon_\nu^* \left[A_0(q^2) \frac{2m_V q^\mu q^\nu}{q^2} + A_1(q^2) (m_B + m_V) \eta^{\mu\nu} \right. \\ \left. - A_2(q^2) \frac{(p_B + p_V)_\sigma q^\nu}{m_B + m_V} \eta^{\mu\sigma} \right], \end{aligned} \quad (21)$$

where we have introduced the polarization vector ϵ_ν of the vector meson with $\epsilon p_V = 0$, and $\eta^{\mu\nu} = g^{\mu\nu} - q^\mu q^\nu / q^2$ is the transverse part of the metric.

For heavy mesons like B and $D^{(*)}$ it is useful to switch to a description in terms of velocities [see Eq. (12)] and to define w -dependent form factors:

$$\frac{\langle D(v_D) | \bar{c} \gamma^\mu b | B(v_B) \rangle}{\sqrt{m_B m_D}} = h_+(w) (v_B + v_D)^\mu + h_-(w) (v_B - v_D)^\mu, \quad (22)$$

$$\frac{\langle D^*(v_{D^*}, \epsilon) | \bar{c} \gamma^\mu b | B(v_B) \rangle}{\sqrt{m_B m_{D^*}}} = h_V(w) \epsilon^{\mu\nu\rho\sigma} v_{B,\nu} v_{D^*,\rho} \epsilon_\sigma^*, \quad (23)$$

$$\begin{aligned} \frac{\langle D^*(v_{D^*}, \epsilon) | \bar{c} \gamma^\mu \gamma^5 b | B(v_B) \rangle}{\sqrt{m_B m_{D^*}}} \\ = i h_{A_1}(w) (1 + w) \epsilon^{*\mu} - i [h_{A_2}(w) v_B^\mu + h_{A_3}(w) v_{D^*}^\mu] \epsilon^* \cdot v_B. \end{aligned} \quad (24)$$

D. Heavy-quark methods

Methods based on the fact that some of the quark masses are large compared to the QCD scale Λ_{QCD} have become standard in B physics. These *heavy-quark methods* have been developed over the last two decades and lead to a significant reduction of model dependences.

The key idea is to perform an expansion of the QCD matrix elements in powers of Λ_{QCD}/m_Q , where m_Q is the mass of the heavy quark. The leading term corresponds to the infinite-mass limit, in which the heavy quark degenerates to a static source of a color field. Such a nonrecoil approximation is in fact well known since the work of Bloch and Nordsieck (1937), who considered the soft radiation of an electron in this approximation. Applying the same idea to QCD leads to some important conclusions, which were first formulated by Shifman and Voloshin (1988) and Isgur and Wise (1989, 1990). The main observation is that in the infinite-mass limit QCD exhibits new and additional symmetries, the so-called *heavy-quark symmetries* (HQS).

The physical origin of these symmetries can be easily understood. The interaction of quarks and gluons does not refer to the mass, i.e., all quark flavors have the same interaction with gluons. For massless light quarks this leads to the well-known chiral and isospin symmetries, while in the

infinite-mass limit the same argument leads to a heavy-flavor symmetry, connecting heavy (static) quarks moving with the same velocity. Treating b and c quarks as heavy quarks, this leads to relations between matrix elements involving bottom and charm hadrons.

The second symmetry originates from the fact that the coupling of a gauge field to the spin of a fermion scales with the inverse power of the mass and thus vanishes in the infinite-mass limit. In other words, in the infinite-mass limit the heavy-quark spin decouples, and rotations of the heavy-quark spin become a symmetry. This symmetry is called the heavy-quark spin symmetry.

Details on this can be retrieved from textbooks dealing specifically with this subject (Manohar and Wise, 2000; Mannel, 2004), where one also finds the formulation of the heavy-quark limit as an effective field theory, the heavy-quark effective theory (HQET). Here we restrict ourselves to quoting the main results relevant to semileptonic B decays.

The first result is that, due to HQS, the number of form factors reduces. For a heavy-to-heavy quark transition, one can express all form factors in terms of a single one, the Isgur-Wise function $\xi(w)$. Using the definitions in Eqs. (22)–(24), one obtains

$$h_+(w) = h_{A_1}(w) = h_{A_3}(w) = h_V(w) = \xi(w), \quad (25)$$

$$h_-(w) = 0 = h_{A_2}(w). \quad (26)$$

Furthermore, from HQS one also obtains a normalization statement of the Isgur-Wise function. In a simple wave function picture, the Isgur-Wise function describes the overlap of the wave functions of the light degrees of freedom of the initial and final states. However, due to HQS, the final-state wave function is the same as the initial-state one, up to the boost related to the momentum of the final state. Consequently, at the point $v_B = v_{D^{(*)}}$, corresponding to $w = 1$, the overlap is maximal and corresponds to the normalization of the wave function. Deviations from this normalization originate either from finite-mass corrections or through hard gluons. Making use of the general theorem (Ademollo and Gatto, 1964) stating that symmetry breaking corrections to matrix elements involving the currents generating the symmetry are of quadratic order in the symmetry breaking, we obtain for the form factors in Eqs. (22)–(24) (Luke, 1990)

$$h_+(1) = 1 + \mathcal{O}(\alpha_s) + \mathcal{O}((\Lambda_{\text{QCD}}/m_Q)^2), \quad (27)$$

$$h_-(1) = 0 + \mathcal{O}(\alpha_s) + \mathcal{O}(\Lambda_{\text{QCD}}/m_q), \quad (28)$$

$$h_{A_1}(1) = 1 + \mathcal{O}(\alpha_s) + \mathcal{O}((\Lambda_{\text{QCD}}/m_Q)^2), \quad (29)$$

where m_Q is the charm-quark mass for the cases under consideration.

Exclusive heavy-to-light transitions are not as much constrained by HQS. Still a few relations may be obtained which relate B decays to D decays, implying a certain scaling. Since we are not going to use these relations and rather use different theoretical tools to treat heavy-to-light transitions, we will not go into detail here.

A related methodology has been developed for inclusive decays, which is called the *heavy-quark expansion* (HQE) (Chay, Georgi, and Grinstein, 1990; Bigi *et al.*, 1993; Mannel, 1994). The starting point is the optical theorem which relates the decay rates to the forward matrix element of a scattering amplitude:

$$\Gamma = \text{Im} \int d^4x \langle B(p_b) | T[H_{\text{eff}}(x)H_{\text{eff}}(0)] | B(p_B) \rangle. \quad (30)$$

The time-ordered product can be written in terms of an *operator product expansion* (OPE). The OPE allows us to write

$$\int d^4x T[H_{\text{eff}}(x)H_{\text{eff}}(0)] = \sum_{n,i} \frac{1}{m_Q^n} C_{n,i} \mathcal{O}_{n+3,i}, \quad (31)$$

where $\mathcal{O}_{l,i}$ is a set (labeled by i) of operators of dimension l , and $C_{n,i}$ are [in terms of $\alpha_s(m_Q)$] perturbatively calculable coefficients, called the Wilson coefficients.

Taking the forward matrix element of this expression, we obtain the decay rate in terms of the Wilson coefficients and the matrix elements of the operators $\mathcal{O}_{n+3,i}$, which encode the nonperturbative input into the decay rate. The HQE has some specific and general features as follows:

- The leading operators are $n = 0$ and hence are dimension 3. It turns out that up to corrections of higher order in $1/m_Q$ all operators can be related to the matrix element
- $$\langle B(p_b) | \bar{b} \gamma_\mu b | B(p_B) \rangle,$$
- which is normalized even in full QCD due to the conservation of the bottom current. Thus there is no unknown hadronic matrix element to leading order, and the coefficient C_0 is the decay rate of a free b quark, i.e., the partonic rate including also the perturbative QCD corrections.
- All dimension-4 operators ($n = 1$) can be rewritten in terms of dimension 5 ($n = 2$) and higher, using the equation of motion for the b quark. Consequently, there are no contributions of order $1/m_b$ to the free quark decay appearing at leading order.
 - The first nontrivial nonperturbative contributions emerge at $n = 2$, corresponding to dimension-5 operators. These may be written in terms of two matrix elements:

$$2m_B \mu_\pi^2 = -\langle B(p_B) | \bar{b}_v (iD)^2 b_v | B(p_B) \rangle, \quad (32)$$

$$2m_B \mu_G^2 = \langle B(p_B) | \bar{b}_v \sigma_{\mu\nu} (iD^\mu) (iD^\nu) b_v | B(p_B) \rangle. \quad (33)$$

Here we have defined $b_v(x) = \exp[im_b(vx)]b(x)$ such that the derivative acting on the field b_v corresponds to the residual momentum $k = p_B - m_b v$, where v is the velocity of the hadron containing the b quark. The parameter μ_π^2 corresponds to the kinetic energy of the heavy quark inside the heavy meson, while μ_G^2 is the chromomagnetic moment of the heavy quark inside the heavy meson.

- At dimension 6 ($n = 3$), there are again two matrix elements,

$$2m_B \rho_D^3 = - \langle B(p_B) | \bar{b}_v (iD_\mu) (ivD) (iD^\mu) b_v | B(p_B) \rangle, \quad (34)$$

$$2m_B \rho_{LS}^3 = \langle B(p_B) | \bar{b}_v \sigma_{\mu\nu} (iD^\mu) (ivD) (iD^\nu) b_v | B(p_B) \rangle, \quad (35)$$

which are the Darwin term and the spin-orbit term.

- At higher orders ($n \geq 4$) the number of nonperturbative parameters proliferates. Details on this can be found in [Dassinger, Mannel, and Turczyk \(2007\)](#) and [Mannel, Turczyk, and Uraltsev \(2010\)](#).

The HQE may also be set up for differential rates. We will discuss the corresponding expression when we discuss specific processes and spectra.

E. Lattice QCD

The only known method to deal with a quantum field theory in a nonperturbative way is to compute its correlation functions on a lattice. The starting point is the generating functional of a quantum field theory, written as a functional integral

$$Z[J] = \int [d\phi] \exp \left[iS + \int d^4x J(x) \phi(x) \right], \quad (36)$$

where the integration runs over all possible field configurations. The variable ϕ is a place holder for all the fields that appear in the corresponding theory; in QCD this would be the quark and gluon fields. Because of the anticommuting nature of the fermions, the fermionic fields have to be represented by anticommuting Grassman variables. Without going into detail, this fact leads to specific problems in the numerical implementation of fermions.

Lattice QCD computes the functional integral in Eq. (36) on a space-time lattice which serves as a regularization of this integral. The functional integral in Eq. (36) is ill defined from a mathematical point of view, as soon as an interaction field theory is considered. The usual perturbation theory may be considered as a perturbative evaluation of this integral, which still needs renormalization. In this sense the regularization needed in perturbative calculations matches the regularization by a finite lattice spacing a . Obviously, the continuum limit $a \rightarrow 0$ has to be discussed carefully.

Typical modern lattice QCD calculations have lattices of the size 16^4 , which is at the edge of what current computers can handle. Progress in computing power as well as progress in lattice methods has led to enormous progress in lattice QCD, turning it into an important tool for QCD calculations of nonperturbative quantities such as form factors and decay constants.

While a more detailed description of lattice methods is beyond the scope of this review, we list a few specific points relevant to semileptonic decays:

- Early lattice simulations of QCD were performed in the so-called quenched approximation, since calculations

without quenching (unquenched calculations) need much higher computing power. The quenched approximation concerns the integration over the fermionic degrees of freedom in Eq. (36),

$$\int [d\psi][d\bar{\psi}] \exp \left[i \int d^4x \bar{\psi} (i\mathcal{D} - m) \psi \right], \quad (37)$$

which yields after the lattice regularization a determinant of a large matrix. The quenched approximation replaces the functional in Eq. (37) by a constant value, although it still depends on the gluon fields. Comparing this to the perturbative approach, quenching corresponds to the omission of all Feynman diagrams with closed fermion loops. Although it is qualitatively clear what the approximation means, its quantitative impact was not under control. The power of modern computers has allowed us to overcome this approximation, such that the quantities relevant for the leptonic and semileptonic processes are nowadays known from unquenched calculations.

- As pointed out above, the variables appearing in functional integrals for fermions should be anticommuting Grassman variables. For the numerical implementation of this case one may set up different ways to represent the fermions, which all coincide in the limit $a \rightarrow 0$. Nevertheless, the choice of the fermion representation remains an issue, which, however, for the leptonic and semileptonic matrix elements is under control.
- The continuum limit $a \rightarrow 0$ needs careful discussion, since it involves the renormalization of the QCD parameters. In other words, performing the continuum limit requires simulations at different lattice spacings a . However, the coupling constant α_s is a function of the lattice spacing $\alpha_s = \alpha_s(a)$. Because of asymptotic freedom, the corresponding β function can be taken from perturbation theory, once a is small enough, but also nonperturbative methods for renormalization have been developed.
- Heavy quarks on the lattice are difficult to simulate, since the lattice spacing has to be chosen to be smaller than the inverse mass of the heavy quark. In order to simulate a hadron of typical size $1/\Lambda_{\text{QCD}}$ this requires very large lattices. For the strange and the charm quark this is feasible, and for bottom quarks this only very recently became possible. A workaround for this problem is to use the static approximation, i.e., to simulate HQET on the lattice. This leads to problems that do not appear in full QCD, which, however, can be solved such that the nonperturbative quantities of HQET and of the HQE can be obtained from the lattice.
- Likewise, it is difficult to simulate objects with large momenta. This is the reason why form factors for decays of heavy mesons cannot be computed in regions where the outgoing meson has a large momentum in the rest frame of the decaying meson. This means that form factor simulations are restricted to the region of maximum momentum transfer to the leptons.

Overall, lattice simulations for quantities relevant for leptonic and semileptonic decays have become quite reliable.

Unquenched results from different groups are available which are compatible with each other. This concerns mainly the lattice values for f_B , the heavy-to-light form factors in the region of maximum momentum transfer to the leptons, and the heavy-to-heavy form factors, again in the region of maximum momentum transfer. We quote the relevant lattice results in the sections where they are used.

F. Other methods: Sum rules and quark models

The remaining methods depend more or less on additional assumptions or even models.

One method, which certainly has its roots in QCD, is based on the various kinds of QCD sum rules. The main idea is to perform a perturbative calculation of suitably chosen correlation functions in those kinematic regions, where perturbation theory is valid. These perturbative results are then extrapolated into the (usually nonperturbative) regions of interest by using unitarity and analyticity, i.e., by using a dispersion relation. The simplest example is the correlator involving two electromagnetic currents of quarks,

$$\int d^4x e^{-iqx} \langle 0 | T[j_\mu(x) j_\nu(0)] | 0 \rangle = (g_{\mu\nu} q^2 - q^\mu q_\nu) T(q^2), \quad (38)$$

which can be computed for large negative q^2 in QCD perturbation theory. In fact, one can apply the technique of the OPE, which yields an expansion of Eq. (38) in inverse powers of $-q^2$. The leading term is simply the perturbative result, while the subleading terms can be computed in terms of vacuum matrix elements of local operators (sometimes called ‘‘condensates’’), multiplied by perturbatively calculate coefficients.

On the other hand, $T(q^2)$ satisfies a dispersion relation in terms of a spectral function $\rho(s)$,

$$T(s) = \int \frac{ds'}{2\pi i} \frac{\rho(s')}{s - s' + i\epsilon}, \quad (39)$$

where $\rho(s)$ contains all nonperturbative information and is nonvanishing in the physical region $s > 4m_\pi^2$.

The original sum rules were formulated by [Shifman, Vainshtein, and Zakharov \(1979\)](#) for exactly this case and have been used to extract information on the ρ meson, which is the lowest state that can appear in the spectral function $\rho(s)$.

The technicalities of QCD sum rules have been refined since then. The standard repertoire for sum rule estimates consists of the following:

- In order to reduce the contribution of the states with large mass s in the dispersion relation in Eq. (39), one usually performs a Borel transformation defined as

$$T(s) = \sum a_n s^n \rightarrow T(M^2) = \sum \frac{a_n}{n!} M^n,$$

which transforms the denominator of Eq. (39) as

$$\frac{1}{s - s'} \rightarrow \frac{1}{s} e^{-s'/M^2},$$

turning the power suppression into an exponential one.

- Above a certain threshold s_0 , one may assume duality, which means that the hadronic spectral function is replaced by the partonic one. This assumption introduces uncertainties, which are hard to quantify. To this end, the sum rule will depend on two parameters M^2 and s_0 .
- The two parameters M^2 and s_0 have to be determined. In principle, there should be a plateau in both parameters where the extracted nonperturbative quantities should be largely independent of M^2 and s_0 . For many quantities this is also the case, and in practical applications values are taken that are known to lie within such a plateau. Nevertheless, this is the point where a QCD sum rule estimate becomes model dependent. However, one can get a feeling of the quality of the sum rule by varying M and s_0 .
- The sum rules discussed up to here turn out to not be very stable for the calculation of form factors, in particular, for heavy-to-light transitions. Up to this point we relied on the local OPE applied to Eq. (38). However, instead of setting up an OPE for the limit $x \rightarrow 0$ in Eq. (38), one may as well replace this limit by the limit $x^2 \rightarrow 0$, which is a light-cone expansion. This is also studied in QCD and corresponds to the twist expansion in deep inelastic scattering. One may set up sum rules based on the twist expansion which are usually called *light-cone sum rules* (LCSR). These sum rules require as the nonperturbative input also light-cone distributions of mesons, usually the one of the light meson, defined as

$$\langle \pi(q) | \bar{u}(x) \gamma_\mu \gamma_5 d(0) | 0 \rangle_{x^2=0} = -i q_\mu f_\pi \int_0^1 du e^{iuqx} \phi_\pi(u), \quad (40)$$

where f_π is the pion decay constant and ϕ_π can be interpreted as the distribution of the (light-cone component of the) momentum between the two quarks. To this end, the light-cone distribution is a nonperturbative input to the sum rule, in addition to M and s_0 .

Finally, we make a few remarks concerning quark models. Although there are a variety of methods based or at least rooted in QCD, one may still resort to a quark model for estimates of hadronic matrix elements if no other option is left. Clearly such models have a few serious shortcomings:

- Since the connection to QCD remains unclear, the use of a model introduces a basically uncontrollable systematic uncertainty, making an uncertainty estimate almost impossible. This is in contrast to all the other approaches described, where in all cases uncertainties can be estimated.
- An explicit treatment of bound states is up to now only possible in nonrelativistic quantum mechanics, which is the basis for any nonrelativistic quark model. Such a model treats a meson as a two-particle state bound by an (instantaneous) potential, which has to be modeled from phenomenology. As far as spectroscopy is concerned,

such models are phenomenologically quite successful, once the parameters are fixed properly. However, even if a relatively large constituent mass is assigned to the light quarks, the nonrelativistic assumption is questionable.

- Instead of solving a Schrödinger equation one may try to include relativistic effects by moving to a Dirac equation, interpreted as a two-body equation. This allows for an inclusion of relativistic effects, but still only as small corrections, since otherwise the two-body description breaks down.

As far as leptonic and semileptonic decays are concerned, quark models have fortunately become completely obsolete, since sum rules, HQE, and lattice QCD calculations are available for all relevant nonperturbative quantities. Nevertheless, quark models are still useful for estimates of some subleading effects, such as the matrix elements of the HQE or the form factors for decays into orbitally or radially excited states. We quote the relevant results in the sections where they are needed.

III. EXPERIMENTAL OVERVIEW

In this section, we give an overview of the production and detection of B mesons at particle colliders. The reconstruction of leptonic and semileptonic B decays and the experimental techniques used to analyze them are introduced.

A. Accelerators and detectors

1. B -meson production at colliders

Studies of B -meson decays have been performed in electron-positron collisions at the $\Upsilon(4S)$ resonance with the following colliders and experiments: DORIS (ARGUS experiment), CESR (CLEO experiment), PEP-II ($BABAR$ experiment), and KEKB (Belle experiment). CLEO, Belle, and $BABAR$ also collected data at or near the $\Upsilon(5S)$ resonance, providing samples of excited B mesons and B_s mesons. Samples of b -flavored hadrons of different types are available from production at higher energies, in e^+e^- collisions on the Z resonance at LEP (ALEPH, DELPHI, L3, and OPAL experiments) and SLC (SLD experiment), as well as in hadron collisions at the Tevatron (CDF and D0 experiments) and the LHC (LHCb, ATLAS, and CMS experiments).

The cross sections for the process $e^+e^- \rightarrow b\bar{b}$ at the $\Upsilon(4S)$, $\Upsilon(5S)$, and Z resonances are 1.1, 0.3, and 6.6 nb, respectively. The cross section for b -hadron production in hadron collisions is much larger, e.g., $\sigma(pp \rightarrow b\bar{b}) \sim 300 \mu\text{b}$ at a center-of-mass energy of $\sqrt{s} = 7 \text{ TeV}$. Table I gives an overview of the data samples recorded by the various experiments.

Semileptonic and leptonic B decays are best studied in e^+e^- collisions, where the four-momentum of the initial state is known and the events are comparatively clean. Their study in hadron collisions is difficult due to the large hadronic background and the unknown initial state, which makes reconstruction of the neutrino challenging. Furthermore, hadron-collider experiments must trigger on specific exclusive decay modes and typically require charged particles in the final state. The B -factory experiments can reconstruct a large

TABLE I. Overview of the b -hadron samples recorded by various experiments. For LEP and SLC, the number of produced Z bosons, N_Z , is given instead of the integrated luminosity $\int \mathcal{L} dt$. For the LHC experiments, only the run 1 data samples are considered.

Experiment	\sqrt{s} (GeV)	$\int \mathcal{L} dt$ (fb $^{-1}$) or N_Z	$B\bar{B}/b\bar{b}$ pairs
Belle	10.58	711	$7.72 \times 10^8 B\bar{B}$
$BABAR$	10.58	426	$4.68 \times 10^8 B\bar{B}$
CLEO	10.58	16	$1.71 \times 10^7 B\bar{B}$
ARGUS	10.58	0.2	$2 \times 10^5 B\bar{B}$
LEP ^{a,b}	~ 91	$\sim 4 \times 10^6 Z$	$\sim 6 \times 10^5 b\bar{b}$
SLD	~ 91	$\sim 6 \times 10^5 Z$	$\sim 9 \times 10^4 b\bar{b}$
LHCb	7000, 8000	3.2	$2.6 \times 10^{11} b\bar{b}$
ATLAS, CMS ^b	7000, 8000	25	$\sim 10^{12} b\bar{b}$
Tevatron ^{c,b}	1960	10	$\sim 10^{11} b\bar{b}$

^aLEP represents ALEPH, DELPHI, L3, and OPAL.

^bQuoted numbers are per experiment.

^cTevatron represents CDF and D0.

variety of B -meson decay modes with a high efficiency and are thus able to perform inclusive measurements.

The measurements of the high-luminosity B -factory experiments Belle and $BABAR$ are the focus of this article. They currently provide the most precise results on $B \rightarrow \ell\nu$ and $B \rightarrow X\ell\nu$ decays. If competitive results from other experiments exist, they are also mentioned. The PEP-II and KEKB colliders were in operation from 1998 to 2008 and 1998 to 2010, respectively. They operated at a center-of-mass energy of $\sqrt{s} = 10.58 \text{ GeV}$, equal to the mass of the $\Upsilon(4S)$.

The production of B mesons in e^+e^- collisions at the $\Upsilon(4S)$ resonance is illustrated in Fig. 4. The $\Upsilon(4S)$ is the lightest $b\bar{b}$ resonance with a mass above the $B\bar{B}$ pair production threshold: $m_{\Upsilon(4S)} = 10.58 \text{ GeV} > 2m_B = 10.56 \text{ GeV}$. It decays almost exclusively to B -meson pairs, with about equal probability to B^+B^- and $B^0\bar{B}^0$. The current upper limit for non- $B\bar{B}$ decays of the $\Upsilon(4S)$ is 4% at the 95% confidence level (Olive *et al.*, 2014).

The energies of the colliding electron and positron beams were chosen to be asymmetric to boost the $\Upsilon(4S)$ resonance and the B mesons produced in its decay. This boost allows for a better spatial separation of the two B -meson decay vertices. The flight lengths of the B mesons are used to determine their lifetimes and are thus important for time-dependent measurements, in particular, the measurement of time-dependent CP asymmetries. Table II lists some of the operating parameters of the KEKB and PEP-II colliders.

2. Detectors

The detection of $B \rightarrow \ell\nu$ and $B \rightarrow X\ell\nu$ decays requires a reliable reconstruction and identification of the charged lepton $\ell = e, \mu$ and, in the case of semileptonic decays, the hadrons

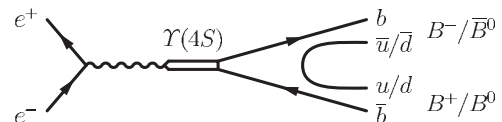


FIG. 4. B -meson production in e^+e^- collisions at the $\Upsilon(4S)$ resonance.

TABLE II. Operating parameters of the e^+e^- colliders running at the $\Upsilon(4S)$ resonance. For the asymmetric-energy colliders, LER and HER denote the low-energy e^+ ring and high-energy e^- ring, respectively.

	KEKB	PEP-II	CESR
Beam energy (GeV)	LER: 3.5 HER: 8.0	LER: 3.1 HER: 9.0	5.29
Lorentz boost $\beta\gamma$	0.425	0.56	0
Circumference (m)	3018	2199	768
Peak luminosity ($\text{cm}^{-2} \text{s}^{-1}$)	2.1×10^{34}	1.2×10^{34}	0.08×10^{34}

that form the hadronic final state X . The other particles in the event also need to be reconstructed to infer the kinematics of the undetected neutrino either from the missing energy and momentum in the event or from the reconstruction of the second B meson. For this reason, a good hermeticity of the detectors is important.

Figure 5 shows schematics of the Belle and *BABAR* detectors. Both detectors have a similar overall design. They are laid out in a cylindrical geometry and feature the following subdetector components (from inside to outside):

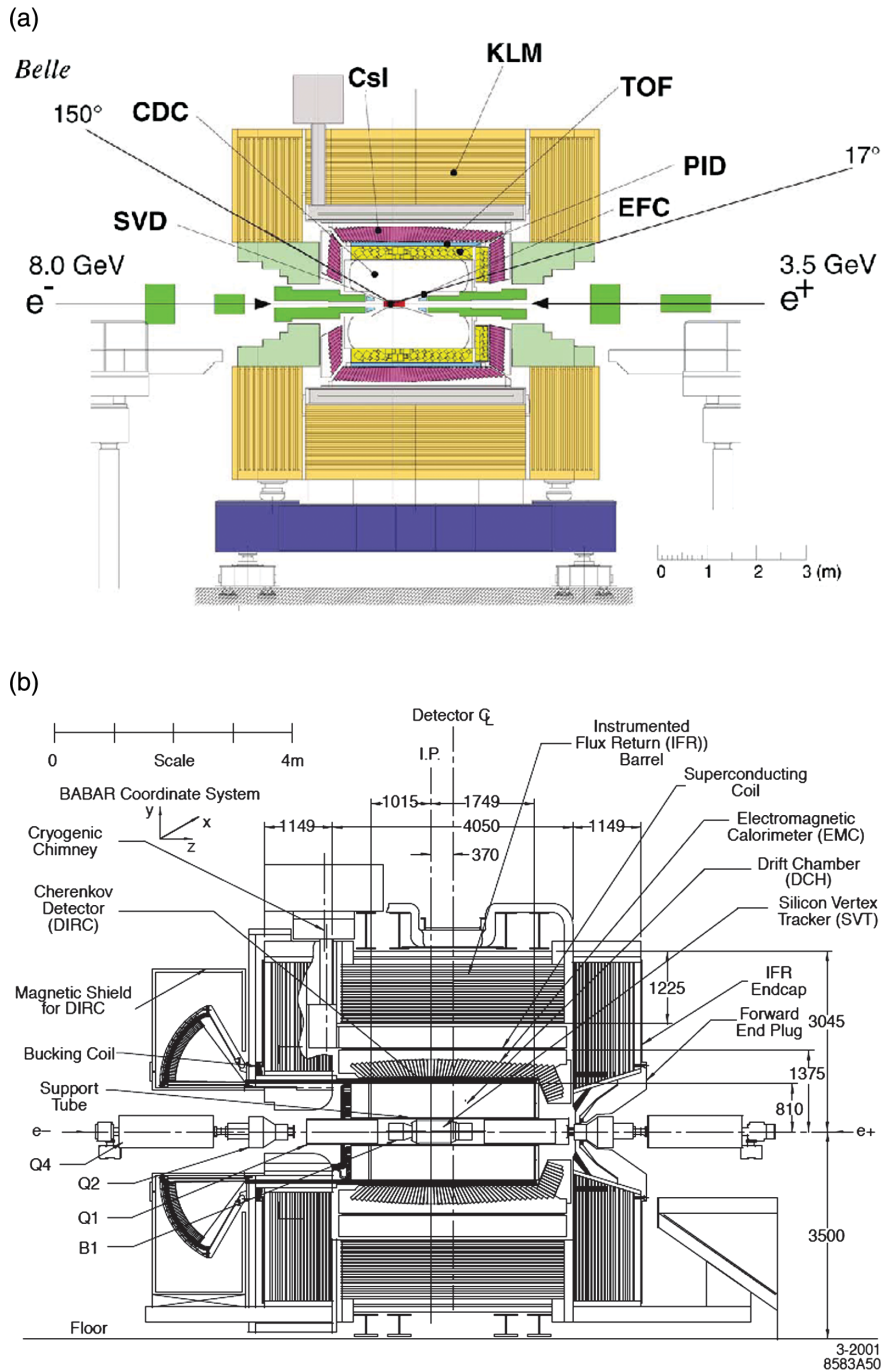


FIG. 5. Side views of (a) the Belle and (b) *BABAR* detectors. The acronyms used for the subdetector components of Belle are SVD = silicon vertex detector, CDC = central drift chamber, PID = particle identification system, TOF = time-of-flight counter, CsI = CsI crystal calorimeter, KLM = K_L^0/μ on system, and EFC = extreme forward calorimeter. From [Abashian et al., 2002](#) and [Aubert et al., 2002](#).

- a multilayer silicon-strip detector for the reconstruction of decay vertices and precision track reconstruction close to the interaction point;
- a large, low-material drift chamber to reconstruct tracks of charged particles and measure their momenta;
- a particle identification (PID) system to identify charged particles;
- a crystal calorimeter with TI-doped CsI crystals for the measurement of electromagnetic showers created by electrons and photons;
- a solenoid magnet enclosing the tracking detectors and the calorimeter, which provides 1.5 T axial magnetic field to bend charged-particle tracks for the measurement of their momentum and charge;
- and an iron flux return instrumented with resistive-plate chambers or limited streamer tubes for muon and K_L^0 detection (“ K_L^0 /muon system”).

The largest difference between the Belle and *BABAR* detectors lies in their PID systems. *BABAR* used a novel Cherenkov detector system that was based on the detection of internally reflected Cherenkov light (DIRC) produced in long quartz radiator bars. Belle relied on a threshold Cherenkov detector with aerogel as radiator and photon multiplier tubes as photon detectors and time-of-flight plastic scintillation counters situated radially outside of the drift chamber. In both experiments, specific energy loss (dE/dx) measurements in the drift chamber are used in combination with the Cherenkov and scintillation counter information to identify particles. Because of the asymmetric beam energies, both detectors have a forward-backward-asymmetric design and are instrumented down to smaller polar angles in the forward (e^- -beam) direction. The detector acceptance in polar angle is $17^\circ < \theta < 150^\circ$. Another consequence of the asymmetric design is a reduced solid angle coverage in the center-of-mass frame compared with detectors at symmetric colliders, e.g., CLEO. Detailed descriptions of the Belle and *BABAR* detectors can be found in [Abashian *et al.* \(2002\)](#) and [Aubert *et al.* \(2002, 2013\)](#), respectively.

B. Reconstruction of leptonic and semileptonic B decays

B mesons have a mass of 5.279 GeV and a mean lifetime of $\tau_{B^0} = 1.519 \pm 0.005$ ps for neutral B mesons and $\tau_{B^\pm} = 1.638 \pm 0.004$ ps for charged B mesons ([Olive *et al.*, 2014](#)). Their mean flight length at the B -factory experiments is $\beta\gamma c\tau_B \approx 0.2$ mm, so they decay inside the beam pipe, close to the interaction point. Therefore, B mesons must be reconstructed from their stable or long-lived decay products: charged pions, charged kaons, protons, photons, electrons, or muons. The key signature of $B \rightarrow \ell\nu$ and $B \rightarrow X\ell\nu$ decays is the charged lepton. The hadronic final state X in semileptonic decays can be reconstructed either inclusively or exclusively. In the exclusive case, X is reconstructed in a specific decay mode, while in the inclusive case, X is not explicitly reconstructed and represents the sum over all possible resonant and potentially also nonresonant hadronic final states. An example semileptonic decay in the *BABAR* detector is shown in Fig. 6.

1. Lepton identification

The reconstruction of a leptonic or semileptonic B decay starts with the identification of a high-momentum lepton candidate.¹ The typical minimum lepton momentum requirement used in analyses of leptonic or semileptonic B decays is $p_\ell^* > 1.0$ GeV.² The identification of electrons is based on a match of a track reconstructed in the central tracking system with an energy cluster in the electromagnetic calorimeter. Variables used to discriminate electrons from other particles include the shower shape in the calorimeter and the ratio of the cluster energy to the track momentum E/p , which is expected to be close to unity for electrons. Muons are identified by their ability to traverse the whole detector and leave tracks in the muon system. Energy deposits in the muon system are matched to a track in the central tracking system. The quality of this match is evaluated in terms of a χ^2 value computed from the transverse deviations of the energy deposits in the muon system from the position of the drift chamber track extrapolated to the muon system. Additional variables used for muon identification are the length and shape of the cluster of energy deposits in the muon system, the shape of the cluster of energy depositions in the calorimeter, dE/dx , and Cherenkov detector information.

The performance of the lepton identification is studied with large control samples of electrons and muons from $e^+e^- \rightarrow e^+e^-(\gamma)$ and $e^+e^- \rightarrow \mu^+\mu^-$ processes or from $J/\psi \rightarrow e^+e^-$, $\mu^+\mu^-$ decays. The misidentification of pions and kaons as electrons or muons is studied with control samples of $D^{*+} \rightarrow D^0\pi^+ \rightarrow K^-\pi^+\pi^+$ and $K_S \rightarrow \pi^+\pi^-$ decays. In Belle and *BABAR*, electrons are identified with an efficiency of up to 98%, corresponding to a pion misidentification probability of a few per mil (for lab-frame momenta above 1 GeV). Muons are identified with an efficiency of 90%–95% and the corresponding pion misidentification probability is a few percent (for lab-frame momenta above 1.5 GeV).

Tau leptons are identified through their leptonic decay modes, $\tau^+ \rightarrow e^+\nu_e\bar{\nu}_\tau$, $\tau^+ \rightarrow \mu^+\nu_\mu\bar{\nu}_\tau$, or hadronic decay modes, $\tau^+ \rightarrow X^+\bar{\nu}_\tau$, where the hadronic final state X most of the time consists of one or three charged pions and possibly additional neutral pions.

2. Hadron reconstruction

Semileptonic B decays predominantly produce a final state containing a charm meson X_c . Reconstruction of the D^0 and D^+ mesons (the lightest charm mesons) is of particular importance and is performed by choosing decay modes, which produce a kaon and at least one pion. The invariant mass of the decay products is used for identification.

The experimentally most favorable decay modes are $D^0 \rightarrow K^-\pi^+$ and $D^+ \rightarrow K^-\pi^+\pi^+$. A list of further decay modes commonly used to reconstruct D mesons is given in Table III. Neutral pions and neutral kaons that appear in these decays are reconstructed in their dominant decay modes $\pi^0 \rightarrow \gamma\gamma$ and $K_S^0 \rightarrow \pi^+\pi^-$, and narrow mass windows around their nominal masses are applied. D^* mesons are identified by their decay to

¹From here on, we refer to charged leptons simply as leptons.

²The asterisk (*) denotes variables in the $\Upsilon(4S)$ rest frame.

TABLE III. Ground-state charm mesons (D and D^*), their masses, the most important decay modes, and branching fractions (Olive *et al.*, 2014).

Meson	Mass (MeV)	Decay modes	\mathcal{B} (%)
D^0	1864.86 ± 0.13	$D^0 \rightarrow K^- \pi^+$	3.88 ± 0.05
		$D^0 \rightarrow K^- \pi^+ \pi^- \pi^+$	8.08 ± 0.20
		$D^0 \rightarrow K^- \pi^+ \pi^0$	13.9 ± 0.5
		$D^0 \rightarrow K_S^0 \pi^0$	1.19 ± 0.04
		$D^0 \rightarrow K_S^0 \pi^+ \pi^-$	2.83 ± 0.20
		$D^0 \rightarrow K_S^0 \pi^0 \pi^0$	0.91 ± 0.11
		$D^0 \rightarrow K_S^0 \pi^+ \pi^- \pi^0$	5.2 ± 0.6
		$D^0 \rightarrow K^- \pi^+ \pi^- \pi^+ \pi^0$	4.2 ± 0.4
D^+	1896.62 ± 0.15	$D^+ \rightarrow K^- \pi^+ \pi^+$	9.13 ± 0.19
		$D^+ \rightarrow K^- \pi^+ \pi^+ \pi^0$	5.99 ± 0.18
		$D^+ \rightarrow K_S^0 \pi^+ \pi^+ \pi^-$	3.12 ± 0.11
		$D^+ \rightarrow K_S^0 \pi^+ \pi^0$	6.99 ± 0.27
		$D^+ \rightarrow K_S^0 \pi^+$	1.47 ± 0.07
D^{*0}	2006.99 ± 0.15	$D^{*0} \rightarrow D^0 \pi^0$	61.9 ± 2.9
		$D^{*0} \rightarrow D^0 \gamma$	38.1 ± 2.9
D^{*+}	2010.29 ± 0.13	$D^{*+} \rightarrow D^0 \pi^+$	67.7 ± 0.5
		$D^{*+} \rightarrow D^+ \pi^0$	30.7 ± 0.5

a D meson and a slow pion or a low-energy photon. The pions or photons from D^* decays have characteristically low energies, since the mass difference between D and D^* mesons is only marginally larger than the pion mass $m_{D^{*+}} - m_{D^+} = 140.66 \pm 0.10$ MeV, $m_{D^{*0}} - m_{D^0} = 145.42 \pm 0.01$ MeV (Olive *et al.*, 2014). As the experimental uncertainties in the reconstruction of the D and D^* masses are correlated, their difference, $\Delta m = m_{D^*} - m_D$ or $m_{D^*} - m_D$, can be measured more precisely. The uncertainties largely cancel out in the difference and the Δm distribution exhibits a very narrow peak for correctly reconstructed D^* candidates. Higher-mass charm mesons, e.g., the orbitally excited D^{**} mesons, are reconstructed in their decays to the ground-state D and D^* mesons and a transition pion (see Sec. VII.B.4).

Semileptonic B decays to charmless final states X_u are suppressed with respect to charm final states by the ratio of CKM matrix elements $|V_{ub}|^2/|V_{cb}|^2$. The most relevant charmless mesons for $B \rightarrow X_u \ell \nu$ analyses are the pseudoscalar mesons π^+ , π^0 , η , and η' and the vector mesons ρ^+ , ρ^0 , and ω . Table IV shows their masses and main decay modes. Charmless mesons with masses above 1 GeV have not yet been observed in semileptonic B decays.³

3. Neutrino reconstruction

The neutrino in $B \rightarrow \ell \nu$ and $B \rightarrow X \ell \nu$ decays is not directly detected. If there is only one neutrino in the $B\bar{B}$ event, its four-momentum can be inferred from the missing energy and momentum of the whole event:

$$\begin{aligned}
 P_\nu &= (E_\nu, \vec{p}_\nu) = (E_{\text{miss}}, \vec{p}_{\text{miss}}) \\
 &= (E_{\Upsilon(4S)}, \vec{p}_{\Upsilon(4S)}) - \left(\sum_i E_i, \sum_i \vec{p}_i \right), \quad (41)
 \end{aligned}$$

³Belle recently reported the first signs of the decay $B^+ \rightarrow f_2 \ell^+ \nu$ at a hadronic mass of ~ 1.3 GeV (Sibidanov *et al.*, 2013).

 TABLE IV. Charmless mesons (with masses below 1 GeV), their masses, the most important decay modes, and branching fractions (Olive *et al.*, 2014).

Meson	Mass (MeV)	Decay modes	\mathcal{B} (%)
π^0	134.9766 ± 0.0006	$\pi^0 \rightarrow \gamma\gamma$	98.823 ± 0.034
π^+	139.57018 ± 0.00035	$\pi^+ \rightarrow \mu \nu^a$	99.98770 ± 0.00004
η	547.862 ± 0.018	$\eta \rightarrow \gamma\gamma$	39.41 ± 0.20
		$\eta \rightarrow \pi^0 \pi^0 \pi^0$	32.68 ± 0.23
		$\eta \rightarrow \pi^+ \pi^- \pi^0$	22.92 ± 0.28
ρ^+	775.11 ± 0.34	$\rho^+ \rightarrow \pi^+ \pi^0$	~ 100
ρ^0	775.26 ± 0.25	$\rho^0 \rightarrow \pi^+ \pi^-$	~ 100
ω	782.65 ± 0.12	$\omega \rightarrow \pi^+ \pi^- \pi^0$	89.2 ± 0.7
		$\omega \rightarrow \pi^0 \gamma$	8.28 ± 0.28
η'	957.78 ± 0.06	$\eta' \rightarrow \eta \pi^+ \pi^-$	42.9 ± 0.7
		$\eta' \rightarrow \rho^0 \gamma$	29.1 ± 0.5
		$\eta' \rightarrow \eta \pi^0 \pi^0$	22.2 ± 0.8

^aBecause of their long lifetime ($\tau_\pi = 2.6 \times 10^{-8}$ s), charged pions can be considered as stable particles in B -physics experiments.

where the index i runs over all detected particles. The squared missing mass in the event $M_{\text{miss}}^2 = P_\nu^2$ is expected to be compatible with zero (i.e., with a negligible neutrino mass). As the neutrino reconstruction depends on the measurement of the energies and momenta of all particles in the event, the experimental resolution of P_ν is moderate and the M_{miss}^2 distribution has long tails. Better resolution can be achieved if the second B meson in the $B\bar{B}$ event is fully reconstructed (see Sec. III.C.3). In this case, the four-momentum P_B of the signal B meson decaying via $B \rightarrow \ell \nu$ or $B \rightarrow X \ell \nu$ can be derived from that of the fully reconstructed B meson. The neutrino four-momentum can then be precisely calculated as

$$P_\nu = P_B - P_\ell (-P_X), \quad (42)$$

resulting in a narrow peak around zero for correctly reconstructed signal decays.

C. Background suppression and experimental techniques

The e^+e^- cross section at the $\Upsilon(4S)$ resonance includes sizable contributions from non- $B\bar{B}$ events. Only about 25% of all hadronic events produced at this energy contain a $B\bar{B}$ pair. Table V gives the effective cross sections for the different processes in e^+e^- collisions at $\sqrt{s} = m_{\Upsilon(4S)}$.

The two main background sources for the analyses of B decays are as follows:

- (1) *Continuum background:* $e^+e^- \rightarrow q\bar{q}$ ($q = u, d, s, c$) processes involving quarks lighter than the b quark and lepton pair production in $e^+e^- \rightarrow \ell^+ \ell^-$ ($\ell = e, \mu, \tau$) processes.
- (2) *Combinatorial background:* $B\bar{B}$ events where one or more particles have been wrongly assigned to the signal B decay (typically originating from the other B decay).

The suppression of these backgrounds is a crucial part of any B -decay analysis and is discussed in more detail in the

TABLE V. Effective cross sections (expected cross sections within the experimental acceptance) for $e^+e^- \rightarrow b\bar{b}$, $e^+e^- \rightarrow q\bar{q}$ ($q = u, d, s, c$) and $e^+e^- \rightarrow \ell^+\ell^-$ ($\ell = e, \mu, \tau$). The numbers are valid for the acceptance of the *BABAR* detector; they are very similar for Belle.

$e^+e^- \rightarrow q\bar{q}$	Cross section (nb)
$b\bar{b}$	1.05
$c\bar{c}$	1.30
$s\bar{s}$	0.35
$d\bar{d}$	0.35
$u\bar{u}$	1.39
$\tau^+\tau^-$	0.94
$\mu^+\mu^-$	1.16
e^+e^-	~ 40

following. In addition to data taking at the $\Upsilon(4S)$ resonance (*on-resonance* data), the B factories dedicated a part of their data taking to *off-resonance* data recorded at a center-of-mass energy 60 MeV (Belle) or 40 MeV (*BABAR*) below the $\Upsilon(4S)$ mass. This off-resonance data sample can be used to estimate the continuum background under the $\Upsilon(4S)$ peak, after scaling the cross section and the magnitudes of the particle momenta to those expected for on-resonance collisions.

1. Continuum background suppression

In e^+e^- collisions at the $\Upsilon(4S)$ resonance, B mesons are produced slightly above the kinematic threshold for $B\bar{B}$ pair production. Their momentum in the $\Upsilon(4S)$ rest frame is only about 320 MeV. For this reason, they decay almost isotropically in the $\Upsilon(4S)$ rest frame, leading to a spherical distribution of the final-state particles. The average charged-particle multiplicity in $B\bar{B}$ events is 10.7 (Brandenburg *et al.*, 2000), i.e., 5.4 charged particles per B decay (3.9 for semileptonic B decays). Events from continuum processes have a lower particle multiplicity, larger particle momenta, and are more directional. The hadronization of the quarks in $e^+e^- \rightarrow q\bar{q}$ ($q = u, d, s, c$) processes leads to a two-jet topology. Continuum background can be suppressed by asking for a minimum number of tracks, typically at least three or four, and by applying criteria on event-shape variables that quantify how jetlike or spherical an event is.

Examples of commonly used event-shape variables are the *thrust* and thrust-related variables. The thrust axis \hat{T} of a collection of N particles is defined as the unit vector that maximizes the sum of the projections $|\vec{p}_i \cdot \hat{T}|$ over all particle momenta \vec{p}_i . The thrust itself is defined as

$$T = \frac{\sum_{i=1}^N |\vec{p}_i \cdot \hat{T}|}{\sum_{i=1}^N |\vec{p}_i|}. \quad (43)$$

Often two thrust axes are computed for an event and are compared with each other, for instance the thrust axis of the visible decay products of the signal B decay and that of the rest of the event (ROE). These two axes are uncorrelated for $B\bar{B}$ events due to the isotropic B decays. In continuum events, the particles are aligned along the directions of the two jets and the thrust axis of the B candidate and that of the rest of the event are collinear. As shown in Fig. 7, the magnitude of the

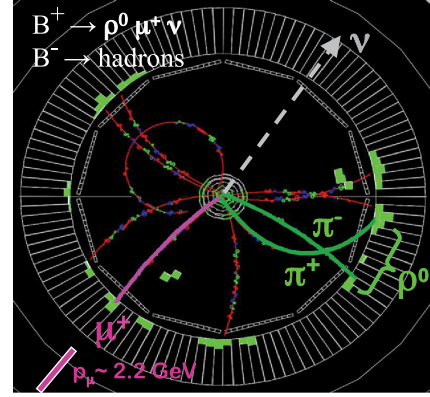


FIG. 6. Event display of a $B^+ \rightarrow \rho^0 \mu^+ \nu$ ($\rho^0 \rightarrow \pi^+ \pi^-$) decay in the *BABAR* detector. The neutrino is not detected and can be only indirectly reconstructed; its flight direction is indicated by the dashed arrow. The second B meson in the event decayed hadronically.

cosine of the angle between the two thrust axes $|\cos \Delta\theta_T| = |\hat{T}_{\text{cand}} - \hat{T}_{\text{ROE}}|$ is uniformly distributed between 0 and 1 for signal, while it is strongly peaked at 1 for continuum events.

Further examples of event-shape variables are sphericity, aplanarity, Fox-Wolfram moments (Fox and Wolfram, 1979), and variables describing the particle momentum flow around the thrust axis of the B candidate. See Bevan *et al.* (2014) for a discussion of these variables. To achieve an optimum continuum suppression, several event-shape variables are typically combined in a multivariate discriminant, e.g., a Fisher discriminant or a neural network.

2. Combinatorial background suppression

The combinatorial $B\bar{B}$ background as well as the continuum background can be suppressed by testing the kinematic consistency of the reconstructed B candidate with a B meson. Two largely uncorrelated kinematic variables used for such tests are the difference between the reconstructed and expected energy of the B candidate, ΔE , and the beam-constrained mass of the B candidate, m_{bc} (or m_{ES} ⁴). They are defined as

$$\Delta E = E_B^* - E_{\text{beam}}^*, \quad (44)$$

$$m_{\text{bc}} = \sqrt{E_{\text{beam}}^{*2} - p_B^{*2}}, \quad (45)$$

where E_B^* is the energy of the B candidate and E_{beam}^* is the beam energy in the $\Upsilon(4S)$ rest frame. The beam-energy constraint in m_{bc} makes use of the fact that the energies of the colliding beam particles are precisely known and hence improves the mass resolution compared to the standard invariant mass definition. For a correctly reconstructed B candidate, $\Delta E \approx 0$ and $m_{\text{bc}} \approx m_B$. Example distributions of ΔE and m_{bc} are shown in Fig. 8.

⁴Belle uses the nomenclature m_{bc} (beam-constrained mass), while *BABAR* uses m_{ES} (energy-substituted mass). For simplicity, we use only m_{bc} in this article.

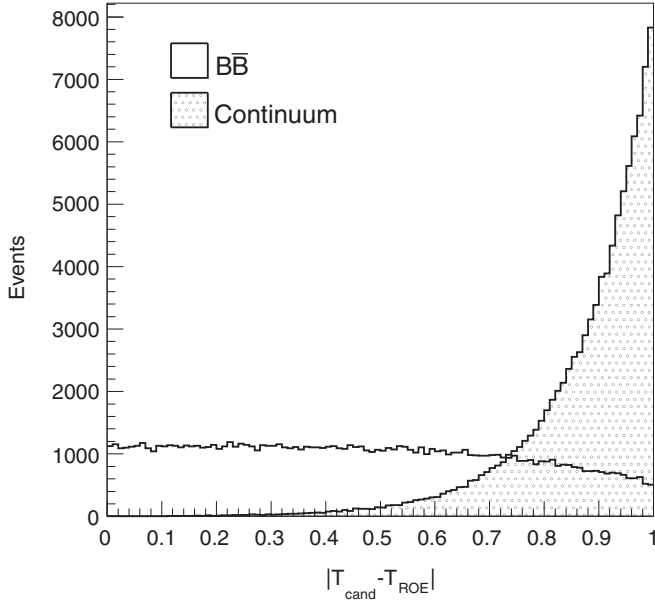


FIG. 7. Distribution of $|\cos \Delta\theta_T| = |\hat{T}_{\text{cand}} - \hat{T}_{\text{ROE}}|$ for $B\bar{B}$ events (open histogram) and continuum events (shaded histogram).

Another useful variable for analyses of $B \rightarrow X\ell\nu$ decays is the angle θ_{BY} between the B candidate and the visible system $Y = X\ell$ [see Fig. 9(a)]. If the only missing particle in the event is the neutrino from the semileptonic decay, $\cos\theta_{BY}$ can be derived from four-momentum conservation ($P_B = P_Y + P_\nu$) and the assumption that the neutrino is massless:

$$\begin{aligned} P_\nu^2 &= 0 \\ &= (P_B - P_Y)^2 \\ &= m_B^2 + m_Y^2 - 2(E_B E_Y - p_B p_Y \cos \theta_{BY}) \\ \Rightarrow \cos \theta_{BY} &= \frac{2E_B E_Y - m_B^2 - m_Y^2}{2p_B p_Y}. \end{aligned} \quad (46)$$

Under these assumptions, the variable $\cos\theta_{BY}$ is distributed between -1 and 1 , up to resolution and photon radiation effects. For incorrectly reconstructed semileptonic B decays or background events, $\cos\theta_{BY}$ does not correspond to the cosine of a physical angle and the distribution is spread out much further, as shown in Fig. 9(b).

3. B tagging

A further suppression of the continuum and combinatorial background can be achieved by reconstructing not only the B decay of interest but also the second B meson in the $B\bar{B}$ event. This approach is referred to as B tagging. In addition to identifying the event as a $B\bar{B}$ event, B tagging provides kinematic constraints that allow for a precise reconstruction of the neutrino four-momentum or other kinematic variables such as the squared four-momentum transfer q^2 . The second B meson can be either fully reconstructed in a hadronic decay mode (*hadronic tag*) or partially reconstructed in a semileptonic decay mode (*semileptonic tag*) and is referred to as a

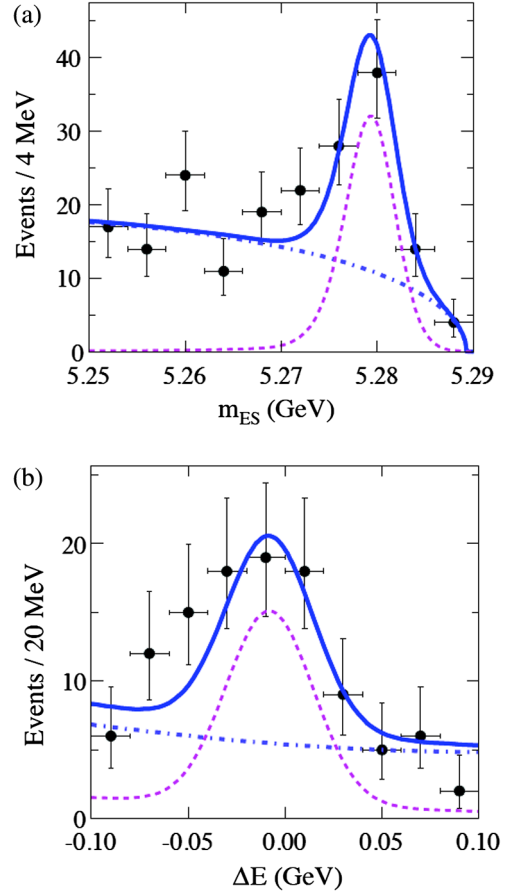


FIG. 8. Observed distributions of (a) m_{bc} ($= m_{ES}$) and (b) ΔE from an analysis of hadronic B decays (Aubert *et al.*, 2008f). The data are compared with the result of a fit of two functions representing correctly reconstructed B candidates (dashed lines) and the total continuum and combinatorial $B\bar{B}$ background (dash-dotted lines). The sum of the signal and background functions is shown as solid lines.

B_{tag} candidate. B -tagging methods usually require that all charged-particle tracks in the event are assigned to one of the two B candidates and that there is only a small amount of remaining energy from unassociated photon candidates or energy deposits in the calorimeter, allowing for beam background, calorimeter noise, etc.

A full reconstruction of the B_{tag} four-momentum $P_{B_{\text{tag}}}$ in a hadronic decay mode allows the four-momentum of the signal B meson P_B to be inferred

$$P_B = P_{\Upsilon(4S)} - P_{B_{\text{tag}}}, \quad (47)$$

where $P_{\Upsilon(4S)}$ is the four-momentum of the $\Upsilon(4S)$. In addition, the charge and the flavor of the signal B candidate are uniquely determined from the charge and the flavor of the B_{tag} candidate (apart from $B^0\bar{B}^0$ mixing).

A large number of different decay modes, mostly with a $b \rightarrow c$ quark transition that lead to final states with a D^0 , D^+ , D^+_s , or a J/ψ meson, are considered for the hadronic B_{tag} reconstruction. The charm meson is combined with additional charmless mesons (π^\pm , K^\pm , π^0 , K^0_S) to reconstruct a large

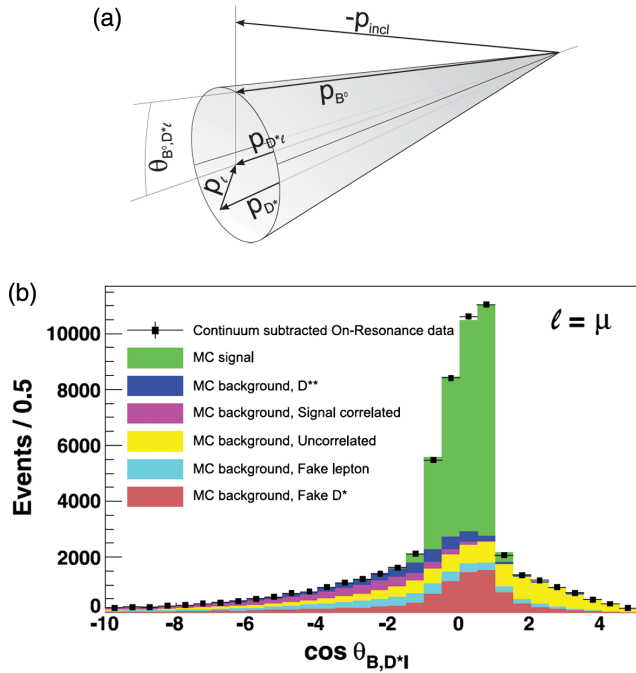


FIG. 9. The variable $\cos\theta_{BY}$ for $B^0 \rightarrow D^{*-}\ell^+\nu$ decays: (a) reconstruction of the angle θ_{BY} , and (b) distribution of $\cos\theta_{BY}$ for correctly reconstructed $B^0 \rightarrow D^{*-}\ell^+\nu$ decays (top-most histogram) and various backgrounds (other histograms). From *Dungel et al., 2010*.

number of exclusive B_{tag} decay modes. The tagging efficiency and purity depend on the number of charged and neutral particles in the decay and are highest for decay modes with low-multiplicity final states. Since the branching fractions of the individual hadronic decays are small, typically of the order of 10^{-5} – 10^{-3} , the inclusion of higher-multiplicity final states is necessary to reach a sufficient tagging efficiency. The variables ΔE and m_{bc} introduced in Eqs. (44) and (45) can be used to distinguish correctly reconstructed from combinatorial B_{tag} candidates and to estimate the tagging efficiency and purity.

Both Belle and *BABAR* updated their hadronic B -tagging algorithms during the course of the experiment, leading to an improvement of about a factor of 2 in the tagging efficiency at a comparable background level compared with the previous versions. In the latest *BABAR* algorithm, B_{tag} candidates are reconstructed in nearly 1800 decay modes. Mode-dependent selection windows in ΔE and m_{bc} are applied. If there are multiple B_{tag} candidates per event, the one reconstructed in the decay mode with the highest purity is chosen. The recent Belle algorithm uses a more hierarchical approach which employs a four-stage B_{tag} reconstruction (as illustrated in Fig. 10) combined with a neural-network classification (*Feindt, 2004*). At the first stage, π^+ , K^+ , K_S^0 , γ , π^0 , e , and μ candidates are reconstructed from tracks and from clusters in the electromagnetic calorimeter. Then D , D_s , and J/ψ candidates as well as D^* and D_s^* candidates are formed. At the last stage, the B_{tag} candidates are reconstructed and classified. At each stage, neural networks are used to estimate the probability that the particles have been correctly

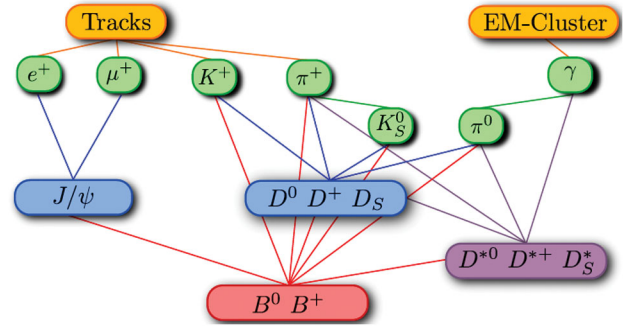


FIG. 10. The selection and classification stages of the hadronic B -tagging algorithm in Belle. From *Feindt et al., 2011*.

reconstructed. The neural-network outputs of each stage are used as input to the next stage, where the particles are combined to reconstruct parent particles. Additional information is provided to the neural networks at each stage, such as invariant masses, angles between particles, and vertexing information. At the end, the kinematic consistency of the B_{tag} candidates with a B decay is checked using m_{bc} . The final neural-network output is used to rank the B_{tag} candidates, allowing the best to be easily selected. Typical efficiencies achieved for hadronic B tagging at the B factories are $\sim 0.3\%$ for B^+B^- and $\sim 0.2\%$ for $B^0\bar{B}^0$ events with purities of (10–30)%.

For semileptonic B tagging, usually the four decay modes $B^0 \rightarrow D^-\ell^+\nu$, $B^0 \rightarrow D^{*-}\ell^+\nu$, $B^+ \rightarrow \bar{D}^0\ell^+\nu$, and $B^+ \rightarrow \bar{D}^{*0}\ell^+\nu$ ($\ell = e, \mu$) are reconstructed. They have a combined branching fraction of about 8% for B^+ and 7% for B^0 , per lepton mode. Sometimes semi-inclusive $B \rightarrow DX\ell\nu$ decays are also used, where X denotes an unspecified hadronic final state. This more inclusive reconstruction includes D^* and higher-mass charm mesons, without having to reconstruct the slow pion or low-energy photon from the D^* decay. This approach leads to a somewhat increased tagging efficiency at the expense of higher backgrounds. Backgrounds and wrongly reconstructed B_{tag} candidates can be suppressed by selecting only events in the signal region of the $\cos\theta_{BY}$ ($Y = D^{(*)}\ell$) distribution [see Eq. (46)]. The efficiency for semileptonic tags is about 0.5%–1%. It is larger than that for hadronic tags because of the sizable semileptonic branching fractions and the relatively high reconstruction efficiencies for these decays. However, the background level is higher and the kinematic constraints are not as tight as for hadronic tags due to the neutrino in the tag decay. In general, semileptonic tags (in contrast to hadronic tags or no tags) represent a compromise between signal efficiency and background suppression. As the various tagging techniques are statistically independent and have largely uncorrelated systematic uncertainties, measurements based on different tagging techniques are complementary and can easily be combined.

D. Branching fraction measurement

The most fundamental quantities of interest in studies of B decays are the total branching fraction \mathcal{B} and the partial branching fractions $\Delta\mathcal{B}$ of the studied decay mode in certain

kinematic regions. The total branching fraction can be calculated from the number of selected data events N_{data} , the estimated number of background events N_{bkg} , the signal selection efficiency ϵ_{sig} (obtained from simulation), and the number of $B\bar{B}$ events $N_{B\bar{B}}$ in the data sample:

$$\mathcal{B} = \frac{N_{\text{data}} - N_{\text{bkg}}}{2\epsilon_{\text{sig}}N_{B\bar{B}}}. \quad (48)$$

The factor of 2 accounts for the presence of two B mesons in a $B\bar{B}$ event. The number of $B\bar{B}$ events is computed as $N_{B\bar{B}} = \sigma(e^+e^- \rightarrow \Upsilon(4S) \rightarrow B\bar{B}) \int \mathcal{L} dt$, where $\int \mathcal{L} dt$ is the integrated luminosity. The trigger efficiency for $B\bar{B}$ events at the B -factory experiments is close to 100%. Branching fractions are usually measured for B^0 or B^+ , not for an admixture of the two. In this case, the ratio of the $\Upsilon(4S)$ branching fractions to charged and neutral B mesons, $f_{\pm}/f_0 = 1.055 \pm 0.025$ (Olive *et al.*, 2014), needs to be taken into account. Partial branching fractions are computed in the same way with the event numbers and signal efficiency for the corresponding kinematic region.

Having discussed the production and reconstruction of B decays and the relevant experimental techniques for their analysis, we now turn to the measurements of leptonic and semileptonic B decays.

IV. LEPTONIC B DECAYS

B mesons can decay into a charged lepton and a neutrino $B \rightarrow \ell\nu$ if the quark and the antiquark inside the meson annihilate each other and produce a virtual W boson [see Fig. 1(a)]. These purely leptonic decays are possible only for charged B mesons. As no hadrons appear in the final state, these decays are quite easy to deal with from the theoretical side. Experimentally they are more difficult, since the annihilation of a b and a \bar{u} quark into a W^- boson involves the CKM parameter $|V_{ub}|$, making these decays quite rare.

A. Theory

The hadronic input to the description of purely leptonic decays is mainly given by the decay constant f_B of the B meson defined in Eq. (16). The decay rate to leading order is given by

$$\Gamma(B \rightarrow \ell\nu) = \frac{G_F^2 m_B^3 f_B^2}{8\pi} |V_{ub}|^2 x^2 (1-x)^2 \quad (49)$$

and involves the product $f_B^2 |V_{ub}|^2$. Here $x = m_\ell/m_B$ is the ratio of the lepton and B -meson masses. The decay constant f_B can be obtained either from QCD sum rules or from lattice calculations. The most recent values are (Dowdall *et al.*, 2013; Gelhausen *et al.*, 2013)

$$f_B = \begin{cases} (186 \pm 4) \text{ MeV} & \text{from lattice QCD} \\ & \text{(Dowdall et al., 2013),} \\ (207_{-9}^{+17}) \text{ MeV} & \text{from QCD sum rules} \\ & \text{(Gelhausen et al., 2013),} \end{cases} \quad (50)$$

which turn out to be consistent with each other within the uncertainties (at the $\sim 2\sigma$ level). From the lattice result for f_B and the $|V_{ub}|$ average of $(3.70 \pm 0.38) \times 10^{-3}$ (see Sec. VIII.B.6) one can derive a SM value for the $B \rightarrow \tau\nu$ branching fraction of

$$\mathcal{B}(B^+ \rightarrow \tau^+\nu) = (0.83 \pm 0.17) \times 10^{-4}. \quad (51)$$

The branching fractions for $B \rightarrow e\nu$ and $B \rightarrow \mu\nu$ are much smaller due to helicity suppression. They are suppressed by factors of $\sim 10^7$ and ~ 220 relative to $B \rightarrow \tau\nu$, respectively.

The factor m_ℓ^2 in the decay rate reflects the helicity suppression due to the left handedness of the charged current, which is a typical feature of the SM. However, this suppression can be overcome by the radiation of an additional photon, i.e., the process $B \rightarrow \ell\nu\gamma$ does not suffer from the factor x^2 , but has an additional factor of α (the electromagnetic coupling constant) due to the photon emission. For the light leptons $\ell = e, \mu$ the predicted $B \rightarrow \ell\nu\gamma$ branching fractions are considerably larger than those without radiation.

The decay rate for the radiative decay is

$$\frac{d\Gamma}{dy} = \frac{\alpha G_F^2 m_B^5 |V_{ub}|^2}{48\pi^2} y^3 (1-y) [f_A^2(y) + f_V^2(y)], \quad (52)$$

where f_V and f_A are the vector and the axial-vector form factors for the $B \rightarrow \gamma$ transition,

$$\begin{aligned} \langle \gamma(p, \epsilon) | \bar{u}\gamma^\mu (1 - \gamma_5) b | B(v) \rangle \\ = \sqrt{4\pi\alpha} \epsilon_\nu^* [e^{\mu\nu\alpha\beta} v_\alpha p_\beta f_V(y) + i(g^{\mu\nu} + v^\nu p^\mu) f_A(y)], \end{aligned} \quad (53)$$

and y is the rescaled photon energy $y = 2E_\gamma/m_B$.

The SM prediction for this process depends strongly on the theoretical input. Calculations based on QCD factorization yield branching fractions $\mathcal{B}(B \rightarrow \ell\nu\gamma) \sim \mathcal{O}(10^{-6})$, depending also on the energy cut applied to the photon. It was advertised by Beneke and Rohrwild (2011) to use the measurement to extract theoretical parameters appearing in the QCD factorization.

In addition to the determination of the standard model parameters $|V_{ub}|$ or f_B , $B \rightarrow \ell\nu$ decays are particularly interesting as probes for new physics. In models beyond the SM with an extended Higgs sector, a charged Higgs boson can be exchanged instead of a W boson. In particular, within a type-II two-Higgs doublet model (2HDM), which also represents the Higgs sector of supersymmetric models, there are additional tree-level contributions from the exchange of a charged Higgs boson. The rate in the 2HDM is given by

$$\Gamma_{2\text{HDM}}(B \rightarrow \ell\nu) = r_H \Gamma_{\text{SM}}(B \rightarrow \ell\nu) \quad (54)$$

with

$$r_H = \left(1 - \frac{m_B^2 \tan^2 \beta}{m_H^2}\right)^2, \quad (55)$$

where m_H is the mass of the charged Higgs boson and $\tan \beta$ is the ratio of the Higgs vacuum expectation values that appear in

the 2HDM. This shows that measurements of $B \rightarrow \ell\nu$ branching fractions can be used to indirectly search for charged Higgs bosons and to constrain the 2HDM parameter space or to look for other unknown heavy charged particles.

B. Measurements

1. $B \rightarrow \ell\nu$ ($\ell = e, \mu$)

While $B \rightarrow e\nu$ decays in the SM are experimentally out of reach at current particle colliders, the predicted $B \rightarrow \mu\nu$ branching fraction of $\sim 5 \times 10^{-7}$ is close to being accessible with the B -factory data samples. It is nevertheless interesting to study both $B \rightarrow e\nu$ and $B \rightarrow \mu\nu$ decays as they could have significantly enhanced branching fractions in models beyond the SM.

Identification of $B \rightarrow e\nu$ and $B \rightarrow \mu\nu$ decays exploits three main event characteristics. The most distinctive signature is the monoenergetic lepton in the rest frame of the decaying B meson, since the decay is a two-body decay. A peak in the distribution of the lepton momentum in the B rest frame, p_ℓ^B , is expected at ~ 2.6 GeV (half the B -meson mass). Second, if there is no additional neutrino from the other B decay in the event, the M_{miss}^2 distribution should peak around zero. Third, the consistency of the second B candidate in the event with a B decay can be checked. This check is done for the second B meson as the signal B decay cannot be fully reconstructed because of the neutrino.

The most important backgrounds in $B \rightarrow \ell\nu$ searches are $e^+e^- \rightarrow \ell^+\ell^-$ events (as well as other continuum processes) and $B \rightarrow X_u\ell\nu$ decays. $B \rightarrow X_c\ell\nu$ decays make little contribution, as the expected lepton momentum lies significantly beyond the kinematic limit for these decays. The background from hadronic B decays is strongly suppressed by the requirement of a well-reconstructed high-momentum lepton, as hadrons misidentified as leptons tend to have lower momenta.

The decays $B \rightarrow e\nu$ and $B \rightarrow \mu\nu$ have been searched for by Belle (Satoyama *et al.*, 2007; Yook *et al.*, 2015), BABAR (Aubert *et al.*, 2008g, 2009e, 2010a), and CLEO (Artuso *et al.*, 1995), in both untagged and tagged analyses. We discuss only the most recent analyses from Belle and BABAR in detail, as they have the best signal sensitivity.

In the untagged analyses, the second B meson in the event is reconstructed inclusively. After identification of a well-reconstructed electron or muon, the four-momentum of all remaining particles in the event is computed and assigned to the second B meson. Its consistency with a B decay is ensured using m_{bc} and ΔE (see Sec. III.C.2). As the four-momentum of the signal B meson is not known, the $\Upsilon(4S)$ rest frame is used as an approximation of the B rest frame. This approximation results in a smeared-out peak between ~ 2.3 and 3.0 GeV in the p_ℓ^B distribution [see Fig. 11(a)]. The inclusive reconstruction of the second B meson yields an estimate of the four-momentum of the signal B meson, which somewhat improves the approximation of the B rest frame. Events with more than one identified charged lepton are vetoed, as charged leptons are mostly produced in conjunction with neutrinos (leading to multineutrino final states) or come from continuum production of lepton pairs. As discussed in Sec. III.C.1, continuum events are reduced by using event-shape variables.

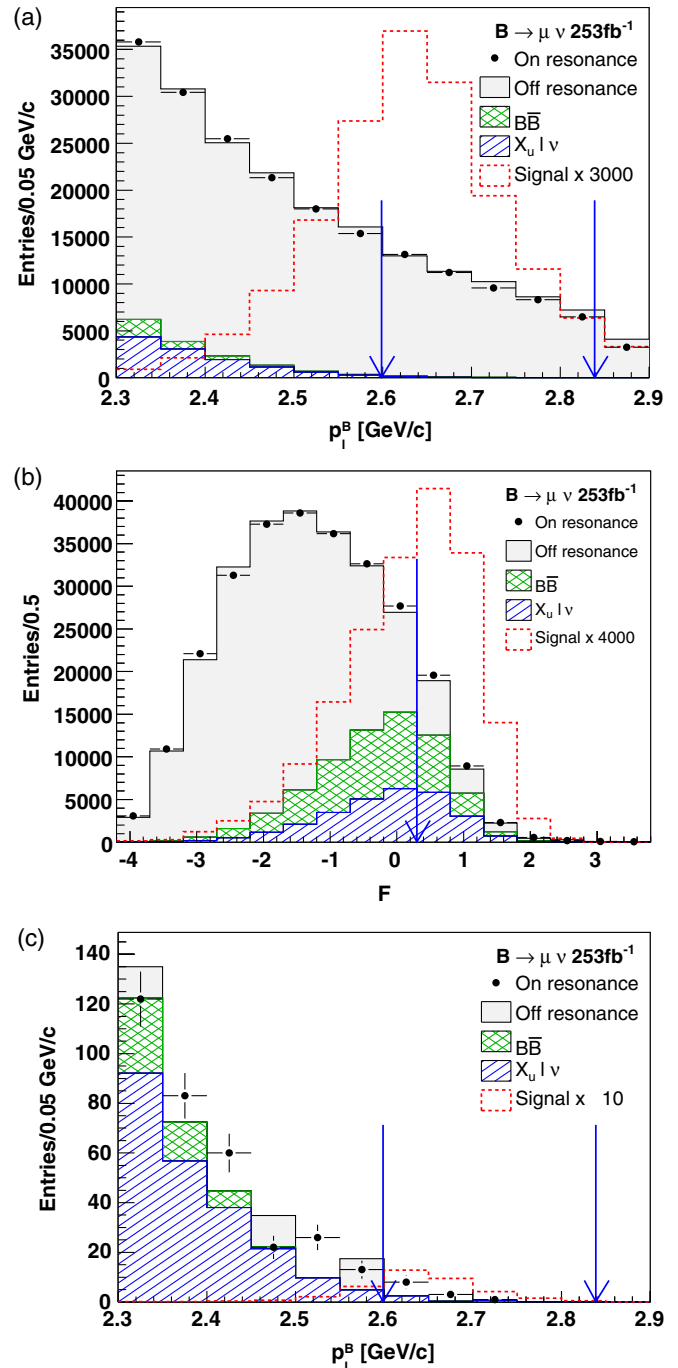


FIG. 11. Distributions from the untagged $B \rightarrow \mu\nu$ analysis by Belle: (a) lepton momentum in the B rest frame p_ℓ^B , (b) Fisher discriminant F used for continuum suppression, and (c) p_ℓ^B after a cut on the Fisher discriminant ($F > 0.3$). The arrows indicate the selection criteria applied on these variables. From Satoyama *et al.*, 2007.

Both Belle and BABAR combine these variables in a Fisher discriminant to achieve an optimum continuum suppression. Belle and BABAR extract the $B \rightarrow \ell\nu$ signal from the distributions of p_ℓ^B , m_{bc} , and ΔE . In the BABAR analysis (Aubert *et al.*, 2009e), events are selected in the range $-2.25 < \Delta E < 0$ GeV. A Fisher discriminant is built from the lepton momentum in the $\Upsilon(4S)$ frame p_ℓ^B and in the B rest frame p_ℓ^{B*} to discriminate the signal against the remaining

TABLE VI. Branching fraction upper limits for $B \rightarrow \ell\nu$ ($\ell = e, \mu$) decays.

Experiment	$\int \mathcal{L} dt$ (fb $^{-1}$)	Upper limit at 90% C.L.	
		$\mathcal{B}(B \rightarrow e\nu)$	$\mathcal{B}(B \rightarrow \mu\nu)$
CLEO untagged (Artuso <i>et al.</i> , 1995)	2	15×10^{-6}	21×10^{-6}
Belle untagged (Satoyama <i>et al.</i> , 2007)	253	1.0×10^{-6}	1.7×10^{-6}
BABAR untagged (Aubert <i>et al.</i> , 2009e)	426	1.9×10^{-6}	1.0×10^{-6}
BABAR semileptonic tag (Aubert <i>et al.</i> , 2010a)	418	11×10^{-6}	8×10^{-6}
BABAR hadronic tag (Aubert <i>et al.</i> , 2008g)	342	5.6×10^{-6}	5.2×10^{-6}
Belle hadronic tag (Yook <i>et al.</i> , 2015)	711	3.4×10^{-6}	2.7×10^{-6}
HFAG average (Amhis <i>et al.</i> , 2014)		1.0×10^{-6}	1.0×10^{-6}

continuum and $B\bar{B}$ backgrounds [see Fig. 11(b)]. The signal is extracted in a joint fit to the Fisher discriminant and m_{bc} . In the Belle analysis (Satoyama *et al.*, 2007), events are required to lie in the regions $-0.8 < \Delta E < 0.4$ GeV and $2.6 < p_\ell^B < 2.84$ GeV, and the signal is extracted in a fit to the m_{bc} distribution. The signal efficiency is 2%–3% in the Belle analysis and 5%–6% in the BABAR analysis. No evidence for $B \rightarrow e\nu$ or $B \rightarrow \mu\nu$ decays has been observed. Both experiments set upper limits on the $B \rightarrow e\nu$ and $B \rightarrow \mu\nu$ branching fractions. The results are presented in Table VI.

Belle and BABAR also searched for $B \rightarrow \ell\nu$ decays using tagged $B\bar{B}$ samples (Aubert *et al.*, 2008g, 2010a; Yook *et al.*, 2015). While the signal yields are much lower than for untagged analyses, tagged measurements provide better kinematic constraints. The full reconstruction of the B_{tag} allows for a precise determination of the four-momentum of the signal B meson and thus a precise reconstruction of the B rest frame. As can be seen in Fig. 12, the resolution of the p_ℓ^B peak is much improved, providing better suppression of the continuum and $B\bar{B}$ backgrounds. The hadronic-tag analysis is almost background free. Semileptonic-tag $B \rightarrow e\nu$ and $B \rightarrow \mu\nu$ analyses were carried out by BABAR as part of their $B \rightarrow \tau\nu$ analysis, where the electron and muon final states contribute to the leptonic τ decay channels. The exclusion limits obtained with the tagged measurements are also shown in Table VI. The best limits from hadronic-tag analyses are about a factor of 2–3 higher than for the most precise untagged

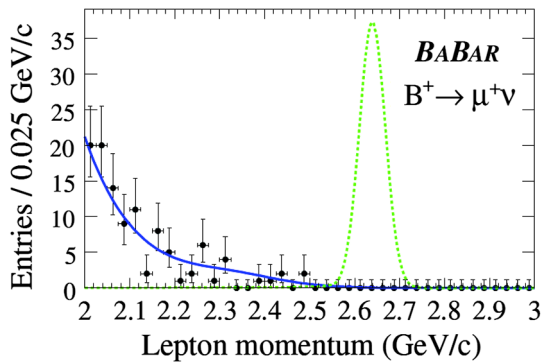


FIG. 12. Distribution of the lepton momentum in the B rest frame p_ℓ^B for the hadronic-tag $B \rightarrow \mu\nu$ analysis by BABAR. The observed distribution (points) is compared with the fit of a signal (dotted line) and a background (solid line) function to data. The signal is shown with an arbitrary normalization. From Aubert *et al.*, 2008g.

measurements. Because of the excellent p_ℓ^B resolution and the low background, tagged measurements have a promising future in $B \rightarrow \ell\nu$ searches with the larger data samples expected at Belle II, the upgrade of Belle at the Japanese SuperKEKB collider, which is expected to start operation in 2017 or 2018.

The current exclusion limits for the combination of all $B \rightarrow \ell\nu$ measurements are

$$\begin{aligned} \mathcal{B}(B \rightarrow e\nu) &< 1.0 \times 10^{-6}, \\ \mathcal{B}(B \rightarrow \mu\nu) &< 1.0 \times 10^{-6} \end{aligned} \quad (56)$$

at the 90% confidence level (Amhis *et al.*, 2014).

Besides the purely leptonic decay modes, radiative decays $B \rightarrow \ell\nu\gamma$ with their enhanced branching fractions compared to their $B \rightarrow \ell\nu$ counterparts are of interest. The current upper limit on the $B \rightarrow \ell\nu\gamma$ branching fraction for photon energies above 1 GeV is 3.5×10^{-6} at the 90% confidence level (Heller *et al.*, 2015). $B \rightarrow \ell\nu\gamma$ decays also allow the parameters of the B -meson light-cone distribution amplitude to be determined [see, e.g., Beneke and Rohrwild (2011)], which will become feasible with the Belle II data set.

2. $B \rightarrow \tau\nu$

The $B \rightarrow \tau\nu$ decay has by far the largest branching fraction of all leptonic B decay modes. Experimentally it is challenging because of the presence of several neutrinos in the final state, so it does not provide many constraints that can be used to suppress backgrounds. The multiple neutrinos make a complete reconstruction of the two-body decay kinematics impossible. Analyses of $B \rightarrow \tau\nu$ decays must rely on the reconstruction of the second B meson in the event to reach a tolerable signal-to-background ratio. Both hadronic-tag and semileptonic-tag analyses have been performed and show a comparable sensitivity with the current data sets.

The τ candidate is typically reconstructed in decay modes with a single charged particle (leptonic and one-prong hadronic decays). The track belonging to the τ candidate and the B_{tag} are required to have opposite charges. After both the B_{tag} and the τ candidate have been reconstructed, there should be no remaining particles in the event. Events with additional charged particles are vetoed. In addition, the remaining energy in the electromagnetic calorimeter $E_{\text{extra}}^{\text{ECL}}$ is computed from all energy clusters (above a certain energy threshold) that are not assigned to the B_{tag} or the τ candidate. Signal events tend to have very little remaining energy and are

located in a peak around zero in $E_{\text{extra}}^{\text{ECL}}$, while background events often contain additional photons or neutral pions. In practice, there is always some amount of extra energy in the calorimeter due to beam backgrounds, detector effects, and fragments of hadronic showers of pions and kaons, so-called hadronic split offs, that are identified as separate clusters. The dominant background that peaks at $E_{\text{extra}}^{\text{ECL}} \approx 0$ is $B \rightarrow D^{(*)} \ell \nu$, if the D meson decays semileptonically or to final states with one or more K_L^0 . Also charmless semileptonic decays $B^+ \rightarrow \pi^0 \ell^+ \nu$ or radiative decays $B \rightarrow K^* \gamma$ contribute to the peaking background. A reliable reconstruction of $E_{\text{extra}}^{\text{ECL}}$ is one of the most important but also most challenging tasks in $B \rightarrow \tau \nu$ analyses.

The first searches for $B \rightarrow \tau \nu$ decays were already performed before the start of the B factories, by ALEPH (Barate *et al.*, 2001), ARGUS (Albrecht *et al.*, 1995), CLEO (Artuso *et al.*, 1995; Browder *et al.*, 2001), and L3 (Acciarri *et al.*, 1997). These analyses led to an upper limit on the $B \rightarrow \tau \nu$ branching fraction of 5.7×10^{-4} (Hagiwara *et al.*, 2002) at the 90% confidence level. In 2006, the Belle experiment reported the first evidence of $B \rightarrow \tau \nu$ decays (Ikado *et al.*, 2006) in a hadronic-tag analysis using a data sample of 414 fb^{-1} . A branching fraction of $\mathcal{B}(B \rightarrow \tau \nu) = (1.79^{+0.56}_{-0.49\text{stat}} \text{ } ^{+0.46}_{-0.51\text{syst}}) \times 10^{-4}$ was measured, corresponding to a signal significance of 3.5σ . Two years later, also BABAR published a 2.2σ evidence for $B \rightarrow \tau \nu$ decays in a hadronic-tag analysis using a data sample of 346 fb^{-1} (Aubert *et al.*, 2008a), and measured a branching fraction consistent with the Belle result.

Both Belle and BABAR have recently published updates of their hadronic-tag analyses using the full data sets (Adachi *et al.*, 2013; Lees *et al.*, 2013b). These analyses benefit not only from the larger data samples, but also from improvements in the hadronic B -tagging algorithms. The results are summarized in Table VII.

The τ lepton is reconstructed in the four decay modes $\tau^+ \rightarrow e^+ \nu_e \bar{\nu}_\tau$, $\tau^+ \rightarrow \mu^+ \nu_\mu \bar{\nu}_\tau$, $\tau^+ \rightarrow \pi^+ \bar{\nu}_\tau$, and $\tau^+ \rightarrow \rho^+ \bar{\nu}_\tau \rightarrow \pi^+ \pi^0 \bar{\nu}_\tau$, which have a combined branching fraction of 72%. Belle extracts the signal in a joint fit to the $E_{\text{extra}}^{\text{ECL}}$ and M_{miss}^2 distributions. The reconstruction of $E_{\text{extra}}^{\text{ECL}}$ and M_{miss}^2 is validated in data with a sample of $B^+ \rightarrow \bar{D}^{*0} \ell^+ \nu$ decays after removing the \bar{D}^{*0} decay products from the event to obtain a similar event topology as for the $B \rightarrow \tau \nu$ signal. The signal fit is performed simultaneously for all four τ decay modes, taking the different reconstruction efficiencies and τ branching fractions into account. The $E_{\text{extra}}^{\text{ECL}}$ distribution after the fit is shown in Fig. 13(a). In the BABAR analysis, a

likelihood ratio is constructed from the signal and background likelihoods to suppress $B\bar{B}$ backgrounds. The likelihoods are obtained from the product of the probability density functions of two variables for $\tau^+ \rightarrow \pi^+ \bar{\nu}_\tau$ and four variables for $\tau^+ \rightarrow \rho^+ \bar{\nu}_\tau \rightarrow \pi^+ \pi^0 \bar{\nu}_\tau$: the momentum of the hadron, the polar angle of the missing momentum, and in the case of $\tau^+ \rightarrow \rho^+ \bar{\nu}_\tau$, also the masses of the π^0 and the ρ^+ candidate. The signal and background yields are determined from a fit to the $E_{\text{extra}}^{\text{ECL}}$ distribution in the four decay modes simultaneously. Templates for signal and background events in which the B_{tag} is correctly reconstructed are taken from simulation. The template for the combinatorial background is taken from a sideband of the m_{bc} distribution of the B_{tag} candidate. Differences between data and simulation for these distributions are studied and corrected using *double-tag* events, where the signal B meson is replaced by a second reconstructed B_{tag} candidate. As seen in Table VII, the branching fraction measured by BABAR is larger than the one obtained by Belle; the two measurements lie about 1.7σ apart. The experimental uncertainties on the individual measurements are 30%–40%, dominated by the statistical uncertainty.

As the hadronic-tag results are still statistically limited, Belle and BABAR have also measured $B \rightarrow \tau \nu$ decays in semileptonic-tag analyses (Aubert *et al.*, 2010a; Kronenbitter *et al.*, 2015). The two tagging techniques provide independent measurements, both statistically and to a large extent also systematically. Belle reconstructs semileptonic tags in the decay modes $B^+ \rightarrow \bar{D}^0 \ell^+ \nu$ and $B^+ \rightarrow \bar{D}^{*0} \ell^+ \nu$. BABAR uses a more inclusive approach and reconstructs $B \rightarrow DX \ell \nu$ decays by selecting only a D meson and a lepton without any requirement on the presence of any additional hadrons (X). In the BABAR analysis, two likelihood ratios per signal mode are constructed from kinematic and event-shape variables to suppress backgrounds, one for the $B\bar{B}$ background, and the other for the continuum background. Selection criteria on the two likelihood ratios and on $E_{\text{extra}}^{\text{ECL}}$ are chosen to maximize the signal significance in each decay mode separately and to determine the signal yields. Belle uses neural networks for background suppression and extracts the signal with a two-dimensional fit in $E_{\text{extra}}^{\text{ECL}}$ and the momentum of the visible τ decay products. The $E_{\text{extra}}^{\text{ECL}}$ distribution is presented in Fig. 13(b). The results of the semileptonic-tag analyses are also shown in Table VII.

A graphical overview of the branching fraction measurements is shown in Fig. 14. The results are still statistically

TABLE VII. Overview of $B \rightarrow \tau \nu$ results from Belle and BABAR. The uncertainty on the number of signal events N_{sig} is statistical, and the uncertainties on the branching fractions are statistical and systematic.

Experiment	$\int \mathcal{L} dt$ (fb^{-1})	N_{sig}	$\mathcal{B}(B \rightarrow \tau \nu)$ (10^{-4})	Significance (σ)
Belle semileptonic tag (Kronenbitter <i>et al.</i> , 2015)	711	222 ± 50	$1.25 \pm 0.28 \pm 0.27$	3.8
Belle hadronic tag (Adachi <i>et al.</i> , 2013)	711	62 ± 23	$0.72^{+0.27}_{-0.25} \pm 0.11$	3.0
Average Belle			0.91 ± 0.22	
BABAR semileptonic tag (Aubert <i>et al.</i> , 2010a)	418	74 ± 39	$1.7 \pm 0.8 \pm 0.2$	2.3
BABAR hadronic tag (Lees <i>et al.</i> , 2013b)	426	62 ± 17	$1.83^{+0.53}_{-0.49} \pm 0.24$	3.8
Average BABAR			1.79 ± 0.48	
Average Belle + BABAR			1.06 ± 0.20	

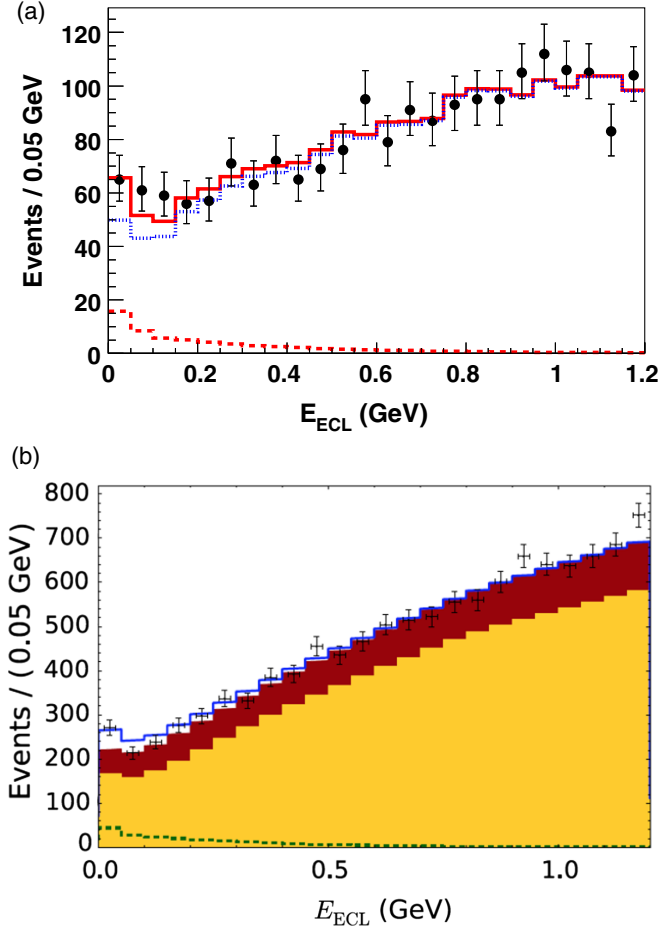


FIG. 13. Distributions of $E_{\text{ECL}}^{\text{extra}}$ for the Belle $B \rightarrow \tau\nu$ analysis using (a) hadronic tags (Adachi *et al.*, 2013) and (b) semileptonic tags (Kronenbitter *et al.*, 2015). The observed distributions (points) are compared with fits of simulated signal (topmost histogram) and background distributions (other histograms) to data.

limited. The leading systematic uncertainty comes from the background modeling, in particular, of the shape of the $E_{\text{ECL}}^{\text{extra}}$ distribution. The combination of the hadronic-tag and semileptonic-tag measurements from Belle and BABAR yields a signal significance of about 5σ , corresponding to an observation of $B \rightarrow \tau\nu$ decays.

3. Interpretation of $B \rightarrow \tau\nu$ results: $|V_{ub}|$, f_B , and new physics

The measured $B \rightarrow \tau\nu$ branching fraction can be compared with the SM prediction computed for given values of f_B and $|V_{ub}|$. The average of the Belle and BABAR measurements in Table VII is found to be in good agreement with the SM prediction in Eq. (51).

The branching fraction average can be translated to a result for the product $f_B|V_{ub}|$. Using the lattice QCD result for f_B , we can then extract the following value for $|V_{ub}|$:

$$|V_{ub}| = (4.19 \pm 0.40) \times 10^{-3}. \quad (57)$$

Alternatively, if the value of $|V_{ub}|$ is known from other measurements, the measured branching fraction can be used to determine the B decay constant. Using

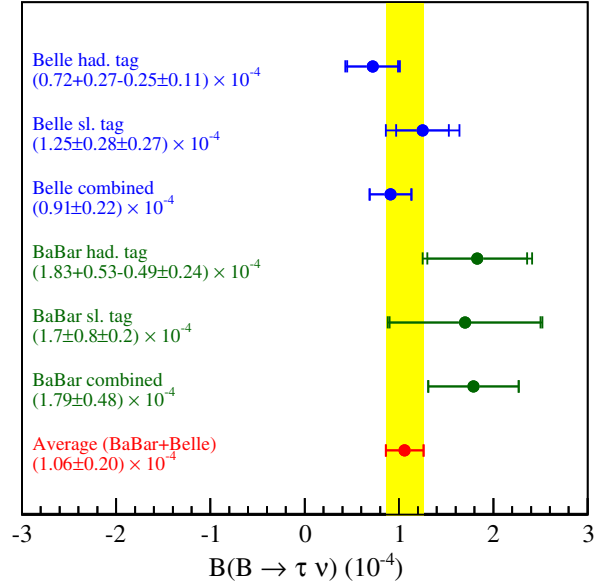


FIG. 14. Comparison of the $B \rightarrow \tau\nu$ results from Belle and BABAR. The inner error bars show the statistical uncertainty, and the outer ones the total experimental uncertainty. For averaged branching fractions, only the total uncertainty is shown.

$|V_{ub}| = (3.70 \pm 0.38) \times 10^{-3}$ (see Sec. VIII.B.6), we obtain

$$f_B = 210 \pm 29 \text{ MeV}. \quad (58)$$

The measured $B \rightarrow \tau\nu$ branching fraction in combination with $|V_{ub}|$ can also be used to constrain new physics models, for instance the ratio r_H in Eq. (55). As an example, Fig. 15 shows the constraints in the $m_{H^\pm} - \tan\beta$ plane for the type-II 2HDM obtained by BABAR (Lees *et al.*, 2013b).

In this article, we focus on charged-current leptonic decays with a neutrino in the final state, which are a domain of the B factories. A number of other interesting leptonic decay modes of the B meson exist and have been studied at the B factories, the Tevatron, and the LHC, for instance $B_{(s)}^0 \rightarrow \mu^+\mu^-$, $B^0 \rightarrow \nu\bar{\nu}$ and lepton flavor violating decays $B \rightarrow e\mu$, $B \rightarrow e\tau$, and $B \rightarrow \mu\tau$. Their discussion is beyond the scope of this article.

V. INCLUSIVE SEMILEPTONIC B DECAYS TO CHARM MESONS

This section describes the current status of studies of inclusive $B \rightarrow X_c \ell \nu$ decays. The large samples of B mesons available from the two B factories allow for high-statistics investigations of $B \rightarrow X_c \ell \nu$ decays, which have a large total branching fraction of about 10% per lepton mode $\ell = e, \mu$. From the theoretical side the methods are in a very mature state, allowing for precise calculations, which lead to extractions of SM parameters, in particular, $|V_{cb}|$ and quark masses, with small uncertainties.

A. Theory

The basis of the precise theoretical prediction for inclusive $B \rightarrow X_c \ell \nu$ decays is the heavy-quark expansion discussed in

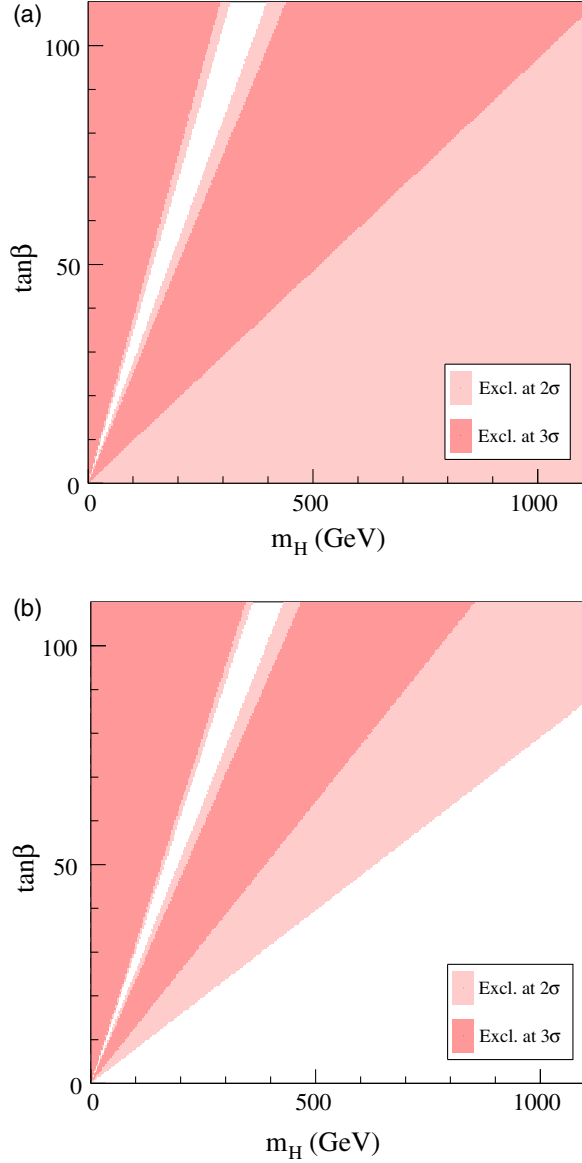


FIG. 15. Constraints on the parameters m_{H^\pm} and $\tan\beta$ in the type-II 2HDM, derived from the $B \rightarrow \tau\nu$ branching fraction of the BABAR hadronic-tag analysis. The exclusion limits are shown for 90% (light-shaded) and 99% (dark-shaded) confidence level and two example $|V_{ub}|$ values: (a) $(3.23 \pm 0.30) \times 10^{-3}$ and (b) $(4.33 \pm 0.28) \times 10^{-3}$. From Lees *et al.*, 2013b.

Sec. II.D. Here we quote the necessary formulas that are used for the determination of $|V_{cb}|$.

For the extraction of $|V_{cb}|$ from inclusive decays, a simultaneous fit is performed to determine $|V_{cb}|$ together with the parameters of the HQE and the quark masses. The observables used are the total rate as well as various moments of differential distributions (lepton energy, hadronic energy, hadronic invariant mass, etc.), which can be computed using the methods presented in Sec. II.D. In contrast to the detailed form of the spectrum, moments of the spectra can be calculated reliably.

The general structure of the expansion (Benson *et al.*, 2003) is

$$\begin{aligned}
 d\Gamma = & d\Gamma_0 + d\Gamma_2 \left(\frac{\Lambda_{\text{QCD}}}{m_b}\right)^2 + d\Gamma_3 \left(\frac{\Lambda_{\text{QCD}}}{m_b}\right)^3 + d\Gamma_4 \left(\frac{\Lambda_{\text{QCD}}}{m_b}\right)^4 \\
 & + d\Gamma_5 \left[a_0 \left(\frac{\Lambda_{\text{QCD}}}{m_b}\right)^5 + a_2 \left(\frac{\Lambda_{\text{QCD}}}{m_b}\right)^3 \left(\frac{\Lambda_{\text{QCD}}}{m_c}\right)^2 \right] + \dots \\
 & + d\Gamma_7 \left(\frac{\Lambda_{\text{QCD}}}{m_b}\right)^3 \left(\frac{\Lambda_{\text{QCD}}}{m_c}\right)^4 + \dots, \quad (59)
 \end{aligned}$$

where the coefficients $d\Gamma_i$ are functions of m_c/m_b that depend on the HQE parameters $\mu_\pi^2, \mu_G^2, \rho_D^3, \rho_{LS}^3, \dots$ [see Eqs. (32)–(36)]. Furthermore, the OPE yields an expansion of the $d\Gamma_i$ in powers of $\alpha_s(m_b)$. It is interesting to note that also inverse powers of the charm-quark mass appear, indicating an infrared sensitivity to the charm-quark mass, which starts with an $\ln m_c$ term at $1/m_b^3$ (Breidenbach *et al.*, 2008; Mannel, Turczyk, and Uraltsev, 2010).

The coefficients $d\Gamma_i$ are known at tree level up to and including $1/m_b^5$ (Dassinger, Mannel, and Turczyk, 2007; Mannel, Turczyk, and Uraltsev, 2010), the corrections of order α_s (Jezabek and Kuhn, 1989) and α_s^2 (Melnikov, 2008; Pak and Czarnecki, 2008; Brucherseifer, Caola, and Melnikov, 2013) are known for $d\Gamma_0$, while for the subleading terms in $1/m_b$ the α_s corrections are known for the μ_π^2 (Becher, Boos, and Lunghi, 2007) and the μ_G^2 terms (Alberti, Gambino, and Nandi, 2014; Mannel, Pivovarov, and Rosenthal, 2014).

As pointed out in Sec. II.D, the leading term of the HQE is given by the decay rate of a free quark. For dimensional reasons the free decay rate scales with the fifth power of the heavy-quark mass, at least if the final state is assumed to be massless. In the early days of the HQE this was considered a problem for the precision of the predictions, since the result depends strongly on the way the heavy-quark mass is defined. Usual perturbative calculations assume the pole mass, corresponding to the location of the pole in the quark propagator. However, the pole mass cannot be defined to a precision better than a few hundred MeV due to the so-called renormalon problem (Bigi *et al.*, 1994b). Moreover, the radiative corrections calculated in terms of the pole mass turn out to be large, and hence, if the two issues were uncorrelated, the HQE would not yield precise predictions.

Fortunately, the bulk of the radiative corrections are indeed correlated with the mass, and hence it is mandatory to choose a suitable mass definition. The first requirement is to choose a mass definition that is not plagued by the renormalon problem; such mass definitions are called *short-distance masses*. The most commonly used definition of this kind is the mass defined in the so-called modified minimal subtraction scheme ($\overline{\text{MS}}$ scheme) (Bardeen *et al.*, 1978), which depends on a renormalization point μ , usually chosen to be $m_b^{\overline{\text{MS}}}$.

The HQE is an effective theory at scales below m_b . Extrapolating the $\overline{\text{MS}}$ scheme to values below m_b has turned out to not yield the most precise scheme for the HQE; rather two specific mass definitions have been constructed which are both short-distance masses. The first one is the mass definition in the so-called kinetic scheme (Bigi *et al.*, 1997), where a μ -dependent mass is defined from a sum rule for the (non-relativistic) kinetic energy; $m_b^{\text{kin}}(\mu)$ is defined for values of μ below m_b . The second possibility is the so-called 1S scheme

(Hoang, Ligeti, and Manohar, 1999; Bauer *et al.*, 2004), where a short-distance mass value is extracted from the mass of the $\Upsilon(1S)$ state. Both the $1S$ mass and the kinetic mass are short-distance masses, thus they can be related to each other within perturbation theory.

The rate for $B \rightarrow X_c \ell \nu$ decays also depends on the mass of the charm quark. However, it turns out that the total rate as well as the moments depends only on a linear combination of the two masses. In fact, from the semileptonic moments one may precisely determine a linear combination

$$m_b^{\text{kin}}(1 \text{ GeV}) - am_c, \quad (60)$$

where a is in the range 0.7–0.8, depending on the choice of the scheme for the charm-quark mass.

The radiative corrections are under good control in both schemes. Including the terms of the HQE up to $1/m_b^3$, the theoretical uncertainty is at the level of 2%. The higher-order terms can be estimated to be (Mannel, Turczyk, and Uraltsev, 2010)

$$\frac{\Delta\Gamma_{1/m^3}}{\Gamma_{\text{tree}}} = -0.030, \quad (61)$$

$$\frac{\Delta\Gamma_{1/m^4}}{\Gamma_{\text{tree}}} = 0.007, \quad (62)$$

$$\frac{\Delta\Gamma_{1/m^5}}{\Gamma_{\text{tree}}} = 0.006, \quad (63)$$

where the terms of the order of $1/m_b^3$ are taken into account in the analysis. The terms of the order of $1/m_b^4$ and higher yield only a very small shift in $|V_{cb}|$, which is well under 1%. Thus the HQE yields a very precise prediction of the rate and also of the moments, which are given in terms of the HQE parameters in Eqs. (32)–(36). These are extracted in a simultaneous fit to data in various moments and hence also yield a contribution to the overall uncertainty. If one assigns this uncertainty to be theoretical, the overall (relative) theoretical uncertainty for the extraction of $|V_{cb}|$ is now below 2%.

Additional sources of uncertainty such as duality violations have been discussed in the literature (Bigi and Uraltsev, 2001; Bigi and Mannel, 2002), however, they are hard to quantify. Following the arguments of Bigi and Mannel (2002), duality violations should show up as unnaturally large coefficients in higher orders in the HQE when extracting them from the data. As there is no evidence for this in the present data, no additional uncertainty for possible duality violations is assigned to $|V_{cb}|$.

B. Measurements

1. Measurements of moments of inclusive spectra

The shapes of kinematic distributions, e.g., lepton energy and hadronic mass spectra, of $B \rightarrow X_c \ell \nu$ decays are sensitive to the HQE parameters. Moments of inclusive distributions are measured to characterize their shapes and the HQE parameters are determined by fitting the HQE to these moments.

The moments of the distribution of an observable O for semileptonic decays are defined as

$$\langle O^n \rangle_{E_{\text{cut}}} = \frac{\int_{E_{\text{cut}}}^{E_{\text{max}}} O^n (d\Gamma/dO) dO}{\int_{E_{\text{cut}}}^{E_{\text{max}}} (d\Gamma/dO) dO}, \quad (64)$$

where E_{cut} denotes the minimum energy required for the lepton. The moments are measured as a function of the minimum lepton energy, as their dependence on E_{cut} contains information on the HQE parameters and thus provides additional sensitivity for their determination. Moments of order n can be interpreted as follows:

- $n = 0$: According to the definition in Eq. (64) the zeroth moment is unity. What is referred to as the zeroth moment by the experiments is often the partial decay rate, which provides the normalization information needed to determine $|V_{cb}|$:

$$\Delta\Gamma(E_{\text{cut}}) = \int_{E_{\text{cut}}}^{E_{\text{max}}} \frac{d\Gamma}{O} dO. \quad (65)$$

- $n = 1$: The first moment corresponds to the mean of the distribution $\langle O \rangle$.
- $n \geq 2$: As the moments with $n \geq 2$ are correlated with the mean, it is advantageous to remove this correlation by defining *central moments* μ_n about the mean of the distribution:

$$\mu_n^O(E_{\text{cut}}) = \langle (O - \langle O \rangle)^n \rangle_{E_{\text{cut}}}. \quad (66)$$

The second central moment corresponds to the variance, the third to the skewness, and the fourth to the kurtosis of the distribution.

Moments of lepton energy $\langle E_\ell^n \rangle$ and (squared) hadronic mass $\langle m_X^2 \rangle$ have been measured for $B \rightarrow X_c \ell \nu$ decays by several experiments in e^+e^- collisions at the $\Upsilon(4S)$ and the Z resonance, and in $p\bar{p}$ collisions. Table VIII gives an overview of the available moment measurements.

In addition to $B \rightarrow X_c \ell \nu$ decays, moments of the photon energy distribution $\langle E_\gamma^n \rangle$ in radiative decays $B \rightarrow X_s \gamma$ can be used to determine the HQE parameters. Radiative decays contain complementary information on the HQE parameters. As $B \rightarrow X_s \gamma$ is a two-body decay, the b quark is at rest in the B rest frame at the parton level, but the photon energy spectrum is smeared out when taking the Fermi motion of the b quark inside the B meson into account. The measured shape of the E_γ spectrum thus has a high sensitivity to m_b and μ_π^2 .

Hadronic mass moments in $B \rightarrow X_c \ell \nu$ decays have been measured with $\Upsilon(4S)$ data by Belle (Schwanda *et al.*, 2007),

TABLE VIII. Moment measurements for hadronic mass and lepton energy.

Experiment	$\langle m_X^2 \rangle$		$\langle E_\ell^n \rangle$	
	n	E_{cut} (GeV)	n	E_{cut} (GeV)
BABAR	1/2, 1, 3/2, 2, 5/2, 3	0.8–1.9	0, 1, 2, 3	0.6–1.5
Belle	1, 2	0.7–1.9	0, 1, 2, 3	0.4–2.0
CDF	1, 2	0.7
CLEO	1, 2	1.0–1.5	1, 2	0.6–1.5
DELPHI	1, 2, 3, 4, 5	...	1, 2, 3	...

BABAR (Aubert *et al.*, 2004b, 2010b), and CLEO (Cronin-Hennessy *et al.*, 2001; Csorna *et al.*, 2004). Measurements at higher energies come from DELPHI (Abdallah *et al.*, 2006) in e^+e^- collisions and CDF (Acosta *et al.*, 2005) in $p\bar{p}$ collisions.

The CLEO analysis is performed as an untagged analysis and hence the hadronic final state X_c of the $B \rightarrow X_c \ell \nu$ decay cannot explicitly be reconstructed. The mass m_X needs to be determined from kinematics according to

$$m_X^2 = m_B^2 + q^2 - 2E_{\text{beam}}^* (E_\ell + E_\nu) + 2|\vec{p}_B| |\vec{q}| \cos \theta_{B,\ell\nu}. \quad (67)$$

In this equation, $\vec{q} = \vec{p}_\ell + \vec{p}_\nu$ is the momentum of the leptonic system, \vec{p}_B and m_B are the momentum and mass of the B meson, and $\theta_{B,\ell\nu}$ is the angle between the B meson and the leptonic system. The neutrino kinematics are inferred from the missing energy and momentum in the event. As the direction of the B meson is unknown, the last term in Eq. (67) is not known. However, as the average momentum of the B meson is small ($p_B \approx 320$ MeV, see Sec. III.C.1), the omission of the last term in Eq. (67) yields a reasonable approximation of the hadronic mass.

In the Belle and *BABAR* analyses, the second B meson in the event is fully reconstructed in a hadronic decay mode (B_{tag}). After identifying the lepton from the semileptonic decay, the momentum of the hadronic final state X_c is reconstructed as the sum of the momenta of all particles in the event not associated with the B_{tag} and the lepton. The measured m_X distribution needs to be corrected for detector acceptance and resolution effects. In *BABAR*, an event-by-event correction is applied, based on lepton momentum, hadron decay multiplicity, and missing mass in the event. Belle performs an unfolding of the m_X spectrum using a correction matrix determined from simulation. Figure 16(a) shows the m_X^2 distribution measured by Belle. The hadronic mass spectrum in $B \rightarrow X_c \ell \nu$ decays is composed of D , D^* , and higher-mass resonant or nonresonant charm final states (see Sec. VII.B.4 for more details). The experimental m_X resolution is not sufficient to clearly separate these individual contributions. In the measurements at higher energies from DELPHI and CDF, exclusive $B \rightarrow X_c \ell \nu$ decays are reconstructed ($B \rightarrow D \ell \nu$, $B \rightarrow D^* \ell \nu$, and $B \rightarrow D^{**} \ell \nu$), and the hadronic mass spectrum is composed of the sum of these exclusive decays. The main systematic uncertainty in this approach is due to the uncertainties on the exclusive branching fractions. Because of the large average B momentum of ~ 30 GeV at LEP, no minimum lepton momentum requirement is needed.

Lepton energy moments in $B \rightarrow X_c \ell \nu$ decays can be measured more precisely than hadronic mass moments. They have been measured by Belle (Urquijo *et al.*, 2007), *BABAR* (Aubert *et al.*, 2004a, 2010b), CLEO (Mahmood *et al.*, 2004), and DELPHI (Abdallah *et al.*, 2006). The CLEO and the earlier of the two *BABAR* analyses are based on a selection of dilepton events. A tag lepton with momentum above 1.4 GeV is selected and the energy distribution of the second (signal) lepton with momentum above 0.6 GeV is studied. Background from events where the signal lepton comes from a secondary decay of a charm meson can be

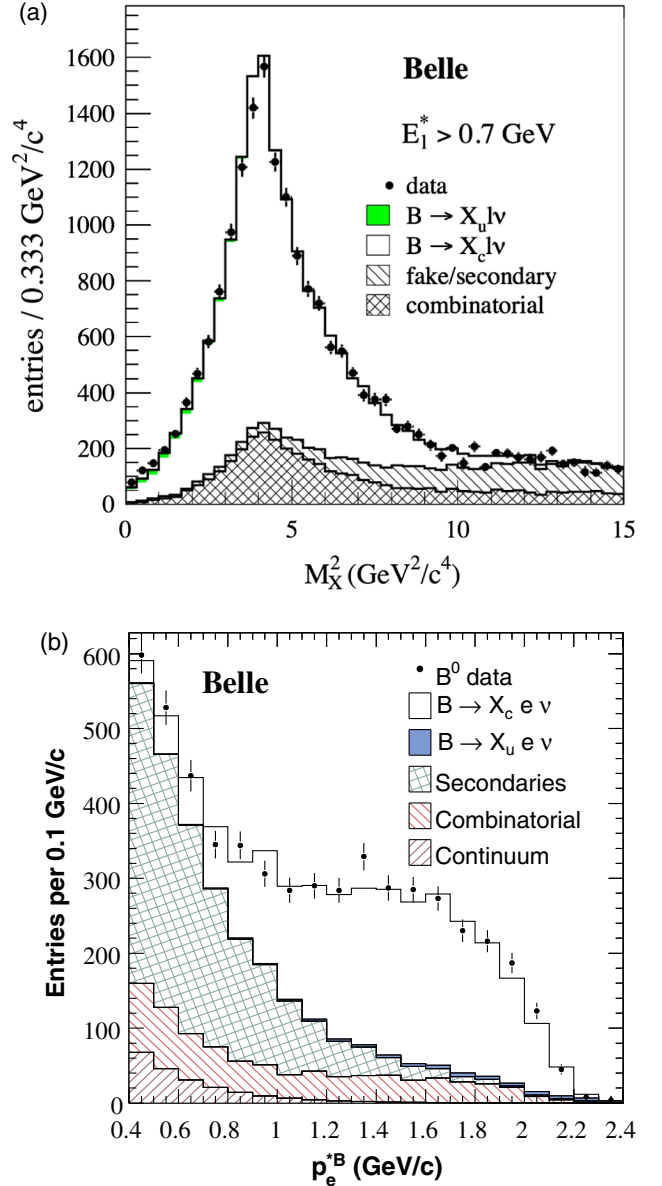


FIG. 16. Inclusive $B \rightarrow X_c \ell \nu$ spectra measured by Belle (Schwanda *et al.*, 2007; Urquijo *et al.*, 2007) for (a) squared hadronic mass and (b) lepton momentum.

controlled by using charge correlation and kinematic properties of the leptons. The more recent analyses by Belle and *BABAR* use hadronic tags and have low combinatorial background. The E_ℓ distribution measured in the Belle analysis is shown in Fig. 16(b).

BABAR also measured combined hadronic mass and hadronic energy (E_X) moments (Aubert *et al.*, 2010b), called *mixed moments* $\langle n_X^{2n} \rangle$. The quantity n_X is defined as

$$n_X^2 = m_X^2 - 2\tilde{\Lambda}E_X + \tilde{\Lambda}^2 \quad (68)$$

with a constant $\tilde{\Lambda} = 0.65$ GeV, as proposed by Gambino and Uraltsev (2004). Mixed moments are supposed to allow for a more reliable extraction of higher-order HQE parameters.

The measured moments need to be known in the B -meson rest frame for a direct comparison with theory calculations.

The translation to the B rest frame is not a large problem for the $\Upsilon(4S)$ analyses, as the $\Upsilon(4S)$ rest frame is quite close to the B rest frame. For hadronic-tag analyses, the four-momentum of the signal B is precisely known from that of the fully reconstructed B_{tag} . Translation of the moments to the B -meson rest frame at the LEP and Tevatron experiments needs to rely on simulation.

2. Determination of $|V_{cb}|$, b -quark mass, and HQE parameters

Belle, *BABAR*, CLEO, and DELPHI performed HQE fits to their measured moments to determine $|V_{cb}|$, the b -quark mass, and the HQE parameters. The most precise results are obtained for global fits that include the moments from all experiments. Global fits have been performed in the kinetic scheme (Buchmüller and Flächer, 2006; Gambino and Schwanda, 2014) and in the 1S scheme (Bauer *et al.*, 2004; Amhis *et al.*, 2014).

As mentioned in Sec. VII.A, $B \rightarrow X_c \ell \nu$ moments are sensitive to a linear combination of m_b and m_c . For a precise determination of m_b , it is useful to include additional, complementary constraints on these masses in the fit. This can be done either by including moments from $B \rightarrow X_s \gamma$ decays, which carry complementary information on m_b , or by using theoretical determinations of m_c , e.g., from QCD sum rules (Chetyrkin *et al.*, 2009; Dehnadi *et al.*, 2013) or lattice QCD (Allison *et al.*, 2008) calculations, and constraining the value of m_c within its uncertainty in the fit. Relatively loose constraints also exist for the HQE parameters μ_G^2 and ρ_{LS}^3 from measurements of the hyperfine splitting between the B and B^* masses and from heavy-quark sum rules, respectively.

The most recent global fit was performed by Gambino and Schwanda (2014) in the kinetic scheme. It is based solely on $B \rightarrow X_c \ell \nu$ moments [including next-to-next-to-leading-order (NNLO) perturbative corrections from Gambino (2011)] and uses a precise mass constraint on m_c from the sum rules calculation by Chetyrkin *et al.* (2009). The only other external inputs are the B -meson lifetime and constraints on μ_G^2 and ρ_{LS}^3 . The fit includes the partial decay rate measurements from Belle and *BABAR*, the lepton energy moments with $n = 1, 2$, and 3 from Belle, *BABAR*, and DELPHI, and the hadronic mass moments with $n = 1, 2$, and 3 from *BABAR* and DELPHI and with $n = 1, 2$ from Belle, CDF, and CLEO for several values of E_{cut} . The moments measured by each experiment are strongly correlated, in particular, the measurements for different E_{cut} values. The full statistical and systematic correlation matrices are taken into account in the fit and only a subset of the available moments has been used to avoid large correlations. Figure 17 shows the results of the global fit. The fit results for $|V_{cb}|$ and m_b (in the kinetic scheme) are

$$\begin{aligned} |V_{cb}| &= (42.42 \pm 0.86) \times 10^{-3}, \\ m_b^{\text{kin}}(1 \text{ GeV}) &= 4.541 \pm 0.023 \text{ GeV}. \end{aligned} \quad (69)$$

The quoted uncertainties are the combined experimental and theoretical uncertainties of the fit. For $|V_{cb}|$, an additional 1.4% theoretical uncertainty on the semileptonic decay rate is included due to missing higher-order corrections in the HQE.

The total average branching fraction for charged and neutral B mesons obtained from the fit is

$$\mathcal{B}(B \rightarrow X_c \ell \nu) = (10.65 \pm 0.16)\%. \quad (70)$$

Using the lifetime ratio $\tau_{B^+}/\tau_{B^0} = 1.078 \pm 0.004$ (Olive *et al.*, 2014), the average branching fraction can be translated to branching fractions for B^0 and B^+ : $\mathcal{B}(B^0 \rightarrow X_c^- \ell^+ \nu) = (10.25 \pm 0.15)\%$ and $\mathcal{B}(B^+ \rightarrow X_c^0 \ell^+ \nu) = (11.05 \pm 0.17)\%$.

The complete set of fitted parameters (including higher-order HQE parameters) can be found in Table IX. Excellent agreement between the measured moments and the HQE fit is seen and gives confidence in the validity of quark-hadron duality and thus the applicability of the HQE. In fact, the χ^2 value per degree of freedom of the fit is significantly smaller than unity ($\chi^2/\text{ndf} = 0.32$, where ndf is the number of degrees of freedom), as already observed in previous moment fits. This may indicate that the theoretical uncertainties are overestimated or the theoretical correlations underestimated. Gambino and Schwanda (2014) discussed various assumptions about the theoretical uncertainties and their correlations and investigated different scenarios in the HQE fit. Figure 18 presents the $\Delta\chi^2 = 1$ contours obtained for $|V_{cb}|$, μ_π^2 , and m_b^{kin} using different scenarios for the theoretical correlations. Even though a reduction of the theoretical uncertainties would lead to a more realistic fit probability, Gambino and Schwanda (2014) pointed out that this would make the use of the extracted values of the HQE parameters in other processes problematic, as higher-order corrections may result in sizable shifts of some of these parameters.

The b -quark mass in the kinetic scheme can be translated to the $\overline{\text{MS}}$ scheme, resulting in $m_b^{\overline{\text{MS}}} = 4.17 \pm 0.04 \text{ GeV}$. The increase in relative uncertainty is due to the additional uncertainty introduced by the translation, which involves perturbative expansions. This result is found to be in good agreement with recent values calculated with lattice QCD, $m_b^{\overline{\text{MS}}} = 4.164 \pm 0.023 \text{ GeV}$ (McNeile *et al.*, 2010), or QCD sum rules, $m_b^{\overline{\text{MS}}} = 4.163 \pm 0.016 \text{ GeV}$ (Chetyrkin *et al.*, 2009).

Global moment fits have also been performed in the 1S scheme (Bauer *et al.*, 2004; Amhis *et al.*, 2014), both for $B \rightarrow X_c \ell \nu$ moments alone and together with $B \rightarrow X_s \gamma$ moments. The 1S fit yields results for $|V_{cb}|$ and also for m_b and μ_π^2 (after translation to a common renormalization scheme) which are consistent with the ones in the kinetic scheme.

HQE fits to mixed moments have been performed only by *BABAR* (Aubert *et al.*, 2010b). From these fits in the kinetic scheme, $|V_{cb}|$ and m_b^{kin} values consistent with those from the m_X fits are obtained, with comparable uncertainties. As the extraction of the HQE parameters from n_X moments is less affected by higher-order corrections than from m_X moments, the consistency of the results gives confidence in the reliability of the uncertainty estimates.

In conclusion, the magnitude of the CKM parameter V_{cb} has been determined with very good precision from inclusive spectra in $B \rightarrow X_c \ell \nu$ decays. The uncertainty on $|V_{cb}|$ obtained from the global moment fits is 2.0% in the kinetic scheme and 1.1% in the 1S scheme, dominated by the theoretical uncertainty. The difference in the final uncertainty

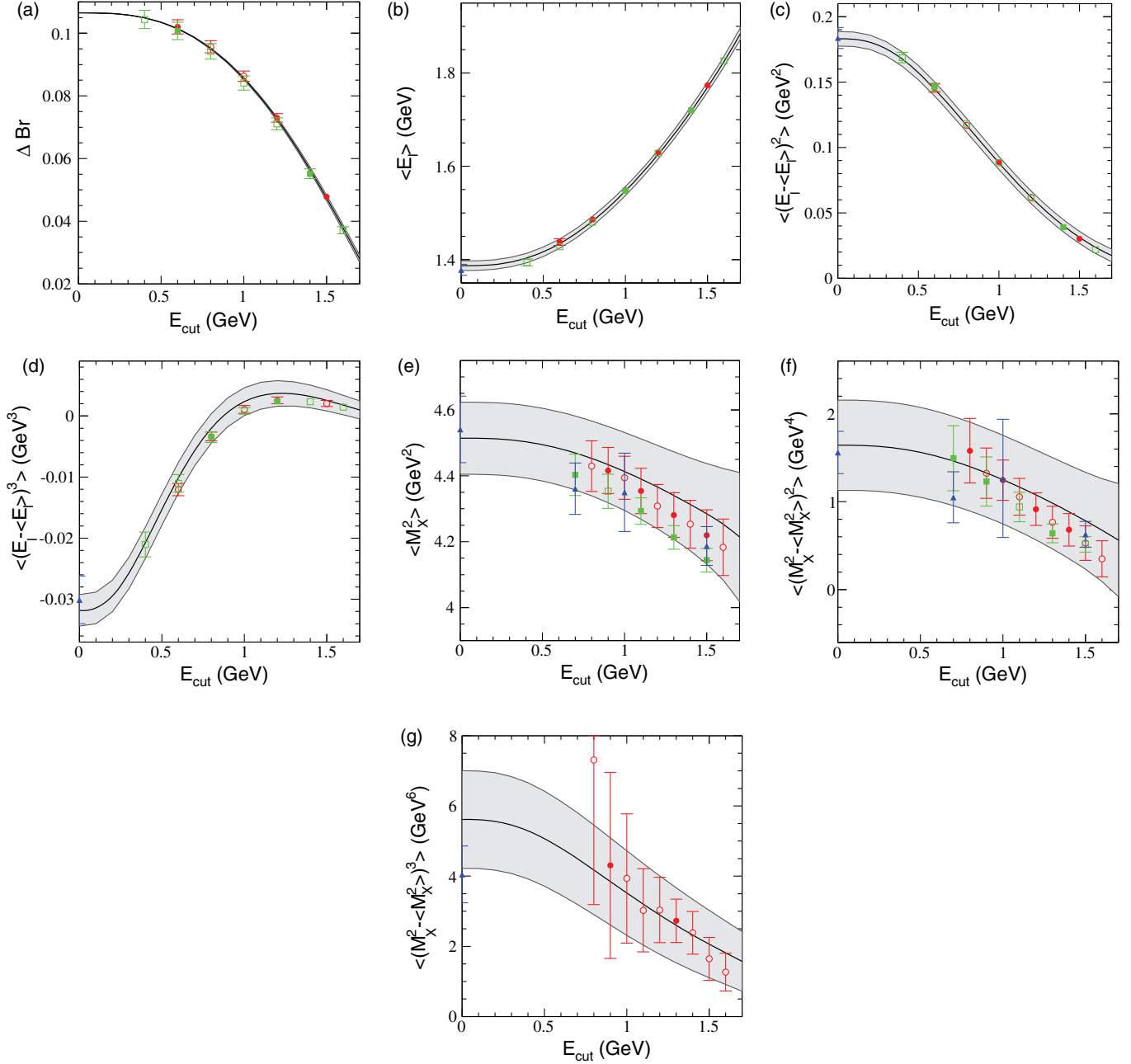


FIG. 17. Results of the global fit to the various E_ℓ and m_X moments (a)–(g) in $B \rightarrow X_c \ell \nu$ decays by [Gambino and Schwanda \(2014\)](#). The shaded bands correspond to the theoretical uncertainty of the HQE on the moments. The measured moments are shown as circles for *BABAR*, squares for *Belle*, and triangles for *CDF*, *CLEO*, and *DELPHI*. Measurements represented by filled symbols are included in the fit, and those with open symbols are not.

is mostly due to different estimates for the theoretical uncertainties and the determination of $|V_{cb}|$ in the $1S$ scheme employs a $1/m_c$ expansion and does not include $\mathcal{O}(\alpha_s^2)$ corrections.

In this article, we choose to quote the result obtained from the latest global fit to $B \rightarrow X_c \ell \nu$ moments by [Gambino and Schwanda \(2014\)](#) as the result for $|V_{cb}|$ from inclusive decays:

$$|V_{cb}| = (42.42 \pm 0.86) \times 10^{-3}. \quad (71)$$

In the future, the precision on $|V_{cb}|$ and the HQE parameters can be further improved by calculations of higher-order

perturbative corrections to the coefficients of the HQE parameters in Eq. (59) and potentially by the inclusion of higher moments ($n = 4, 5, \dots$) in the global fit, which may improve the sensitivity to higher-order terms in the HQE.

VI. INCLUSIVE CHARMLESS SEMILEPTONIC B DECAYS

We now discuss the charmless inclusive semileptonic decays of B mesons. They involve a $b \rightarrow u$ quark transition and are thus well suited for the determination of the magnitude of the CKM matrix element $|V_{ub}|$. The main challenge in the analysis of inclusive $B \rightarrow X_u \ell \nu$ decays is that they are

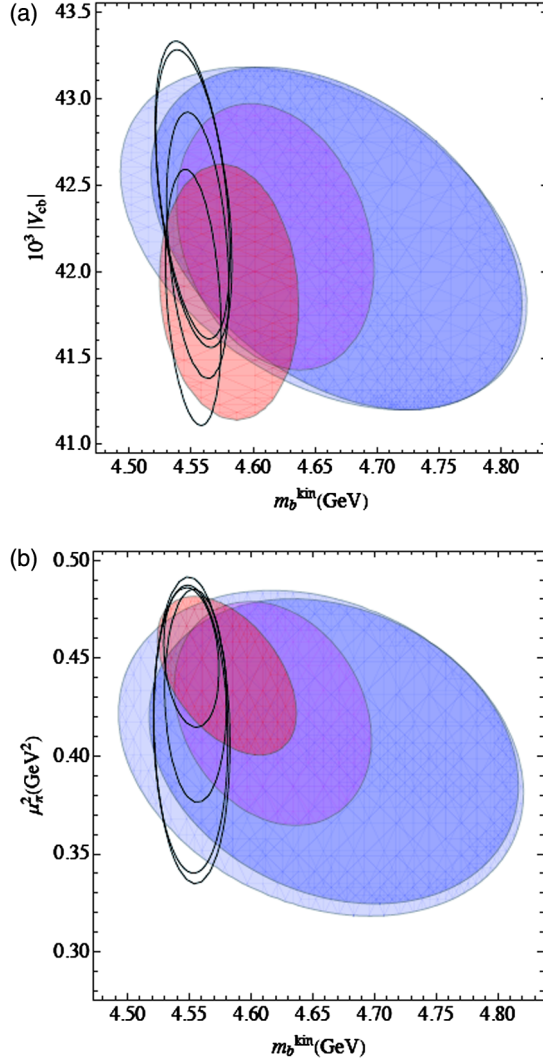


FIG. 18. $\Delta\chi^2 = 1$ contours for the $|V_{cb}|$, μ_π^2 , and m_b results of the global $B \rightarrow X_c \ell \nu$ moment fit by Gambino and Schwanda (2014). The various ellipses correspond to different scenarios for the theoretical correlations. Shaded ellipses represent the fits without m_c constraint and open ellipses those with m_c constraint; see Gambino and Schwanda (2014) for details.

suppressed by a factor of $|V_{ub}|^2/|V_{cb}|^2$, making their observation possible only in kinematic regions that are not polluted by the much more frequent $b \rightarrow c$ transitions. This fact is not only relevant for the experimental analysis, but it is also of particular relevance for the theoretical description of $B \rightarrow X_u \ell \nu$ decays, since the methods applied here differ significantly from the ones used for the $B \rightarrow X_c \ell \nu$ case.

A. Theory

The theoretical treatment of inclusive charmless semileptonic B decays could in principle follow along the same lines

as the one for inclusive $b \rightarrow c$ transitions. However, in most of the phase space $b \rightarrow u$ transitions are completely overwhelmed by $b \rightarrow c$ transitions. For this reason, the extraction of $b \rightarrow u$ transitions requires cuts on the phase space of the final state, which in most cases render the HQE as it is set up for the $b \rightarrow c$ case useless, since the final state is no longer sufficiently inclusive to apply the local OPE.

This problem can easily be illustrated by looking at the lepton energy spectrum, which extends to larger values for $b \rightarrow u$ transitions than for the $b \rightarrow c$ case. In the lepton energy window

$$\frac{1}{2m_B}(m_B^2 - m_D^2) \leq E_\ell \leq \frac{1}{2m_B}(m_B^2 - m_\pi^2) \quad (72)$$

one should find only $b \rightarrow u$ transitions. However, looking at the OPE result for the lepton energy, one finds that the actual expansion parameter is not $1/m_b$ but rather $1/m_b(1-x)$ where $x = 2E_\ell/m_b$. Thus the end point region where $x \sim 1$ cannot be described in terms of a local OPE.

This circumstance is related to the fact that close to the end point the inclusive rate is dominated by very few or even a single exclusive state, which is the physical reason for the breakdown of the OPE. In fact, this is true for the resonance region where $(1-x) \sim \Lambda^2/m_b^2$ and one has to resort to exclusive decays described in terms of form factors. If the region $0 \leq (1-x) \leq \Lambda/m_b$ is treated inclusively, one may still use an OPE, however, in a modified way, which corresponds to a partial resummation of the local OPE used for $b \rightarrow c$.

To this end, it is useful to define the so-called *shape function* (SF) (Bigi *et al.*, 1994a; Mannel and Neubert, 1994; Neubert, 1994), which is formally given by

$$2m_B f(k_+) = \langle B(v) | \bar{b}_v \delta(k_+ - iD_+) b_v | B(v) \rangle, \quad (73)$$

corresponding to the distribution of the residual b -quark momentum on the light cone. This function is universal and appears in all inclusive heavy-to-light transitions, once the end point region needs to be described. The moments of this function are related to the HQE parameters

$$f(\omega) = \delta(\omega) + \frac{\mu_G^2}{6} \delta''(\omega) - \frac{\rho_D^3}{18} \delta'''(\omega) + \dots \quad (74)$$

Equation (74) may be compared with the tree-level result for the inclusive $B \rightarrow X_s \gamma$ case obtained by applying the OPE as described in Sec. II.D,

$$\frac{d\Gamma}{dx} = \frac{G_F^2 a m_b^5}{32\pi^4} |V_{ts} V_{tb}^*|^2 |C_7|^2 \left(\delta(1-x) + \frac{\mu_\pi^2 - \mu_G^2}{2m_b^2} \delta'(1-x) + \frac{\mu_\pi^2}{6m_b^2} \delta''(1-x) + \dots \right) \quad (75)$$

with $x = 2E_\gamma/m_b$.

TABLE IX. Results of the global moment fit in the kinetic scheme by Gambino and Schwanda (2014).

Moment fit in kinetic scheme	$ V_{cb} $ (10^{-3})	m_b^{kin} (GeV)	μ_π^2 (GeV^2)	ρ_D^3 (GeV^3)	μ_G^2 (GeV^2)	ρ_{LS}^3 (GeV^3)
$B \rightarrow X_c \ell \nu + m_c$ constraint	42.42 ± 0.86	4.541 ± 0.023	0.414 ± 0.078	0.154 ± 0.045	0.340 ± 0.066	-0.147 ± 0.098

Equation (75) is instructive in various aspects. First of all it shows that the local OPE does not yield a point-by-point description of spectra, at least not in the end point regions, rather it allows for a calculation of moments of spectra, which are inclusive quantities. Furthermore, one can show that the order of derivatives of the δ function corresponds to the order in the $1/m_b$ expansion such that the terms with *leading twist*⁵ are given by

$$\frac{d\Gamma}{dx} = \frac{G_F^2 \alpha m_b^5}{32\pi^4} |V_{ts} V_{tb}^*|^2 |C_7|^2 \left[\sum_i a_i \left(\frac{1}{m_b} \right)^i \delta^{(i)}(1-x) + \mathcal{O}\{(1/m_b)^{i+1} \delta^{(i)}(1-x)\} \right]. \quad (76)$$

Similar to deep inelastic scattering, the leading-twist terms are summed into the shape function, which is in this sense completely analogous to the parton distributions function. To this end, the leading-twist expression for the inclusive decay $B \rightarrow X_s \gamma$ reads

$$\frac{d\Gamma}{dx} = \frac{G_F^2 \alpha m_b^6}{32\pi^4} |V_{ts} V_{tb}^*|^2 |C_7|^2 f(m_b(1-x)). \quad (77)$$

One effect of this resummation is that the spectrum now becomes a smooth function that extends to the physical end point of the spectrum, which is determined by the B -meson mass and not by the b -quark mass. Thus the typical width of $f(\omega)$ has to be $\bar{\Lambda} = m_B - m_b$, moving the end point of the spectrum from $m_b/2$ to $m_B/2$.

The shape function is universal and thus appears also for inclusive charmless semileptonic B decays. The leading-twist expression for the triple differential decay rate can be written as

$$\frac{d^3\Gamma}{dP_+ dP_- dE_\ell} = \frac{G_F^2 |V_{ub}|^2}{192\pi^3} \int d\omega C(P_+, P_-, E_\ell, \omega) f(\omega) + \mathcal{O}\left(\frac{\Lambda_{\text{QCD}}}{m_b}\right), \quad (78)$$

where C is a perturbatively calculable function and $f(\omega)$ is the shape function.

Although the moments of $f(\omega)$ are given in terms of the HQE parameters, the shape function is a source of uncertainty in this approach, in particular, if phase space regions are considered in which the full nonperturbative form of $f(\omega)$ is needed. Despite this, information on the shape function can be extracted from all heavy-to-light processes, so in practical terms the information from $B \rightarrow X_s \gamma$ and $B \rightarrow X_u \ell \nu$ is combined. There are attempts of a data-driven determination of the shape function similar to fits of parton distribution functions, for instance in [Bernlochner et al. \(2013\)](#).

Subleading shape functions have also been investigated ([Bauer, Luke, and Mannel, 2002, 2003](#); [Beneke et al., 2005](#)). However, there are a large number of subleading functions,

which again have moments that can be related to matrix elements of local operators. Nevertheless, the simple relation between the different heavy-to-light transitions does not hold at subleading order, as different combinations of subleading functions enter the different decays. For phenomenological use the subleading functions can only be modeled.

The usual procedure is to parametrize the shape function using the parameter $\bar{\Lambda}$ and the HQE parameters, in particular, μ_π^2 . From Eq. (74) we infer that the zeroth moment is the normalization of $f(\omega)$, while the first moment vanishes, which is compatible with the equation of motion for a static quark. The construction of the static limit from QCD requires one to pick a definition for the heavy-quark mass, which is usually the pole mass. Choosing a different definition changes the equation of motion for the static quark, rendering the first moment of the shape function nonzero; this moment becomes $\delta m = m_b^{\text{pole}} - m_b$, where m_b is the mass definition used in the QCD Lagrangian.

Perturbative corrections also induce a nonvanishing first moment, which can be used to define a scheme for the quark mass, called the SF scheme ([Bosch et al., 2004](#)). To this end, one defines $m_b^{\text{SF}} = m_b^{\text{pole}} - \delta m^{\text{pert}}$, where δm^{pert} are the perturbatively calculated contributions to the first moment. This scheme also yields a short-distance mass, which is used in the context of inclusive charmless semileptonic B decays, where shape functions are employed.

Extractions of $|V_{ub}|$ are performed using the work by Bosch, Lange, Neubert, and Paz (BLNP) ([Lange, Neubert, and Paz, 2005](#)) and by Gambino, Giordano, Ossala, and Uraltsev (GGOU) ([Gambino et al., 2007](#)). These approaches are model independent. Model-dependent methods are also considered, among which the dressed gluon exponentiation (DGE) ([Andersen and Gardi, 2006](#)) is often used.

BLNP uses the kinematic region in which $P_+ \ll P_-$ [see Eq. (14)] and includes the resummation of Sudakov logarithms to next-to-next-to-leading (NNL) logarithmic order. The perturbative expansion of C includes the α_s corrections, treating m_b in the shape function scheme. The effects of subleading shape functions are modeled and included.

GGOU treats both kinematic regions $P_+ \ll P_-$ and $P_+ \sim P_-$ and computes the coefficient C to order α_s , but also includes the $\mathcal{O}(\beta_0 \alpha_s)$ terms. The perturbative expansion in this approach is performed in the kinetic scheme, and subleading shape function effects are also included.

Finally, DGE constructs a model for the shape function starting from the structure of the perturbative result. The perturbative part includes the summation of Sudakov logarithms, while the nonperturbative part uses the perturbative renormalon structure to model this contribution.

In both BLNP and GGOU, the remaining uncertainties can be estimated and are comparable, resulting in an extraction of $|V_{ub}|$ with a relative uncertainty of 5%–10%. DGE is to some extent model dependent, but was claimed to be able to perform an estimate of the uncertainty which is comparable to the two other approaches.

A new approach has been advertised which combines the advantages of BLNP and GGOU ([Ligeti, Stewart, and Tackmann, 2008](#)). This is achieved by an improved treatment of the shape function, which is expanded in terms of properly

⁵The nomenclature is borrowed from the one in deep inelastic scattering and it is in fact in one-to-one correspondence, once one identifies shape functions with parton distribution functions.

chosen basis functions. One will be able to further improve the determination of $|V_{ub}|$ using these new basis functions in a combined fit to $B \rightarrow X_s \gamma$ and $B \rightarrow X_u \ell \bar{\nu}$.

B. Measurements

1. Measurement of partial branching fractions

Charmless semileptonic B decays were first observed by CLEO (Bartelt *et al.*, 1993) in the lepton momentum spectrum above the $B \rightarrow X_c \ell \nu$ kinematic end point of 2.3 GeV. Subsequently, several analyses of $B \rightarrow X_u \ell \nu$ decays were performed by Belle, BABAR, and CLEO, using both untagged and tagged data samples.

In untagged analyses, the signal must be extracted in a very restricted region of phase space not populated by $B \rightarrow X_c \ell \nu$ background due to the low signal-to-background ratio. Most of the untagged analyses extract the signal in the region of high lepton momenta. However, as the HQE does not converge properly in this part of phase space the theoretical predictions needed to determine $|V_{ub}|$ are affected by large uncertainties. It has thus been tried to push the minimum lepton momentum requirement down as low as possible. In the existing untagged analyses, the minimum lepton momentum is 1.9 GeV or higher, corresponding to signal acceptances of up to $\sim 30\%$. Because of the steeply increasing $B \rightarrow X_c \ell \nu$ background, the extension of an untagged analysis to much lower momenta is difficult, as the uncertainty related to the subtraction of the $B \rightarrow X_c \ell \nu$ background becomes too large. Backgrounds can be further reduced by reconstructing the neutrino from the missing energy and momentum in the event (Aubert *et al.*, 2005).⁶ However, this comes at the expense of a lower signal efficiency and additional systematic uncertainties from the modeling of sources of missing momentum (imperfect track and cluster reconstruction, additional undetected particles, etc.).

Figure 19 presents the electron momentum spectrum of the most precise end point analysis, performed by BABAR on a data sample of 80.4 fb^{-1} (Aubert *et al.*, 2006c). In this analysis, an event sample with a well-defined electron is selected. This sample contains background contributions from continuum events and $B\bar{B}$ production. The latter consists mostly of $B \rightarrow X_c \ell \nu$ decays, but also hadronic decays contribute, where the electron comes from the misidentification of a hadron or from a secondary decay [$D \rightarrow K \ell \nu$, $J/\psi \rightarrow \ell^+ \ell^-$, or $\Upsilon(2S) \rightarrow \ell^+ \ell^-$]. The relative contributions of the $B \rightarrow X_u \ell \nu$ signal, continuum, and $B\bar{B}$ background are determined in a fit to the on- and off-resonance data. The shapes of the electron momentum spectrum are obtained from simulation for $B \rightarrow X_u \ell \nu$ and $B\bar{B}$ background and are parametrized for the continuum background. An OPE calculation (De Fazio and Neubert, 1999) of the electron momentum spectrum is used for the signal shape and known contributions

⁶This analysis is based on a reconstruction of the neutrino. With the knowledge of the neutrino momentum, the squared four-momentum transfer in the decay $q^2 = (P_\ell + P_\nu)^2$ can be calculated. The signal is extracted in a region of the two variables p_ℓ^* and s_h^{max} , where s_h^{max} is the maximum kinematically allowed value of m_X^2 for given p_ℓ^* and q^2 .

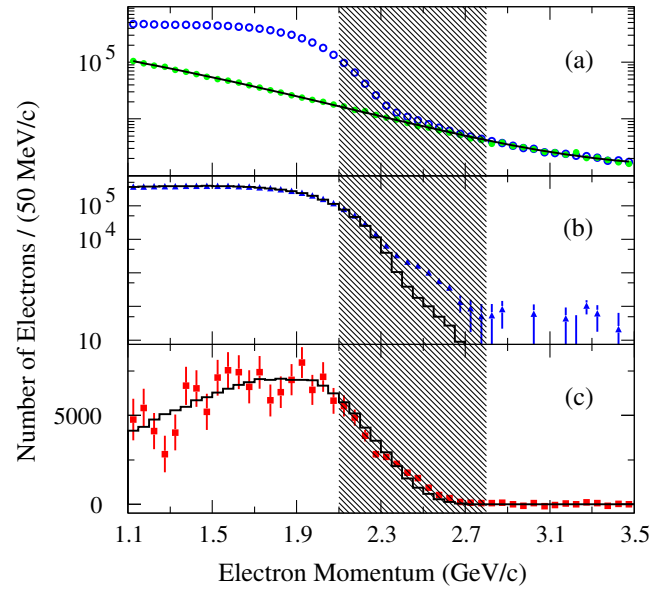


FIG. 19. Electron momentum distribution in the $\Upsilon(4S)$ frame for the BABAR untagged $B \rightarrow X_u \ell \nu$ end point analysis. The distribution is shown for three stages of the analysis: (a) on-resonance data (open circles) and off-resonance data (filled circles). The line shows the parametrization of the continuum background fit to off-resonance data and to on-resonance data above 2.8 GeV, (b) continuum-subtracted on-resonance data (triangles) and $B\bar{B}$ background (histogram), and (c) on-resonance data after subtraction of all backgrounds (squares) compared with the simulated $B \rightarrow X_u \ell \nu$ signal (histogram). The hatched band illustrates the region that is combined into a single bin in the signal fit. From Aubert *et al.*, 2006c.

from charmless resonances are added. As can be seen in Fig. 19, the simulated signal spectrum does not perfectly match the observed data spectrum after subtraction of all backgrounds. To reduce sensitivity to the detailed modeling of the signal shape, the on-resonance data are combined into a single bin for $2.1 < p_\ell^* < 2.8 \text{ GeV}$. The selected signal sample contains about 40 000 events, and a partial branching fraction of $\Delta\mathcal{B}(B \rightarrow X_u \ell \nu) = (0.572 \pm 0.041_{\text{stat}} \pm 0.051_{\text{syst}}) \times 10^{-3}$ is measured. The dominant uncertainty is due to the subtraction of the $B \rightarrow X_c \ell \nu$ background. The total branching fraction can be obtained from $\mathcal{B}(B \rightarrow X_u \ell \nu) = \Delta\mathcal{B}/f_u$, where f_u is the fraction of the electron spectrum that lies within the selected momentum interval. The factor f_u is determined from the BLNP calculation combined with shape function parameters obtained from HQE fits to inclusive $B \rightarrow X_c \ell \nu$ and $B \rightarrow X_s \gamma$ decays. The result for the total branching fraction is

$$\mathcal{B}(B \rightarrow X_u \ell \nu) = (2.27 \pm 0.26_{\text{exp}}^{+0.33} \pm 0.17_{\text{th}}) \times 10^{-3}, \quad (79)$$

where the first uncertainty is experimental, the second is due to the shape function parameters, and the third is the theoretical uncertainty of the HQE.

With the large data samples at the B factories, hadronic-tag $B \rightarrow X_u \ell \nu$ measurements have become feasible. The hadronic

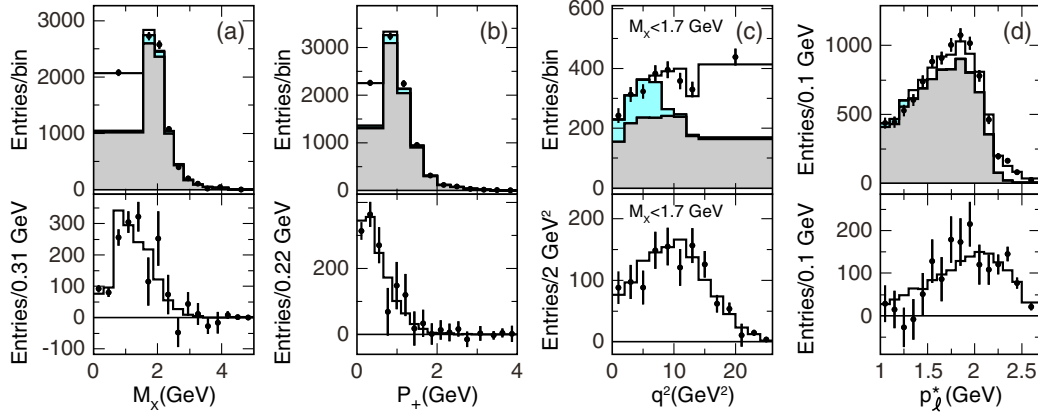


FIG. 20. Measured distributions of (a) m_X , (b) P_+ , (c) q^2 for $m_X < 1.7$ GeV, and (d) p_ℓ^* for the *BABAR* hadronic-tag $B \rightarrow X_u \ell \nu$ analysis. Upper row: Comparison of the data with a fit of the simulated $B \rightarrow X_u \ell \nu$ signal (open histogram) and background (gray, shaded histogram) shapes to data. Lower row: Comparison of the background-subtracted data distributions with the fitted simulated signal distributions (histograms). From *Lees et al., 2012c*.

final state X_u is reconstructed from the sum of all detected particles in the event that are not associated with the B_{tag} or the lepton candidate. Hadronic-tag analyses allow for a precise reconstruction of hadronic variables, such as m_X or P_+ , or the squared momentum transfer in the decay q^2 . The signal yield is rather low, $\mathcal{O}(1000)$ events for the Belle or *BABAR* data sets, but the measured fraction of phase space is large (up to 90%), which significantly reduces the theoretical uncertainties. Combinatorial background is subtracted using the sideband of the m_{bc} distribution of the B_{tag} candidate. Background from $B \rightarrow X_c \ell \nu$ decays can be reduced by vetoing kaons in the reconstructed hadronic final state, as kaons are often produced in charm-meson decays. A veto against slow pions, which are a characteristic signature of D^* decays ($D^* \rightarrow D\pi$), is also frequently imposed. Events with missing particles (in addition to the neutrino) are reduced by requiring that M_{miss}^2 is consistent with zero. The M_{miss}^2 requirement also rejects poorly reconstructed events and hence improves the resolution of the hadronic variables. The normalizations of the signal and the $B \rightarrow X_u \ell \nu$ background are determined in a fit to various kinematic variables. The fits to the m_X , P_+ , q^2 , and p_ℓ^* distributions for the most recent hadronic-tag analysis by *BABAR* (*Lees et al., 2012c*) are shown in Fig. 20.

Using the hadronic-tag samples, partial branching fractions have been measured for different kinematic regions:

- $m_X < 1.55(1.7)$ GeV: Because of the larger mass of the charm quark compared to the up quark, the masses of charmless hadronic final states are significantly lower than for charm final states. The lightest charm meson is the D meson with a mass of $m_D = 1.87$ GeV. Selecting events with $m_X < m_D$ (taking the experimental mass resolution into account) significantly enhances the signal-to-background ratio. However, in the low- m_X region, nonperturbative corrections are kinematically enhanced and make theoretical predictions of partial rates less reliable.
- $m_X < 1.7$ GeV and $q^2 > 8$ GeV²: The requirement on q^2 enhances the relative $B \rightarrow X_u \ell \nu$ contribution, which tends to have higher q^2 values than $B \rightarrow X_c \ell \nu$ decays.

The combined requirement on m_X and q^2 restricts the decay kinematics to the part of the small- m_X region, where $P_+ \sim P_-$ (see Sec. VI.A). In this case, the HQE in terms of local operators can be used again (*Bauer, Ligeti, and Luke, 2001*).

- $P_+ < 0.66$ GeV: $B \rightarrow X_u \ell \nu$ decays have smaller values of P_+ than $B \rightarrow X_c \ell \nu$. Unfortunately, the variable P_+ is very sensitive to reconstruction effects and modeling of the detector resolution.
- $p_\ell^* > 1.3$ GeV: The minimum lepton momentum requirement in hadronic-tag analyses can be lowered much further than in untagged analyses due to the overall much lower background. In the *BABAR* analysis (*Lees et al., 2012c*) the precision of $|V_{ub}|$ is studied for various p_ℓ^* requirements between 1.0 and 2.4 GeV and the smallest total uncertainty is found for $p_\ell^* > 1.3$ GeV.

The latest hadronic-tag analyses by Belle (*Urquijo et al., 2010*) and *BABAR* (*Lees et al., 2012c*) use a two-dimensional fit to the $m_X - q^2$ distribution to measure the partial branching fractions. They cover 80%–90% of the phase space. Figure 21 shows the fit projections in m_X and q^2 for the Belle analysis. The leading systematic uncertainties come from the shape function and the b -quark mass, which have an impact on the simulated signal shapes.

Table X gives an overview of the hadronic-tag $B \rightarrow X_u \ell \nu$ analyses. The relative sizes of the partial branching fractions $\Delta\mathcal{B}$ give some indication of the fraction of phase space covered in each measurement. It is useful to have results from several measurements in various kinematic regions and based on different techniques to test the theoretical predictions of kinematic distributions and to cross-check the experimental results.

2. Determination of $|V_{ub}|$

The CKM parameter $|V_{ub}|$ can be determined from the measured partial branching fraction $\Delta\mathcal{B}$ in combination with a theoretical prediction of the partial rate $\Delta\zeta_{\text{th}} = \Delta\Gamma_{\text{th}}/|V_{ub}|^2$ for the same phase space region according to

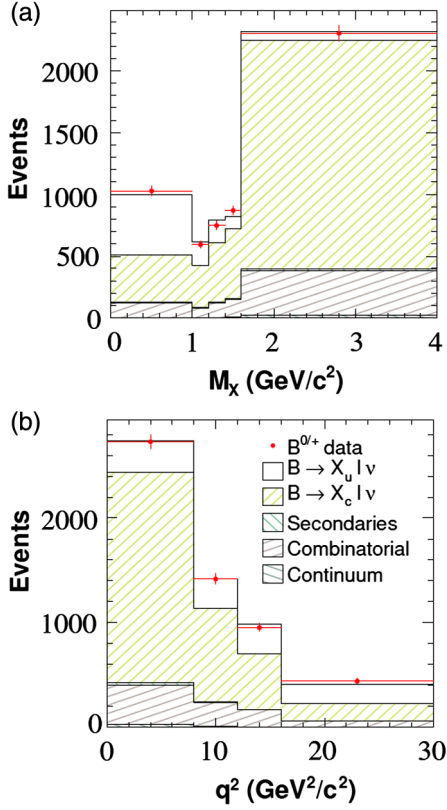


FIG. 21. Projections of measured distributions in (a) m_X and (b) q^2 for the Belle hadronic-tag $B \rightarrow X_u \ell \nu$ analysis (Urquijo *et al.*, 2010). The observed distributions are compared with the result of a two-dimensional fit of the simulated $B \rightarrow X_u \ell \nu$ signal and background to data.

$$|V_{ub}| = \sqrt{\frac{\Delta\mathcal{B}}{\tau_B \Delta\zeta_{\text{th}}}}, \quad (80)$$

where τ_B is the mean B -meson lifetime. Results for $|V_{ub}|$ have been determined for each of the three QCD calculations presented in Sec. VI.A (BLNP, DGE, and GGOU) and are shown in Table X (Amhis *et al.*, 2014). The $|V_{ub}|$ values obtained from the different experiments and in different regions of phase space show good agreement. The consistency between the QCD calculations is also very good. This gives confidence in the validity of the theoretical predictions, in spite of the difficulties involved in their calculation for restricted phase space regions. The most recent hadronic-tag analyses, which cover almost the full phase space, show reduced theoretical uncertainties compared with the kinematically restricted measurements. They have smaller relative systematic uncertainties than the untagged measurements due to much lower background.

A breakdown of the individual uncertainties on $|V_{ub}|$ presented by the Heavy Flavor Averaging Group (HFAG) (Amhis *et al.*, 2014) is given in Table XI for the GGOU result. The uncertainty due to the HQE parameters is dominated by the uncertainty on m_b . The value of m_b used as input to the $|V_{ub}|$ determination is taken from the global $B \rightarrow X_c \ell \nu$ moment fit in the kinetic scheme (see Sec. V.B.1). Another significant source of uncertainty is due to the fact that the calculated $B \rightarrow X_u \ell \nu$ decay rate does not include contributions from weak annihilation, which is discussed in Sec. X.B. Furthermore, the theoretical uncertainty depends on higher-order perturbative and nonperturbative corrections, the functional forms of the leading and subleading shape functions and the matching of scales, and differs for the various QCD calculations.

TABLE X. Partial branching fraction ($\Delta\mathcal{B}$) and $|V_{ub}|$ results from HFAG (Amhis *et al.*, 2014) for various measurements and three QCD calculations (BLNP, DGE, and GGOU). The uncertainties on $\Delta\mathcal{B}$ are statistical and systematic, and those on $|V_{ub}|$ are experimental and theoretical. The values of the HQE parameters used as input for the $|V_{ub}|$ determination are $m_b^{\text{SF}} = 4.569 \pm 0.023 \pm 0.018$ GeV, $\mu_{\pi}^{2,\text{SF}} = 0.145 \pm 0.089^{+0.020}_{-0.040}$ for BLNP (SF scheme), $m_b^{\text{MS}} = 4.177 \pm 0.043$ GeV for DGE ($\overline{\text{MS}}$ scheme), and $m_b^{\text{kin}} = 4.541 \pm 0.023$, $\mu_{\pi}^{2,\text{kin}} = 0.414 \pm 0.078$ for GGOU (kinetic scheme). They were obtained from a global fit to $B \rightarrow X_c \ell \nu$ moments in the kinetic scheme with translation from the kinetic to the SF and $\overline{\text{MS}}$ schemes.

Experiment	Selection	$\Delta\mathcal{B}$ (10^{-4})	$ V_{ub} $ (10^{-3})		
			BLNP	DGE	GGOU
Untagged analyses					
CLEO (Bornheim <i>et al.</i> , 2002)	$2.2 < p_{\ell}^* < 2.6$ GeV	$0.33 \pm 0.02 \pm 0.07$	$4.28 \pm 0.50^{+0.31}_{-0.36}$	$3.90 \pm 0.45^{+0.26}_{-0.28}$	$4.21 \pm 0.49^{+0.23}_{-0.33}$
Belle (Limosani <i>et al.</i> , 2005)	$1.9 < p_{\ell}^* < 2.6$ GeV	$0.85 \pm 0.04 \pm 0.15$	$4.93 \pm 0.46^{+0.27}_{-0.29}$	$4.85 \pm 0.45^{+0.21}_{-0.25}$	$4.93 \pm 0.46^{+0.17}_{-0.22}$
BABAR (Aubert <i>et al.</i> , 2006c)	$2.0 < p_{\ell}^* < 2.6$ GeV	$0.57 \pm 0.04 \pm 0.05$	$4.54 \pm 0.26^{+0.27}_{-0.33}$	$4.34 \pm 0.25^{+0.23}_{-0.25}$	$4.50 \pm 0.26^{+0.18}_{-0.25}$
BABAR (Aubert <i>et al.</i> , 2005)	$p_{\ell}^* > 2.0, s_h^{\text{max}} > 3.5$ GeV ²	$0.44 \pm 0.04 \pm 0.04$	$4.53 \pm 0.22^{+0.33}_{-0.38}$	$4.17 \pm 0.20^{+0.28}_{-0.29}$...
Hadronic-tag analyses					
BABAR (Lees <i>et al.</i> , 2012c)	$m_X < 1.55$ GeV	$1.08 \pm 0.08 \pm 0.06$	$4.30 \pm 0.20^{+0.28}_{-0.27}$	$4.53 \pm 0.21^{+0.24}_{-0.22}$	$4.29 \pm 0.20^{+0.21}_{-0.22}$
BABAR (Lees <i>et al.</i> , 2012c)	$m_X < 1.7$ GeV	$1.15 \pm 0.10 \pm 0.08$	$4.04 \pm 0.22^{+0.23}_{-0.23}$	$4.26 \pm 0.24^{+0.26}_{-0.24}$	$4.09 \pm 0.23^{+0.18}_{-0.19}$
BABAR (Lees <i>et al.</i> , 2012c)	$m_X < 1.7$ GeV, $q^2 > 8$ GeV ²	$0.68 \pm 0.06 \pm 0.04$	$4.30 \pm 0.23^{+0.26}_{-0.28}$	$4.27 \pm 0.22^{+0.20}_{-0.20}$	$4.32 \pm 0.23^{+0.27}_{-0.30}$
BABAR (Lees <i>et al.</i> , 2012c)	$P_+ < 0.66$	$0.98 \pm 0.09 \pm 0.08$	$4.15 \pm 0.25^{+0.28}_{-0.27}$	$4.24 \pm 0.26^{+0.37}_{-0.32}$	$4.24 \pm 0.26^{+0.32}_{-0.32}$
BABAR (Lees <i>et al.</i> , 2012c)	$p_{\ell}^* > 1.3$ GeV	$1.53 \pm 0.13 \pm 0.14$	$4.32 \pm 0.27^{+0.20}_{-0.21}$	$4.44 \pm 0.27^{+0.15}_{-0.14}$	$4.41 \pm 0.27^{+0.10}_{-0.12}$
BABAR (Lees <i>et al.</i> , 2012c)	$m_X - q^2$ (2-dim. fit)	$1.80 \pm 0.13 \pm 0.15$	$4.32 \pm 0.24^{+0.19}_{-0.21}$	$4.46 \pm 0.24^{+0.13}_{-0.13}$	$4.42 \pm 0.24^{+0.09}_{-0.11}$
Belle (Urquijo <i>et al.</i> , 2010)	$m_X - q^2$ (2-dim. fit)	$1.96 \pm 0.17 \pm 0.16$	$4.49 \pm 0.27^{+0.20}_{-0.22}$	$4.63 \pm 0.28^{+0.13}_{-0.13}$	$4.60 \pm 0.27^{+0.10}_{-0.11}$
HFAG average (Amhis <i>et al.</i> , 2014)			$4.45 \pm 0.16^{+0.21}_{-0.22}$	$4.52 \pm 0.16^{+0.15}_{-0.16}$	$4.51 \pm 0.16^{+0.12}_{-0.15}$

TABLE XI. Breakdown of systematic uncertainties on the $|V_{ub}|$ average from HFAG (Amhis *et al.*, 2014) for the GGOU calculation.

Source of uncertainty	Uncertainty on $ V_{ub} $ (%)
Statistical	± 1.9
Experimental (detector)	± 1.7
$B \rightarrow X_c \ell \nu$ modeling	± 1.3
$B \rightarrow X_u \ell \nu$ modeling	± 1.9
HQE parameters	± 1.6
Higher-order corrections	± 1.5
q^2 modeling	± 1.4
Weak annihilation	$+0.0, -2.0$
Shape function parametrization	± 0.2
Total experimental (including modeling)	± 3.4
Total theoretical (including HQE parameter)	$+2.7, -3.3$
Total	$+4.3, -4.7$

The $|V_{ub}|$ results given in Table X do not include NNLO corrections. Greub, Neubert, and Pecjak (2010) presented a partial calculation of the NNLO corrections to the leading term in the $1/m_b$ expansion of the partial decay rate within the BLNP framework. Their result suggests that the NNLO contributions could have a significant impact on the $|V_{ub}|$ determination, leading to an increase of $\sim 8\%$ with respect to the $|V_{ub}|$ value obtained with the BLNP calculation at NLO. As the NNLO corrections are dominated by contributions of order $\alpha_S^2 \beta_0$, which are already included in the GGOU and DGE calculations, no significant change in $|V_{ub}|$ for GGOU or DGE is expected.

The HQE-based calculation by Bauer, Ligeti, and Luke (2001) can be used together with the measurements based on combined m_X and q^2 requirements (Kakuno *et al.*, 2004; Aubert *et al.*, 2006a; Lees *et al.*, 2012c), as this kinematic region is less affected by nonperturbative contributions to the shape functions. The result for $|V_{ub}|$ is somewhat larger but still consistent (at the $\sim 1\sigma$ level) with those obtained from the other calculations in the same phase space region.

Since the results for all QCD calculations are very similar and have comparable total uncertainties, we quote the arithmetic mean of the HFAG averages for the three theoretical predictions as the main $|V_{ub}|$ result from inclusive decays in this article:

$$|V_{ub}| = (4.49 \pm 0.16_{\text{exp-0.18th}})^{+0.16} \times 10^{-3}. \quad (81)$$

The current precision on $|V_{ub}|$ from inclusive decays is about 5%.

VII. EXCLUSIVE SEMILEPTONIC B DECAYS TO CHARM MESONS

The decays $B \rightarrow D \ell \nu$ and $B \rightarrow D^* \ell \nu$ into ground-state charm mesons are the most frequent semileptonic decays of the B meson. The determination of $|V_{cb}|$ from these decays involves theoretical predictions of the hadronic form factors and serves as an independent cross-check of the $|V_{cb}|$ determination with inclusive decays. In this section, we first introduce the relevant form factor calculations and then turn to the measurements of semileptonic B decays to D , D^* , and excited charm states. We present the status of $|V_{cb}|$

determinations from these decays and discuss how well we understand the composition of the total $B \rightarrow X_c \ell \nu$ rate.

A. Theory

Exclusive semileptonic B decays into charm mesons are overall under very good theoretical control, since the leading contribution may be obtained from the infinite-mass limit for both the b and c quarks. Using the normalization of the form factors at zero recoil ($v_B = v_{D^{(*)}}$), one may extract a precise value of $|V_{cb}|$ from these decays. In addition, heavy-quark symmetries constrain also the form factors for decays into excited states.

1. $B \rightarrow D \ell \nu$ and $B \rightarrow D^* \ell \nu$

We first consider the decays into the ground-state charm mesons D and D^* , which make up more than 70% of the inclusive rate. These two mesons constitute the lowest-lying spin-symmetry doublet, since a spin rotation of the charm quark rotates the D into a D^* (see Sec. II.D). Using the form factor definitions in Eq. (22) of Sec. II.C, we obtain for the $B \rightarrow D \ell \nu$ differential decay rate

$$\begin{aligned} \frac{d\Gamma(B \rightarrow D \ell \nu)}{dw} &= \frac{G_F^2}{48\pi^3} |V_{cb}|^2 (m_B + m_D)^2 m_D^3 (w^2 - 1)^{3/2} |\eta_{\text{EW}} \mathcal{G}(w)|^2, \end{aligned} \quad (82)$$

where the form factor \mathcal{G} is given by

$$\mathcal{G}(w) = h_+(w) - \frac{m_B - m_D}{m_B + m_D} h_-(w). \quad (83)$$

The factor η_{EW} represents the electroweak corrections discussed below and $w = v_B v_D$ is the scalar product of the four-velocities.

Because of heavy-quark symmetries, the form factor \mathcal{G} is normalized at $w = 1$, since $h_+(1) = 1$ and $h_-(1) = 0$. To obtain a precision determination of $|V_{cb}|$, corrections to the normalization of \mathcal{G} and information on the shape of \mathcal{G} to extrapolate to the kinematic point $w = 1$ must be considered.

From the form of \mathcal{G} given in Eq. (83) it is clear that the corrections to the normalization of \mathcal{G} will be of the order of $1/m_c$, since $h_-(1) = \mathcal{O}(1/m_c)$. To this end, it has been argued that the determination of $|V_{cb}|$ from $B \rightarrow D^* \ell \nu$ decays is more precise, since in this case the corrections to the normalization turn out to be $\mathcal{O}(1/m_c^2)$.

Aside from the nonperturbative power corrections, there are electroweak as well as QCD perturbative corrections. The QED corrections also involve photon radiation off the charged lepton and hence cannot be lumped into the form factor. The main contributions are the corrections involving the large logarithm $\ln(M_W^2/m_b^2)$, which can be expressed as a multiplicative factor η_{EW} appearing in Eq. (82). These corrections turn out to be small (Sirlin, 1982),

$$\eta_{\text{EW}} = 1.007, \quad (84)$$

and are present in all semileptonic decays.

The QCD correction at the zero-recoil point $w = 1$ has been investigated in detail, using lattice QCD simulations and the

heavy-quark limit. Lattice simulations yield (Bailey *et al.*, 2015b)

$$\mathcal{G}(1) = 1.054 \pm 0.008, \quad (85)$$

while the estimates based on HQE methods yield a slightly lower central value (Uraltsev, 2004)

$$\mathcal{G}(1) = 1.04 \pm 0.02. \quad (86)$$

The w dependence of $G(w)$ must be assumed to extrapolate to the point $w = 1$. The maximum value of w is 1.62 for the $B \rightarrow D$ mode, so one could consider a linear extrapolation

$$\mathcal{G}(w) = \mathcal{G}(1)[1 - \rho_D^2(w-1) + \dots], \quad (87)$$

where ρ_D^2 is the slope parameter. However, the data are more precise and require the inclusion of higher terms of this expansion.

Since form factors are subject to constraints from unitarity and analyticity, a different expansion has been suggested, which is based on a parameter z (Boyd, Grinstein, and Lebed, 1995; Caprini and Neubert, 1996),

$$z = \frac{\sqrt{w+1} - \sqrt{2}}{\sqrt{w+1} + \sqrt{2}}, \quad (88)$$

motivated by a conformal mapping used in the discussion of analytical properties of the form factors. A frequently used expansion is the one proposed by Caprini, Lellouch, and Neubert (1998),

$$\mathcal{G}(w) = \mathcal{G}(1)[1 - 8\rho_D^2 z + (51\rho_D^2 - 10)z^2 - (252\rho_D^2 - 84)z^3], \quad (89)$$

which relates all higher derivatives of $\mathcal{G}(w)$ to the slope parameter ρ_D . The values quoted below are extracted using this parametrization.

Recent lattice calculations by the HPQCD (Na *et al.*, 2015) and FNAL and MILC (Bailey *et al.*, 2015b) Collaborations also provide values of $\mathcal{G}(w)$ for $w > 1$. They make use of model-independent expansions in z , the so-called BCL parametrization (Bourrely, Caprini, and Lellouch, 2009) (see Sec. VIII.A.1 for details) and a similar expansion called the BGL parametrization (Boyd, Grinstein, and Lebed, 1995).

A similar treatment is used for $B \rightarrow D^* \ell \nu$. The differential decay rate as a function of w is given by

$$\frac{d\Gamma(B \rightarrow D^* \ell \nu)}{dw} = \frac{G_F^2 m_B^5}{48\pi^3} |V_{cb}|^2 (w^2 - 1)^{1/2} P(w) |\eta_{EW} \mathcal{F}(w)|^2, \quad (90)$$

where $P(w)$ is a phase space factor,

$$P(w) = r^3 (1-r)^2 (w+1)^2 \left(1 + \frac{4w}{w+1} \frac{1-2rw+r^2}{(1-r)^2} \right) \quad (91)$$

with $r = m_{D^*}/m_B$. The form factor $\mathcal{F}(w)$ is a combination of the form factors $h_V(w)$ and $h_{A_i}(w)$ defined in Sec. II.D and is given by

$$P(w) |\mathcal{F}(w)|^2 = |h_{A_1}(w)|^2 \left\{ 2 \frac{r^2 - 2rw + 1}{(1-r)^2} \left[1 + \frac{w-1}{w+1} R_1^2(w) \right] + \left[1 + \frac{w-1}{1-r} [1 - R_2(w)] \right]^2 \right\}, \quad (92)$$

where the ratios R_1 and R_2 are given by

$$R_1(w) = \frac{h_V(w)}{h_{A_1}(w)}, \quad R_2(w) = \frac{h_{A_3}(w) + r h_{A_2}(w)}{h_{A_1}(w)}. \quad (93)$$

In the heavy-quark limit for the b and c quarks, the form factor $\mathcal{F}(w)$ is normalized to unity at $w = 1$. Furthermore, the leading nonperturbative corrections are of the order of $1/m_c^2$ (Luke, 1990).

The ratios R_1 and R_2 are both unity in the heavy-quark limit for the b and c quarks (see Sec. II.D), independent of w . Estimates of the w dependence at finite quark masses yield only a weak dependence, so for many practical purposes R_1 and R_2 can be taken as approximately constant. However, fits indicate significant deviations from the value obtained in the heavy-quark limit, and hence the w dependence is taken into account for precision measurements.

The value of $\mathcal{F}(1)$ has been estimated using various approaches. Lattice QCD simulations compute the deviation of this form factor from unity and obtain for finite quark masses (Bailey *et al.*, 2014)

$$\mathcal{F}(1) = 0.906 \pm 0.013, \quad (94)$$

while estimates using QCD sum rules at zero recoil tend to yield a smaller value (Gambino, Mannel, and Uraltsev, 2010, 2012),

$$\mathcal{F}(1) = 0.86 \pm 0.03. \quad (95)$$

The sum rule used by Gambino, Mannel, and Uraltsev (2010) yields an upper bound $\mathcal{F}(1) \leq 0.92$, which is only marginally higher than the lattice value.

Finally, for the extrapolation to $w = 1$, one again uses a parametrization of the form factor based on the conformal variable z defined in Eq. (88). A frequently used parametrization is the one introduced by Caprini, Lellouch, and Neubert (1998),

$$\mathcal{F}(w) = \mathcal{F}(1)[1 - 8\rho_{A_1}^2 z + (53\rho_{A_1}^2 - 15)z^2 - (231\rho_{A_1}^2 - 91)z^3], \quad (96)$$

where ρ_{A_1} is the slope parameter of the form factor h_{A_1} .

2. Semileptonic B decays to excited charm mesons

Treating the charm quark as heavy, the excited states can be classified using the heavy-quark spin symmetry. In the limit $m_c \rightarrow \infty$, all charm hadrons fall into spin-symmetry doublets, which are related by the rotation of the heavy-quark spin. The heavy-quark spin decouples in this limit, which means that the total angular momentum of the light degrees of freedom in the heavy hadron j_{light} becomes a good quantum number.

The lowest-lying excited states are the states with one unit of angular momentum, which can be coupled to the spin of the light quark to either $j_{\text{light}} = 1/2$ or $3/2$. Thus one expects to

see an almost degenerate pair of states with quantum numbers $J^P = 0^+$ and 1^+ and another almost degenerate pair with 1^+ and 2^+ . The decays into these states have been investigated in some detail (Colangelo, Nardulli, and Paver, 1992; Leibovich *et al.*, 1998); the general expressions involve a significant number of new form factors, however, they are reduced in the heavy-quark limit for both b and c quarks. Similar to the ground states, there is only a single form factor for each spin-symmetry doublet $\tau_{1/2}(w)$ and $\tau_{3/2}(w)$ describing these decays. Not much is known about these form factors; heavy-quark symmetries do not supply their normalizations, nor any information on their w dependence. Sum rule estimates have been performed for these form factors and have led to simulations for the decay rates, which are still quite uncertain (Colangelo, Nardulli, and Paver, 1992).

B. Measurements

1. $B \rightarrow D\ell\nu$

The measurement of $B \rightarrow D\ell\nu$ decays is challenging because of the large background from $B \rightarrow D^*\ell\nu$ decays, where the slow pion from the $D^* \rightarrow D\pi$ decay has not been detected (“down-feed background”). Combinatorial background from wrongly reconstructed D candidates also contributes. For this reason, the much cleaner tagged measurements are more promising than untagged measurements for this decay mode.

The $B \rightarrow D\ell\nu$ decay has been measured by ALEPH (Buskalic *et al.*, 1997a), CLEO (Bartelt *et al.*, 1999), Belle (Abe *et al.*, 2002; Glattauer *et al.*, 2016), and BABAR (Aubert *et al.*, 2009d, 2010c). The currently most precise results come from the new hadronic-tag analysis by Belle (Glattauer *et al.*, 2016). The previously most precise results come from a hadronic-tag measurement (Aubert *et al.*, 2010c) and a global

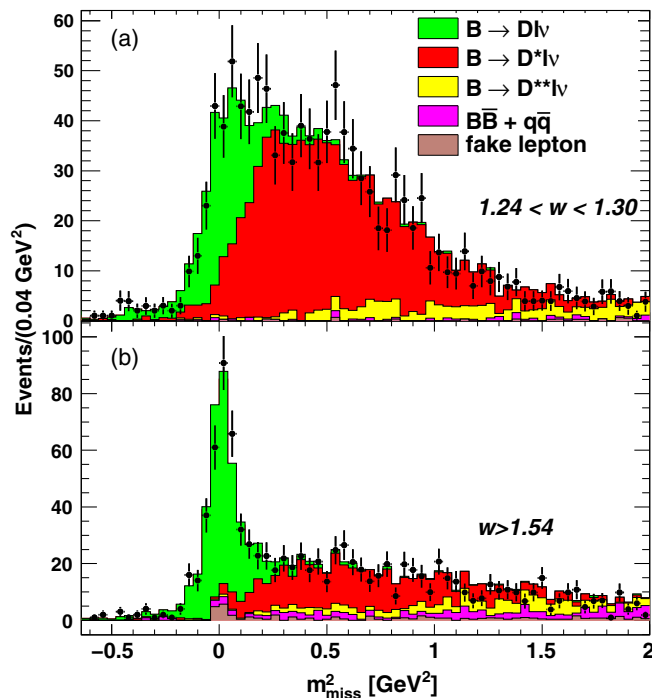


FIG. 22. Distribution of M_{miss}^2 from the hadronic-tag $B \rightarrow D\ell\nu$ analysis by BABAR, for two w intervals. From Aubert *et al.*, 2010c.

analysis of $B \rightarrow D^{(*)}\ell\nu$ decays (Aubert *et al.*, 2009d) by BABAR. The latter is discussed in Sec. VII.B.2. In the hadronic-tag measurements by BABAR and Belle, the decays of both neutral and charged B mesons $B^0 \rightarrow D^-\ell^+\nu$ and $B^+ \rightarrow \bar{D}^0\ell^+\nu$ are studied. The D meson is reconstructed in a large number of decay modes (see, e.g., Table III). The signal yields are determined in a fit to the M_{miss}^2 distribution. The fit is performed in ten bins of w to measure the w dependence of the form factor $\mathcal{G}(w)$.

The M_{miss}^2 distribution from BABAR is shown in Fig. 22 for two different w intervals. Figure 23(a) presents the resulting w spectrum after correcting for reconstruction efficiency. The product $\eta_{\text{EW}}\mathcal{G}(1)|V_{cb}|$ in Eq. (82) and the form factor slope parameter ρ_D^2 are determined with a fit of the parametrization in Eq. (89) to this spectrum. Together with a prediction for the form factor at $w=1$, the product $\eta_{\text{EW}}\mathcal{G}(1)|V_{cb}|$ can be

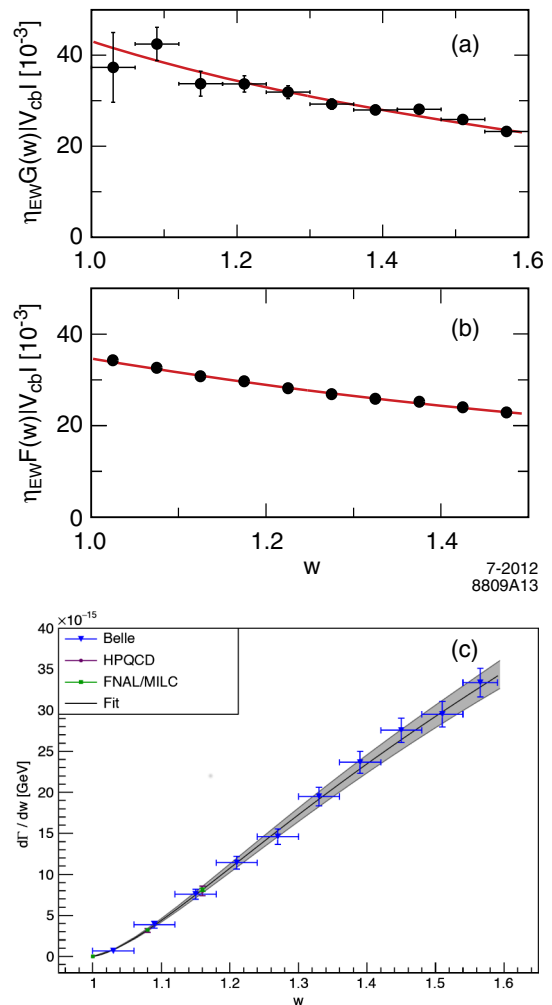


FIG. 23. Dependence of the form factor on w for the BABAR analysis of (a) $B \rightarrow D\ell\nu$ (Aubert *et al.*, 2010c) and (b) $B \rightarrow D^*\ell\nu$ (Aubert *et al.*, 2008b) decays. The distributions have been corrected for reconstruction efficiency. The results of a fit to the w distributions are shown as lines. In (c), the differential width of $B \rightarrow D\ell\nu$ for the Belle hadronic-tag analysis (Glattauer *et al.*, 2016) and the result of the combined fit of the BGL form factor parametrization to the experimental and lattice QCD (FNAL-MILC and HPQCD) data is shown.

TABLE XII. Results of $B \rightarrow D\ell\nu$ and $B \rightarrow D^*\ell\nu$ measurements and the current HFAG averages (Amhis *et al.*, 2014). The branching fractions are quoted for B^0 decays, also for the cases where B^+ decays were measured or both B^+ and B^0 measurements were combined using isospin relations. The uncertainties are statistical and systematic. If only one uncertainty is quoted, it corresponds to the total uncertainty.

$B \rightarrow D\ell\nu$	\mathcal{B} (%)	$\eta_{\text{EW}}\mathcal{G}(1) V_{cb} $ (10^{-3})	ρ_D^2
CLEO untagged (Bartelt <i>et al.</i> , 1999)	$2.19 \pm 0.16 \pm 0.35$	$44.88 \pm 5.96 \pm 3.25$	$1.27 \pm 0.22 \pm 0.12$
Belle untagged (Abe <i>et al.</i> , 2002)	$2.08 \pm 0.12 \pm 0.52$	$40.96 \pm 4.39 \pm 5.03$	$1.12 \pm 0.19 \pm 0.11$
BABAR hadronic tag (Aubert <i>et al.</i> , 2010c)	$2.14 \pm 0.11 \pm 0.08$	$42.45 \pm 1.88 \pm 1.02$	$1.18 \pm 0.09 \pm 0.06$
BABAR global fit (Aubert <i>et al.</i> , 2009d)	$2.16 \pm 0.03 \pm 0.13$	$43.25 \pm 0.80 \pm 2.07$	$1.20 \pm 0.04 \pm 0.06$
HFAG average (Amhis <i>et al.</i> , 2014)	$2.13 \pm 0.03 \pm 0.09$	$42.65 \pm 0.72 \pm 1.35$	$1.19 \pm 0.04 \pm 0.04$
Belle hadronic tag (Glattauer <i>et al.</i> , 2016)	$2.31 \pm 0.03 \pm 0.11$	42.29 ± 1.37	1.09 ± 0.05
$B \rightarrow D^*\ell\nu$	\mathcal{B} (%)	$\eta_{\text{EW}}\mathcal{F}(1) V_{cb} $ (10^{-3})	$\rho_{D^*}^2$
CLEO untagged (Briere <i>et al.</i> , 2002)	$5.62 \pm 0.18 \pm 0.26$	$39.94 \pm 1.23 \pm 1.63$	$1.37 \pm 0.09 \pm 0.09$
Belle untagged (Dungel <i>et al.</i> , 2010)	$4.56 \pm 0.03 \pm 0.26$	$34.60 \pm 0.17 \pm 1.02$	$1.21 \pm 0.03 \pm 0.01$
BABAR untagged $B^0 \rightarrow D^{*-}\ell^+\nu$ (Aubert <i>et al.</i> , 2008b)	$4.54 \pm 0.04 \pm 0.25$	$33.94 \pm 0.30 \pm 0.99$	$1.19 \pm 0.05 \pm 0.03$
BABAR untagged $B^+ \rightarrow \bar{D}^{*0}\ell^+\nu$ (Aubert <i>et al.</i> , 2008d)	$4.97 \pm 0.07 \pm 0.34$	$35.22 \pm 0.59 \pm 1.33$	$1.13 \pm 0.06 \pm 0.06$
BABAR global fit (Aubert <i>et al.</i> , 2009d)	$4.95 \pm 0.02 \pm 0.20$	$35.76 \pm 0.20 \pm 1.10$	$1.19 \pm 0.02 \pm 0.06$
HFAG average (Amhis <i>et al.</i> , 2014)	$4.93 \pm 0.01 \pm 0.11$	$35.81 \pm 0.11 \pm 0.44$	$1.21 \pm 0.02 \pm 0.02$

translated to a value for $|V_{cb}|$. The statistical precision decreases toward small values of w , as the $B \rightarrow D\ell\nu$ differential decay rate is proportional to ρ_D^2 and is thus suppressed at small w . This makes the extrapolation to $w = 1$ more difficult and limits the precision of the $|V_{cb}|$ determination.

An overview of the $B \rightarrow D\ell\nu$ branching fraction $\eta_{\text{EW}}\mathcal{G}(1)|V_{cb}|$ and ρ_D^2 results from various experiments is given in Table XII. The current HFAG average (Amhis *et al.*, 2014) yields

$$\rho_D^2 = 1.19 \pm 0.05,$$

$$\eta_{\text{EW}}\mathcal{G}(1)|V_{cb}| = (42.65 \pm 1.53) \times 10^{-3}. \quad (97)$$

The χ^2 probability of this combination is close to 100%, indicating that the uncertainties on the measurements may be overestimated.

The new hadronic-tag result from Belle has not yet been included in the average. It yields a value of $\eta_{\text{EW}}\mathcal{G}(1)|V_{cb}| = (42.29 \pm 1.37) \times 10^{-3}$ that is consistent with the HFAG average but more precise, and a value of $\rho_D^2 = 1.09 \pm 0.05$ from a fit of the parametrization by Caprini and Neubert (1996) to the w spectrum. Recent lattice data at $w > 1$ also allow for a combined fit to measured data and lattice results. In the new Belle analysis such a fit is performed using the BGL parametrization and the lattice results from FNAL and MILC (Bailey *et al.*, 2015b) and HPQCD (Na *et al.*, 2015), yielding consistent results [see Fig. 23(c)].

2. $B \rightarrow D^*\ell\nu$

The decay $B \rightarrow D^*\ell\nu$ has a larger branching fraction than $B \rightarrow D\ell\nu$ due to the additional helicity degrees of freedom for

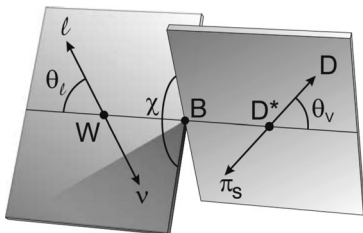


FIG. 24. The helicity angles θ_ℓ , θ_ν , and χ in the decay $B \rightarrow D^*\ell\nu$, $D^* \rightarrow D\pi$.

the vector D^* meson as compared to the pseudoscalar D meson. It was measured by BABAR (Aubert *et al.*, 2008b, 2008d, 2009d), Belle (Dungel *et al.*, 2010), CLEO (Briere *et al.*, 2002), ALEPH (Buskulic *et al.*, 1997a), DELPHI (Abreu *et al.*, 2001; Abdallah *et al.*, 2004), and OPAL (Abbiendi *et al.*, 2000). Compared to $B \rightarrow D\ell\nu$ decays, there is significantly less down-feed background from higher-mass charm states. In addition, the reconstruction of the D^* meson via its characteristic decay into a D meson and a slow pion allows for an effective reduction of combinatorial background.

A precise determination of the w spectrum at small values is important for the extrapolation to $w = 1$ needed to determine $|V_{cb}|$. However, the reconstruction efficiency of the slow pion at small D^* momenta is low in the B -factory experiments, limiting the precision at low w .⁷

The measurements by CLEO and the LEP experiments as well as the first B -factory analyses of $B \rightarrow D^*\ell\nu$ decays determined the product $\eta_{\text{EW}}\mathcal{F}(1)|V_{cb}|$ and the form factor slope parameter $\rho_{D^*}^2$ by measuring the differential decay rate $d\Gamma/dw$ as a function of w . They relied on external measurements of $R_1(1)$ and $R_2(1)$. The fully differential decay distribution gives access to the complete set of form factor parameters for $B \rightarrow D^*\ell\nu$ decays. The first analysis that measured $R_1(1)$, $R_2(1)$, and $\rho_{D^*}^2$ was performed by CLEO (Duboscq *et al.*, 1996). The parameters $R_1(1)$, $R_2(1)$, $\rho_{D^*}^2$, and $\eta_{\text{EW}}\mathcal{F}(1)|V_{cb}|$ were determined in a fit to one-dimensional projections of the differential decay distribution in four variables: w and the three helicity angles θ_ℓ , θ_ν , and χ . The helicity angles are defined as follows (see Fig. 24):

- θ_ℓ is the angle between the directions of the lepton in the virtual W rest frame and the virtual W in the B rest frame.
- θ_ν is the angle between the directions of the D in the D^* rest frame and the D^* in the B rest frame.
- χ is the angle between the W and D^* decay planes.

Belle and BABAR have subsequently published measurements of the branching fraction and form factor parameters of

⁷The measurements of the LEP experiments suffer from a poorer w resolution due to the larger average B momentum, but have a reconstruction efficiency that varies only moderately with w .

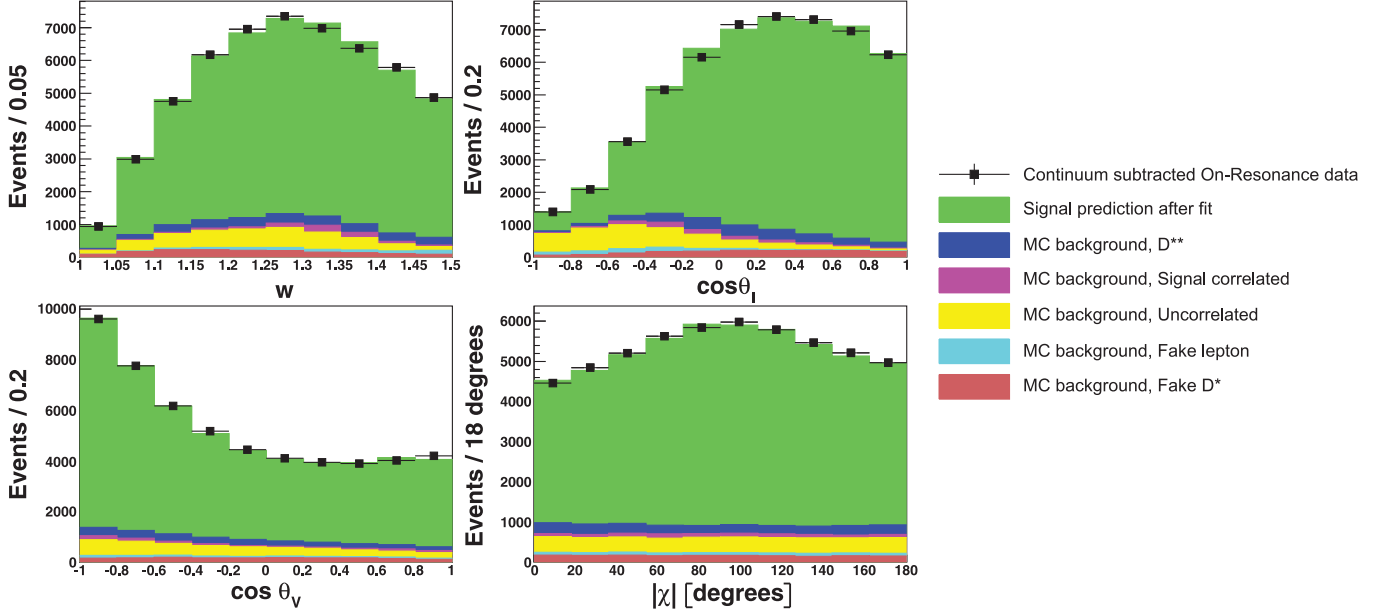


FIG. 25. Distributions of the velocity transfer w , the cosine of the angles θ_ℓ and θ_ν , and the magnitude of the angle χ for the Belle analysis of $B^0 \rightarrow D^{*-}\ell^+\nu$ decays. From [Dungel et al., 2010](#).

$B^0 \rightarrow D^{*-}\ell^+\nu$ decays ([Aubert et al., 2008b](#); [Dungel et al., 2010](#)) using the same approach with one-dimensional projections, but yielding significant improvements in precision. As the same events enter in all four projections, correlations need to be properly taken into account. This is done by combining separate covariance matrices for data, simulated signal, and backgrounds. The *BABAR* analysis uses a data sample of 79 fb^{-1} , while the Belle analysis uses the full Belle data set of 711 fb^{-1} . Both measurements are untagged. An electron or muon with momentum in the range $0.8\text{--}2.4 \text{ GeV}$ (Belle) or $1.2\text{--}2.4 \text{ GeV}$ (*BABAR*) is combined with a D^{*-} candidate reconstructed from the decay chain $D^{*-} \rightarrow \bar{D}^0\pi^-$, $\bar{D}^0 \rightarrow K^+\pi^-$ ($\bar{D}^0 \rightarrow K^+\pi^-, K^+\pi^-\pi^+\pi^-, K^+\pi^-\pi^0$). As the neutrino momentum is not known, the variables w , θ_ℓ , θ_ν , and χ cannot be calculated directly. Assuming massless neutrinos, the direction of the signal B momentum is constrained to a cone centered around the direction of the $Y = D^*\ell$ system (see Sec. III.C.2). The neutrino momentum can be approximated by averaging over the possible B momentum directions, yielding an estimation of w , θ_ℓ , θ_ν , and χ . The distributions of these variables from the Belle analysis are shown in Fig. 25. The background contribution is small and the distributions show a very good agreement between data and simulation.

BABAR performed another analysis of $B^0 \rightarrow D^{*-}\ell^+\nu$ decays ([Aubert et al., 2006d](#)), using a four-dimensional fit to the fully differential decay distribution $d\Gamma/dw d\cos\theta_\ell d\cos\theta_\nu d\chi$. This analysis shows an increased sensitivity to $R_1(1)$ and $R_2(1)$ and an improved precision of $|V_{cb}|$. The results of the two untagged $B^0 \rightarrow D^{*-}\ell^+\nu$ analyses from *BABAR* were combined, taking correlations into account. The combined result was reported by [Aubert et al. \(2008b\)](#). The largest uncertainties in these measurements are due to background subtraction and the uncertainties of the reconstruction efficiencies. For the latter, especially the reconstruction of the slow pion is important.

In addition to the studies of neutral B decays, *BABAR* also published a measurement of the charged B -meson decay $B^+ \rightarrow \bar{D}^{*0}\ell^+\nu$ ([Aubert et al., 2008d](#)). The neutral D^{*0} meson is reconstructed in the decay chain $D^{*0} \rightarrow D^0\pi^0$, $D^0 \rightarrow K^-\pi^+$. The reconstruction efficiency of the slow neutral pion from the D^{*0} decay differs from the one for charged pions from D^{*-} decays. Furthermore, neutral pions can be reconstructed down to lower momenta, allowing for a measurement at smaller values of w . For these reasons, the $B^+ \rightarrow \bar{D}^{*0}\ell^+\nu$ measurement represents a useful cross-check of the results obtained with $B^0 \rightarrow D^{*-}\ell^+\nu$ decays. As can be seen in Table XII, the measured $B^+ \rightarrow \bar{D}^{*0}\ell^+\nu$ branching fraction is consistent with the results obtained for neutral B mesons, taking into account isospin symmetry (see Sec. X.A).

BABAR also carried out a global analysis of $B \rightarrow DX\ell\nu$ decays ([Aubert et al., 2009d](#)). In this analysis, $D^0\ell$ and $D^+\ell$ pairs are reconstructed and a global fit to their kinematic properties is used to determine the branching fractions and form factor parameters of both $B \rightarrow D\ell\nu$ and $B \rightarrow D^*\ell\nu$ decays. Three kinematic variables are used in the fit: $\cos\theta_{BY}$, p_ℓ^* , and p_D^* . An advantage of this approach is that it does not explicitly depend on the reconstruction of the slow pion from D^* decays and its associated uncertainty. The analysis includes signal decays for which the slow pion could not be reconstructed, thus increasing the statistical precision of the measurement.

The current HFAG averages for $B \rightarrow D^*\ell\nu$ decays ([Amhis et al., 2014](#)) are

$$\begin{aligned} \rho_{D^*}^2 &= 1.21 \pm 0.03, \\ R_1(1) &= 1.41 \pm 0.03, \\ R_2(1) &= 0.85 \pm 0.02, \\ \eta_{\text{EW}}\mathcal{F}(1)|V_{cb}| &= (35.81 \pm 0.45) \times 10^{-3} \end{aligned} \quad (98)$$

with a χ^2 probability for the combination of 15%.

3. Determination of $|V_{cb}|$

The measured values of $\eta_{EW}\mathcal{G}(1)|V_{cb}|$ and $\eta_{EW}\mathcal{F}(1)|V_{cb}|$ can be combined with theoretical predictions for $\mathcal{G}(1)$ and $\mathcal{F}(1)$ to determine $|V_{cb}|$. Using the unquenched lattice QCD predictions $\mathcal{G}(1) = 1.054 \pm 0.008$ (Bailey *et al.*, 2015b) for $B \rightarrow D\ell\nu$ and $\mathcal{F}(1) = 0.906 \pm 0.013$ (Bailey *et al.*, 2014) for $B \rightarrow D^*\ell\nu$ gives

$$\begin{aligned} B \rightarrow D\ell\nu: |V_{cb}| &= (40.18 \pm 1.44_{\text{exp}} \pm 0.32_{\text{th}}) \times 10^{-3}, \\ B \rightarrow D^*\ell\nu: |V_{cb}| &= (39.25 \pm 0.49_{\text{exp}} \pm 0.56_{\text{th}}) \times 10^{-3}. \end{aligned} \quad (99)$$

Alternative form factor predictions are available from an HQE calculation for $B \rightarrow D\ell\nu$ (Uraltsev, 2004) and a QCD sum rules calculation for $B \rightarrow D^*\ell\nu$ (Gambino, Mannel, and Uraltsev, 2010). Using these predictions yields $|V_{cb}|$ values that are 1%–2% larger for $B \rightarrow D\ell\nu$ and 5% larger for $B \rightarrow D^*\ell\nu$.

The $|V_{cb}|$ results from both decay modes are compatible with each other. The experimental uncertainty for $B \rightarrow D\ell\nu$ is larger than for $B \rightarrow D^*\ell\nu$ because of the smaller branching fraction, the larger down-feed background, and the less reliable extrapolation to $w = 1$. A combination of the $|V_{cb}|$ results for both decay modes using the lattice form factors and assuming uncorrelated experimental and theoretical uncertainties gives

$$|V_{cb}| = (39.44 \pm 0.66) \times 10^{-3}. \quad (100)$$

This result is smaller than the one obtained from inclusive $B \rightarrow X_c\ell\nu$ decays; the difference corresponds to about 2.8σ . Averaging the $|V_{cb}|$ results from exclusive and inclusive measurements yields

$$|V_{cb}| = (40.54 \pm 1.46) \times 10^{-3}. \quad (101)$$

The χ^2 probability is 0.6%. Because of the marginal agreement, the uncertainty has been scaled by a factor of $\sqrt{\chi^2/\text{ndf}} = 2.8$, following the approach used by the Particle Data Group (Olive *et al.*, 2014).

4. $B \rightarrow D^{**}\ell\nu$

The charm-meson ground states D and D^* have orbital angular momentum $L = 0$. As mentioned in Sec. VII.A.2, there are orbitally excited states with $L = 1$ and masses higher than the D^* mass, which are collectively referred to as D^{**} states. An overview of the various charm-meson states is given in Fig. 26. As discussed in Sec. VII.A.2, the D^{**} states can be grouped into two doublets based on the total angular momentum of the light degrees of freedom $j_{\text{light}} = L \pm 1/2$. The states with $j_{\text{light}} = 1/2$ have spin parity $J^P = 0^+$ (D_0^*) or 1^+ (D_1^*) and decay predominantly through an S -wave transition. These resonances are broad and have widths of a few hundred MeV. The states with $j_{\text{light}} = 3/2$ have spin parity $J^P = 1^+$ (D_1) or 2^+ (D_2^*) and decay predominantly via a D -wave transition. These resonances are narrow and have widths of a few tens of MeV. The 0^+ state decays into $D\pi$, the

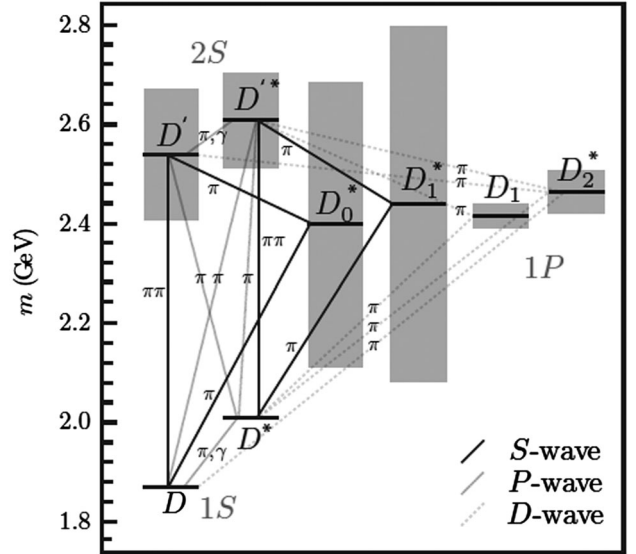


FIG. 26. Excited charm-meson states with orbital angular momentum $L = 0$ and $L = 1$. The shaded boxes indicate the widths of the resonances. The lines show the possible decays involving the emission of one or two pions. The states collectively referred to as D^{**} are $D_0^*(2400)$, $D_1^*(2430)$, $D_1(2420)$, and $D_2^*(2460)$. From Bernlochner, Ligeti, and Turczyk, 2012.

1^+ states into $D^*\pi$, and the 2^+ state can decay into both $D\pi$ and $D^*\pi$.

The experimental knowledge of $B \rightarrow D^{**}\ell\nu$ decays is still rather poor, especially for the broad D^{**} states. The narrow states D_1 and D_2^* have been observed in semileptonic B decays by Belle (Liventsev *et al.*, 2008), BABAR (Aubert *et al.*, 2008c, 2009a), CLEO (Anastassov *et al.*, 1998), ALEPH (Buskulic *et al.*, 1997b), OPAL (Abbiendi *et al.*, 2003), and D0 (Abazov *et al.*, 2005). The broad states D_0^* and D_1^* have been observed by DELPHI (Abdallah *et al.*, 2006), BABAR (Aubert *et al.*, 2008c), and Belle (Liventsev *et al.*, 2008). Table XIII summarizes the averages of $B \rightarrow D^{**}\ell\nu$ branching fraction measurements. As the branching fractions of the D^{**} mesons themselves are not well known, the product of the $B \rightarrow D^{**}\ell\nu$ and $D^{**} \rightarrow D^{(*)}\pi$ branching fractions is quoted.

Belle (Liventsev *et al.*, 2008) and BABAR (Aubert *et al.*, 2008c) performed analyses of $B \rightarrow D^{(*)}\pi\ell\nu$ decays to select $B \rightarrow D^{**}\ell\nu$ candidates with D^{**} mesons decaying to $D^{(*)}\pi$. As an example, Fig. 27 shows the results of the BABAR hadronic-tag analysis. In this analysis, the individual

TABLE XIII. HFAG averages for the branching fractions of $B \rightarrow D^{**}\ell\nu$ decays (Amhis *et al.*, 2014). The quoted branching fractions are the product of the branching fractions of the $B \rightarrow D^{**}\ell\nu$ decay and the subsequent $D^{**} \rightarrow D^{(*)}\pi$ decay (shown in parentheses). The uncertainties are the total experimental uncertainties.

Decay mode	\mathcal{B} (%)
$B^- \rightarrow D_1\ell\nu(D_1 \rightarrow D^{*+}\pi^-)$	0.285 ± 0.018
$B^- \rightarrow D_2^*\ell\nu(D_2^* \rightarrow D^{*+}\pi^-)$	0.078 ± 0.008
$B^- \rightarrow D_1^*\ell\nu(D_1^* \rightarrow D^{*+}\pi^-)$	0.13 ± 0.04
$B^- \rightarrow D_0^*\ell\nu(D_0^* \rightarrow D^+\pi^-)$	0.29 ± 0.05

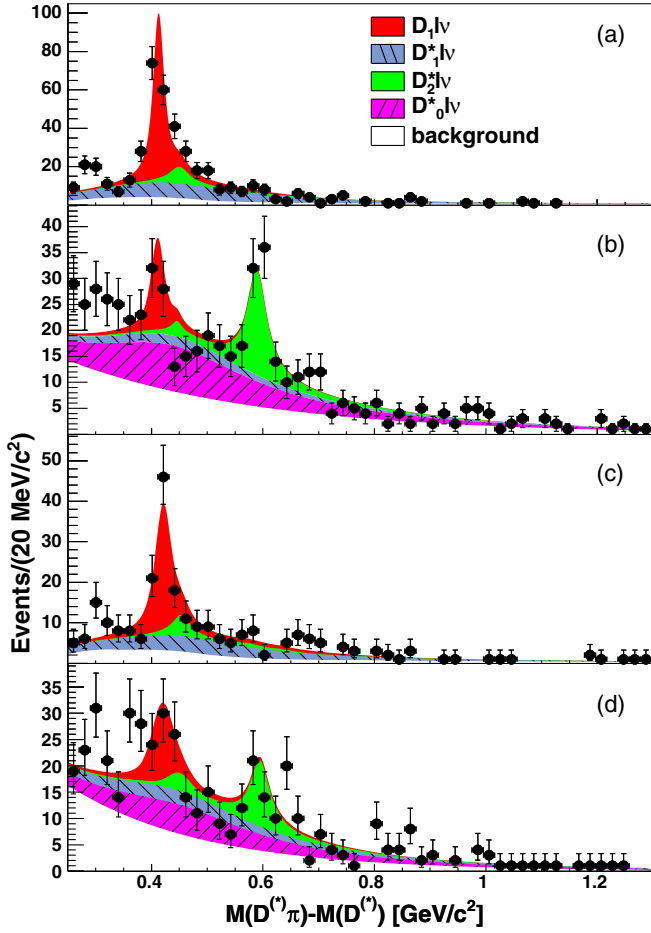


FIG. 27. Distributions of the mass difference $\Delta m = m_{D^{(*)}\pi} - m_{D^{(*)}}$ for the BABAR analysis of $B \rightarrow D^{(*)}\ell\nu$ decays in four different final states: (a) $B^- \rightarrow D^{*+}\pi^-\ell^-\bar{\nu}$, (b) $B^- \rightarrow D^+\pi^-\ell^-\bar{\nu}$, (c) $\bar{B}^0 \rightarrow D^{*0}\pi^+\ell^-\bar{\nu}$, and (d) $\bar{B}^0 \rightarrow D^0\pi^+\ell^-\bar{\nu}$. From [Aubert et al., 2008c](#).

$B \rightarrow D^{**}\ell\nu$ yields are extracted in a simultaneous fit of the simulated signal to the distribution of $\Delta m = m_{D^{(*)}\pi} - m_{D^{(*)}}$ for the four possible $D^{(*)}\pi$ combinations: $D^{*+}\pi^-$, $D^+\pi^-$, $D^{*0}\pi^+$, and $D^0\pi^+$. While the narrow states are clearly visible in the data, the contribution from the broad states is much more difficult to constrain experimentally.

From the theoretical side, the orbitally excited states are described in the heavy-mass limit for both the c and the b quarks by two form factors $\tau_{1/2}(w)$ and $\tau_{3/2}(w)$ (see Sec. VII.A.2). These form factors are constrained by sum rules ([Uraltsev, 2001](#)), which may be used for an estimate together with quark-model as well as lattice calculations to get some idea about the relative contributions of the various states ([Bigi et al., 2007](#)). This yields a dominance of the $j_{\text{light}} = 3/2$ states:

$$\frac{\tau_{1/2}(1)}{\tau_{3/2}(1)} \sim 0.5. \quad (102)$$

Inserting this into the decay rates predicts a significantly smaller rate for the decays to the $j_{\text{light}} = 1/2$ states compared with the ones to the $j_{\text{light}} = 3/2$ states, which is not reflected

by the present data. This constitutes one of the puzzles in the field of semileptonic decays discussed by [Bernlochner, Ligeti, and Turczyk \(2012\)](#). However, these conclusions are drawn on the basis of the heavy-mass limit. The corrections in this case are of the order Λ_{QCD}/m_c , which may significantly alter this conclusion. In particular, these corrections will lead to a mixing among the two spin-symmetry doublets, which may also alter the rates observed for the orbitally excited states.

5. Putting it all together

The branching fractions of semileptonic B decays to charm mesons are summarized in Table XIV for neutral and charged B mesons separately. A comparison of the sum of the exclusive branching fractions with the inclusive $B \rightarrow X_c\ell\nu$ branching fraction makes it clear that the observed exclusive decays do not saturate the inclusive semileptonic decay rate. For both B^0 and B^\pm decays, there is a missing component that amounts to about 15% of the inclusive decay rate. This missing component seems to be too large to be accounted for by nonresonant decays, which have not yet been observed. The contributions from higher-mass resonant states, such as orbitally excited charm states with $L = 2$ or radially excited states (e.g., the $2S$ states labeled D' and D'^* in Fig. 26) that decay into $D^{(*)}\pi$ are still unknown and need to be determined in the future. BABAR recently presented results of a measurement of $B \rightarrow D^{(*)}\pi^-\ell\nu$ and $B \rightarrow D^{(*)}\pi^+\pi^-\ell\nu$ decays ([Lees et al., 2016](#)). The resulting $B \rightarrow D^{(*)}\pi\pi\ell\nu$ branching fraction accounts for almost half of the gap between the inclusive and the sum of exclusive branching fractions.

VIII. EXCLUSIVE CHARMLESS SEMILEPTONIC B DECAYS

The determination of $|V_{ub}|$ from exclusive charmless semileptonic B decays has experimental and theoretical uncertainties that are independent of those for inclusive $B \rightarrow X_u\ell\nu$ decays. The most promising decay mode for determining $|V_{ub}|$, both experimentally and theoretically, is $B \rightarrow \pi\ell\nu$. The corresponding measurements and form factor calculations are discussed in this section. We also briefly summarize the

TABLE XIV. Comparison of inclusive and exclusive $B \rightarrow X_c\ell\nu$ branching fractions, based on the current HFAG averages ([Amhis et al., 2014](#)).

Decay mode	$\mathcal{B}(B^0)$ (%)	$\mathcal{B}(B^\pm)$ (%)
$B \rightarrow D\ell\nu$	2.19 ± 0.12	2.27 ± 0.11
$B \rightarrow D^*\ell\nu$	4.93 ± 0.11	5.69 ± 0.19
$B \rightarrow D\pi^-\ell\nu$	0.42 ± 0.06	0.42 ± 0.05
$B \rightarrow D^*\pi^-\ell\nu$	0.48 ± 0.08	0.60 ± 0.06
$B \rightarrow D\pi^0\ell\nu^a$	0.21 ± 0.03	0.21 ± 0.03
$B \rightarrow D^*\pi^0\ell\nu^a$	0.24 ± 0.04	0.30 ± 0.03
Sum of exclusive decays	8.47 ± 0.20	9.49 ± 0.24
Inclusive $B \rightarrow X_c\ell\nu$	10.25 ± 0.15	11.05 ± 0.17
Missing component (incl. – excl.)	1.78 ± 0.25	1.56 ± 0.29

^a $B \rightarrow D^{(*)}\pi^0\ell\nu$ decays with a neutral pion have not been measured. The branching fractions are assumed to be half of those measured for $B \rightarrow D^{(*)}\pi^-\ell\nu$.

investigations of semileptonic B decays to other charmless mesons (π^0 , η , η' , ρ , and ω).

A. Theory

Exclusive charmless semileptonic B decays are much less constrained by heavy-quark symmetries than those with charm final states. For this reason, the information on the relevant form factors comes either from lattice QCD calculations or from QCD sum rules.

1. $B \rightarrow \pi \ell \nu$

The most precise information on the decay form factors is available for $B \rightarrow \pi \ell \nu$. In the limit of massless leptons, the differential rate for this decay depends only on a single form factor:

$$\frac{d\Gamma(B^0 \rightarrow \pi^- \ell^+ \nu)}{dq^2} = \frac{G_F^2 |V_{ub}|^2}{24\pi^3} |\vec{p}_\pi|^3 |f_{B\pi}^+(q^2)|^2, \quad (103)$$

where \vec{p}_π is the momentum of the pion in the rest frame of the B meson, and $f_{B\pi}^+$ is the form factor of the vector current [see Eq. (19)].

QCD light-cone sum rules and lattice calculations yield complementary information on the form factor. While lattice calculations are restricted to the region close to maximum momentum transfer to the leptons $q^2 \sim q_{\max}^2 = (m_B - m_\pi)^2$, QCD sum rules work best close to $q^2 \sim 0$.

QCD sum rules have been used to calculate the value of the form factor at $q^2 = 0$. A calculation including perturbative QCD corrections to order α_s (Khodjamirian *et al.*, 2011) yields

$$f_{B\pi}^+(0) = 0.281 \pm 0.033, \quad (104)$$

where the uncertainty is due to the parameters entering the QCD light-cone sum rule (Borel parameter, threshold parameter, and the parameters of the pion light-cone distribution). Further estimates of $f_{B\pi}^+(0)$ are available from Bharucha (2012) and Sentitemsu Imsong *et al.* (2015).

At the other end of the phase space, precise lattice simulations are available. Figure 28 shows the data of the lattice simulations from the HPQCD (Gulez *et al.*, 2006) and the Fermilab and MILC (Bailey *et al.*, 2009) Collaborations. The Fermilab and MILC Collaboration recently published a new calculation of the $B \rightarrow \pi \ell \nu$ form factor (Bailey *et al.*, 2015a) with a significantly reduced uncertainty. New lattice results are also available from the RBC and UKQCD Collaboration (Flynn *et al.*, 2015).

Given that the form factor is quite well known at the edges of the phase space, the remaining issue is the interpolation between these two regimes. The interpolation is performed using a specific parametrization motivated by bounds which can be obtained from analyticity and unitarity in a quantum field theory. To this end, we introduce a variable (Bourelly, Caprini, and Lellouch, 2009)

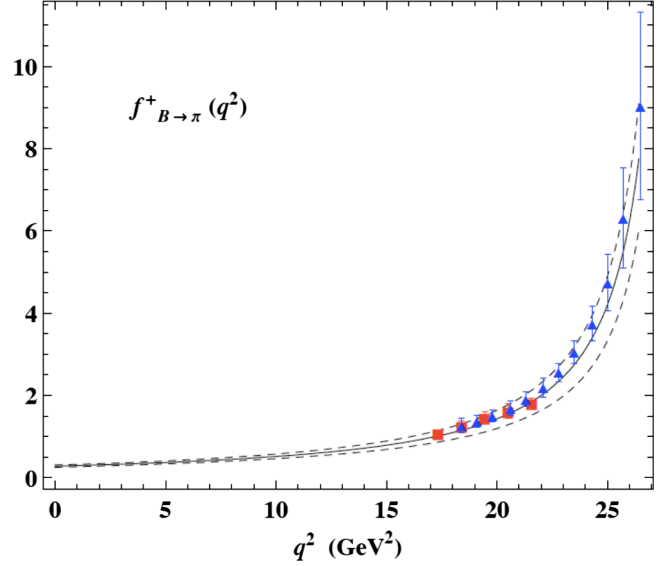


FIG. 28. The form factor $f_{B\pi}^+$ as a function of q^2 . Data points are from lattice QCD simulations; squares: HPQCD (Gulez *et al.*, 2006) and triangles: Fermilab and MILC (Bailey *et al.*, 2009). The value at $q^2 = 0$ is taken from a QCD sum rules calculation (Khodjamirian *et al.*, 2011). The interpolation uses the BCL parametrization (Bourelly, Caprini, and Lellouch, 2009).

$$z(q^2, t_0) = \frac{\sqrt{(m_B + m_\pi)^2 - q^2} - \sqrt{(m_B + m_\pi)^2 - t_0}}{\sqrt{(m_B + m_\pi)^2 - q^2} + \sqrt{(m_B + m_\pi)^2 - t_0}}, \quad (105)$$

where t_0 is an auxiliary parameter to be chosen later. This definition is analogous to the one given in Eq. (88) for heavy-to-heavy transitions.

The form factor interpolation is performed by employing the *BCL parametrization* suggested by Bourelly, Caprini, and Lellouch (2009), which is essentially a polynomial ansatz in z ,

$$f_{B\pi}^+(q^2) = \frac{1}{1 - q^2/m_{B^*}^2} \sum_{k=0}^{K-1} b_k \left[z(q^2, t_0)^k - (-1)^{k-K} \frac{k}{K} z^K \right], \quad (106)$$

where Bourelly *et al.* showed that the optimal choice for t_0 is

$$t_0^{\text{opt}} = (m_B + m_\pi)(\sqrt{m_B} - \sqrt{m_\pi})^2. \quad (107)$$

The known values of the form factor at $q^2 = 0$ and near q_{\max}^2 can be used to fit the coefficients b_k in the BCL parametrization in Eq. (106).

The lines in Fig. 28 show the interpolation obtained from the BCL parametrization. In fact, any other reasonable parametrization such as the BK parametrization (Becirevic and Kaidalov, 2000) yields a similarly good fit. Overall this means that we have sufficient control over the form factor $f_{B\pi}^+$ to perform a precise extraction of $|V_{ub}|$ from $B \rightarrow \pi \ell \nu$ decays.

2. Other charmless semileptonic modes

The form factors for other exclusive charmless semileptonic modes are much more uncertain. This is mainly due to the fact that neither QCD sum rules nor lattice QCD calculations can deal with states like the ρ or ω mesons, which are much heavier than the pion and are unstable. Although some data are available on these decays, a competitive extraction of $|V_{ub}|$ from these decays is currently not possible.

A further problem with these decays is related to the fact that the final states are unstable particles with a significant width. For this reason, the theoretical description should rather provide the full phase space distribution for $B \rightarrow \pi\pi\ell\nu$ (Faller *et al.*, 2014). First attempts to have a QCD-based phenomenological description are available (Kang *et al.*, 2014; Meißner and Wang, 2014).

B. Measurements

1. $B \rightarrow \pi\ell\nu$

The main goal of $B \rightarrow \pi\ell\nu$ analyses is a precise measurement of the branching fraction and q^2 distribution. The latter allows for a comparison of the q^2 dependence of the $B \rightarrow \pi$ form factor $f_{B\pi}^+(q^2)$ with theoretical predictions. The main experimental challenge is the reduction of the background from the much more abundant $B \rightarrow X_c\ell\nu$ decays, but also the down-feed from other $B \rightarrow X_u\ell\nu$ decays with higher-mass X_u final states.

In spite of the large background, untagged analyses have so far provided the most precise $B \rightarrow \pi\ell\nu$ results due to their statistical precision. The first untagged $B \rightarrow \pi\ell\nu$ measurement was performed by CLEO (Alexander *et al.*, 1996) using a data sample of 2.7 fb^{-1} , and was later updated with larger data samples of 10.1 fb^{-1} (Athar *et al.*, 2003) and 16.0 fb^{-1} (Adam *et al.*, 2007). Since untagged analyses need additional constraints to reduce the background, the CLEO analysis uses a neutrino-reconstruction technique in which the four-momentum of the undetected neutrino in the signal decay is inferred from the missing energy and momentum in the whole event [see Eq. (41)]. The reconstructed neutrino is then combined with a charged lepton ($\ell = e, \mu$) and a pion (π^- or π^0) to form a $B^0 \rightarrow \pi^-\ell^+\nu$ or $B^+ \rightarrow \pi^0\ell^+\nu$ candidate. *BABAR* and Belle carried out a series of untagged analyses (Ha *et al.*, 2011; del Amo Sanchez *et al.*, 2011; Lees *et al.*, 2012b) using the same neutrino-reconstruction technique with varying requirements on the quality of the reconstructed neutrino, yielding somewhat different signal-to-background ratios.

The background composition in $B \rightarrow \pi\ell\nu$ analyses varies strongly with q^2 :

- The dominant background at low q^2 is due to $e^+e^- \rightarrow q\bar{q}$ ($q = u, d, s,$ and c) continuum events, where the charged lepton originates from a semileptonic decay of a hadron (mostly produced in $e^+e^- \rightarrow c\bar{c}$) or the misidentification of a charged hadron as an electron or muon. Continuum events are rejected by applying selection criteria on event-shape variables such as $\cos \Delta\theta_T$ (see Sec. III.C.1).
- $B \rightarrow X_c\ell\nu$ decays are the largest background component overall and are most relevant at intermediate values of q^2 . They can be suppressed by selection criteria on

kinematic variables, especially those related to neutrino reconstruction: M_{miss}^2 and the polar angle of the missing momentum vector θ_{miss} . Only loose criteria are applied on the lepton and hadron momenta, as too strict criteria would bias the measurement of the q^2 spectrum.

- At high q^2 , the down-feed from nonsignal $B \rightarrow X_u\ell\nu$ decays becomes important. $B \rightarrow X_u\ell\nu$ decays have similar decay kinematics as the $B \rightarrow \pi\ell\nu$ signal and are thus difficult to reduce. They are mostly located at high q^2 since the X_u state has a higher decay multiplicity than the single pion hadronic final state. If one of the X_u decay particles is wrongly taken as the pion from the $B \rightarrow \pi\ell\nu$ candidate, it tends to have smaller momentum than expected for a signal pion and hence results in a large value of q^2 . The uncertainty on this background is sizable and limits the measurement in the region $q^2 > 20 \text{ GeV}^2$.

In the Belle and *BABAR* untagged analyses, the suppression of all backgrounds is optimized as a function of q^2 to allow for a precise measurement of the q^2 spectrum over the whole range. The $B \rightarrow \pi\ell\nu$ signal yield is extracted in a fit to the two-dimensional $m_{\text{bc}}-\Delta E$ distribution. The fit is performed in bins of q^2 to measure the shape of the q^2 spectrum. Belle uses 13 q^2 bins (Ha *et al.*, 2011), *BABAR* uses 12 bins (Lees *et al.*, 2012b) or 6 bins (del Amo Sanchez *et al.*, 2011), and CLEO uses 4 bins (Adam *et al.*, 2007). Figure 29 shows the m_{bc} and ΔE distributions in two q^2 regions for the 12-bin *BABAR* analysis.

In the CLEO and the 6-bin *BABAR* analyses, a simultaneous fit to several $B \rightarrow X_u\ell\nu$ decay modes is performed (*BABAR*: $X_u = \pi^\pm, \pi^0, \rho^\pm,$ and ρ^0 ; CLEO: $X_u = \pi^\pm, \pi^0, \eta, \eta', \rho^\pm, \rho^0,$ and ω). The simultaneous fit reduces the uncertainties due to $B \rightarrow X_u\ell\nu$ cross feed between signal modes.

The signal distributions in m_{bc} and ΔE for the untagged analyses exhibit long tails, as can be seen in Fig. 29. Therefore the signal-to-background ratio in the whole fit region is low (0.1–0.2). In a narrower region around $m_{\text{bc}} = m_B$ and $\Delta E = 0$ (“signal region”), it increases to about 0.5–1. The signal efficiencies are (7–12)% for the fit region and (2–3)% for the signal region, depending on the analysis.

Recently, a hadronic-tag analysis of $B \rightarrow \pi\ell\nu$ decays (together with several other charmless decay modes) was published by Belle (Sibidanov *et al.*, 2013), using the full $\Upsilon(4S)$ data sample of 711 fb^{-1} . *BABAR* previously published a tagged analysis (Aubert *et al.*, 2006b) on a smaller data sample of 211 fb^{-1} . The use of hadronic B tagging allows for a simpler and more precise reconstruction of the neutrino, but the lower statistical precision is a limitation, in particular, for measuring the q^2 spectrum. Because of the precise reconstruction of the neutrino kinematics, the M_{miss}^2 distribution is ideally suited for signal extraction. In the Belle analysis, the signal yields are determined in a fit to the M_{miss}^2 distribution in 13 bins of q^2 . Figure 30(a) shows the M_{miss}^2 distribution for the whole q^2 range. The signal purity in this measurement is very high and the systematic uncertainties are smaller than for the untagged measurements.

Belle and *BABAR* also performed $B \rightarrow \pi\ell\nu$ measurements with semileptonic B tags (Hokuue *et al.*, 2007; Aubert *et al.*, 2008e). The signal-to-background ratios for the

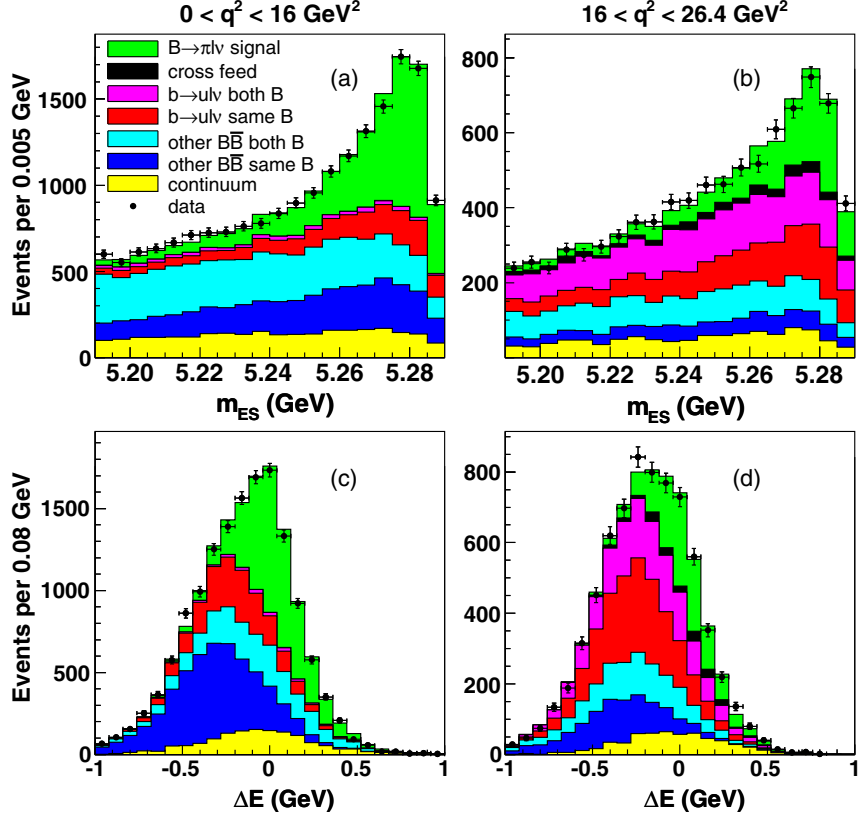


FIG. 29. Observed distributions of m_{bc} and ΔE for the untagged $B \rightarrow \pi \ell \nu$ analysis from *BABAR* (Lees *et al.*, 2012b) in two q^2 regions. The observed distributions (points) are compared with a fit of simulated signal (topmost histogram) and background (other histograms) to data.

semileptonic- and hadronic-tag $B^0 \rightarrow \pi^- \ell^+ \nu$ analyses are roughly in the range 2–3 and 5–10, respectively, for a signal efficiency of $\sim 0.2\%$ for both types of analyses. Since the analyses using different tagging methods are largely uncorrelated, they serve as complementary cross-checks of one another and can be combined.

Table XV summarizes the signal yields of the various $B \rightarrow \pi \ell \nu$ analyses, separately for neutral and charged B mesons ($B^0 \rightarrow \pi^- \ell^+ \nu$ and $B^+ \rightarrow \pi^0 \ell^+ \nu$). The branching fraction results for $B^0 \rightarrow \pi^- \ell^+ \nu$ are summarized in Table XVI. The total branching fraction as well as the partial branching fractions for $q^2 < 12$ and $q^2 > 16$ GeV^2 (the validity regions of the light-cone sum rules and lattice QCD form factor calculations) are shown. The individual measurements are generally in good agreement with each other. For $q^2 > 16$ GeV^2 , however, the difference between the 6-bin *BABAR* and the Belle analyses amounts to $\sim 2\sigma$.

A combination of all untagged $B^0 \rightarrow \pi^- \ell^+ \nu$ measurements results in an average total branching fraction of

$$B(B^0 \rightarrow \pi^- \ell^+ \nu) = (1.45 \pm 0.02_{\text{stat}} \pm 0.04_{\text{syst}}) \times 10^{-4} \quad (108)$$

with a total uncertainty of $\sim 3\%$ (Amhis *et al.*, 2014). The main systematic uncertainties in untagged $B \rightarrow \pi \ell \nu$ analyses are associated with the reconstruction of both charged and neutral particles (which affect the neutrino reconstruction) and with backgrounds from continuum events at low q^2 and $B \rightarrow X_u \ell \nu$ decays at high q^2 . Because of the down-feed from $B \rightarrow \rho \ell \nu$

decays into the $B \rightarrow \pi \ell \nu$ channels ($\rho^\pm \rightarrow \pi^\pm \pi^0$, $\rho^0 \rightarrow \pi^+ \pi^-$), the uncertainties on the $B \rightarrow \rho \ell \nu$ branching fraction and form factors are also relevant. In the hadronic-tag measurement, the systematic uncertainty is dominated by the uncertainty on the B -tagging efficiency.

2. $B \rightarrow \pi$ form factor shape

The q^2 dependence of the $B \rightarrow \pi$ form factor is determined by fitting the BCL parametrization [Eq. (106)] to the measured q^2 spectrum $\Delta B / \Delta q^2$ after correcting the spectrum for detector effects and photon radiation. The BCL parametrization with three parameters (b_0 , b_1 , and b_2) is fitted to the q^2 spectra obtained from all untagged *BABAR* and Belle measurements and the Belle hadronic-tag measurement. The results of the fit in terms of the shape parameters b_1 and b_2 , relative to the normalization parameter b_0 , are

$$\frac{b_1}{b_0} = -0.99 \pm 0.20, \quad \frac{b_2}{b_0} = -1.28 \pm 0.61. \quad (109)$$

The χ^2 probability of the fit is 3%. This relatively low probability is mainly due to the discrepancy between measurements at high q^2 discussed previously, and the rather large fluctuations in the hadronic-tag measurement.

Figure 31(b) shows a comparison of the fitted BCL parametrization with the shapes predicted by various form factor calculations. The measured shape is compatible with the light-cone sum rules and lattice QCD calculations in their

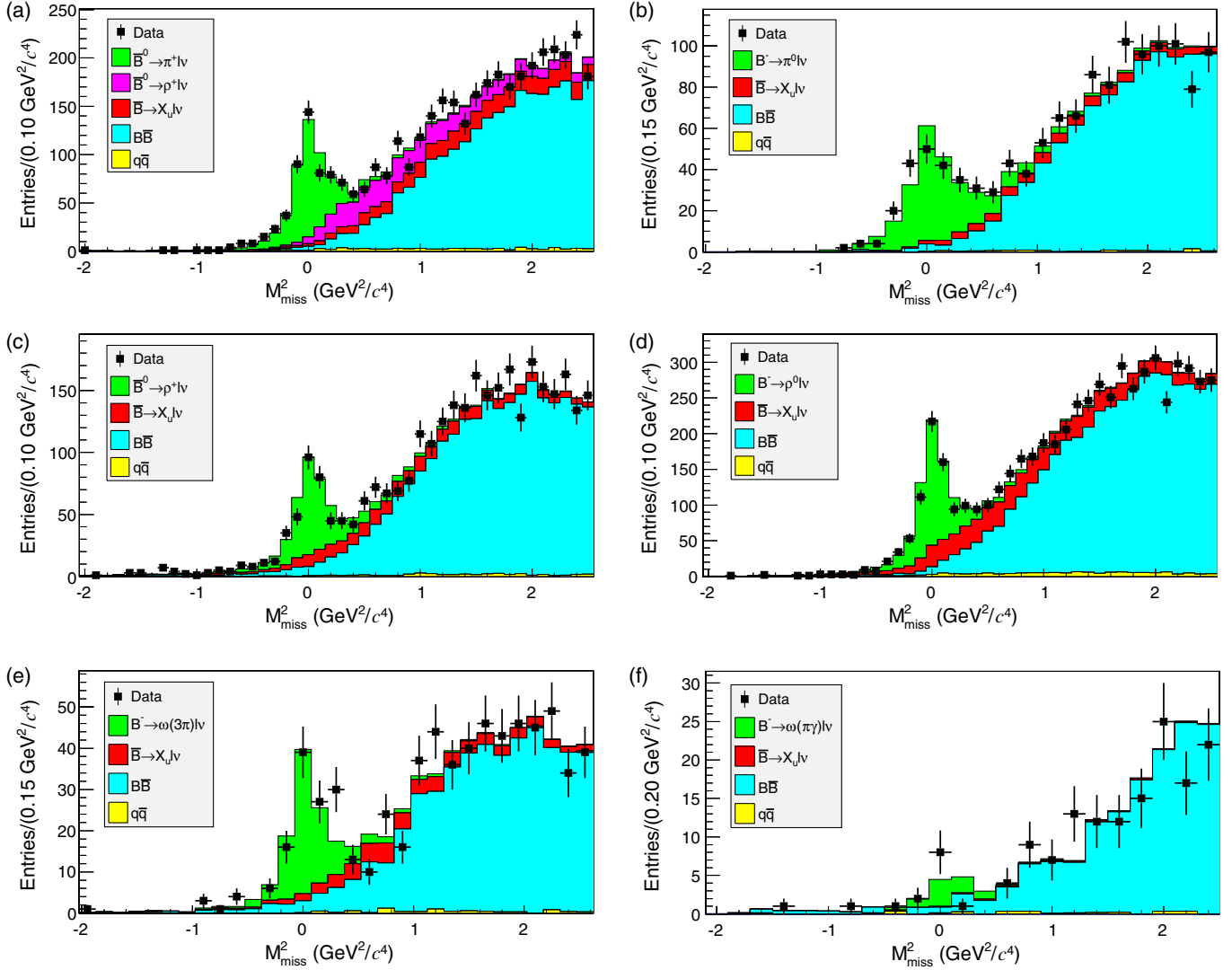


FIG. 30. Distributions of M_{miss}^2 for the hadronic-tag analysis of exclusive charmless semileptonic B decays from Belle (Sibidanov *et al.*, 2013): (a) $B^0 \rightarrow \pi^- \ell^+ \nu$, (b) $B^+ \rightarrow \pi^0 \ell^+ \nu$ with $\pi^0 \rightarrow \gamma\gamma$, (c) $B^0 \rightarrow \rho^- \ell^+ \nu$ with $\rho^- \rightarrow \pi^- \pi^0$, (d) $B^+ \rightarrow \rho^0 \ell^+ \nu$ with $\rho^0 \rightarrow \pi^- \pi^+$, (e) $B^+ \rightarrow \omega \ell^+ \nu$ with $\omega \rightarrow \pi^- \pi^+ \pi^0$, and (f) $B^+ \rightarrow \omega \ell^+ \nu$ with $\omega \rightarrow \pi^0 \gamma$. The data (points) are compared with a fit of the simulated signal (topmost histogram) and background (other histograms) distributions to data.

regions of validity. The relativistic quark model ISGW2 (Isgur *et al.*, 1989; Scora and Isgur, 1995) deviates significantly from the observed shape and can be ruled out.

The fitted BCL parametrization evaluated at $q^2 = 0$ determines the product $f_{B\pi}^+(0)|V_{ub}|$ [see Eq. (103)]:

$$f_{B\pi}^+(0)|V_{ub}| = (0.922 \pm 0.024) \times 10^{-3}. \quad (110)$$

For a given $|V_{ub}|$, this value can be compared with the light-cone sum rules prediction of $f_{B\pi}^+(0)$. Using the $|V_{ub}|$ value obtained with the sum rules calculation for the $B \rightarrow \pi \ell \nu$ average in Table XVII (see Sec. VIII.B.3), we obtain $f_{B\pi}^+(0) = (0.27 \pm 0.03)$, in good agreement with the LCSR result $f_{B\pi}^+(0) = 0.28 \pm 0.03$ (Khodjamirian *et al.*, 2011).

TABLE XV. Overview of $B \rightarrow \pi \ell \nu$ signal yields.^a

Measurement	$\int \mathcal{L} dt$ (fb ⁻¹)	$N_{\text{sig}}(B^0 \rightarrow \pi^- \ell^+ \nu)$	$N_{\text{sig}}(B^+ \rightarrow \pi^0 \ell^+ \nu)$
BABAR untagged 6 bins (del Amo Sanchez <i>et al.</i> , 2011)	349	7 181	3446
BABAR untagged 12 bins (Lees <i>et al.</i> , 2012b)	416	9 297	3204
Belle untagged (Ha <i>et al.</i> , 2011)	605	21 486	...
BABAR semileptonic tag (Aubert <i>et al.</i> , 2008e)	348	150	134
Belle semileptonic tag (Hokuue <i>et al.</i> , 2007)	253	156	69
BABAR hadronic tag (Aubert <i>et al.</i> , 2006b)	211	31	26
Belle hadronic tag (Sibidanov <i>et al.</i> , 2013)	711	463	232

^aThe CLEO analysis is omitted in the table as the exact numbers of signal events are not given in Adam *et al.* (2007).

TABLE XVI. Total and partial branching fraction results for $B^0 \rightarrow \pi^- \ell^+ \nu$ decays and their HFAG average (Amhis *et al.*, 2014). The uncertainties are statistical and systematic.

Measurement	\mathcal{B} (10^{-4})	$\Delta\mathcal{B}(q^2 < 12 \text{ GeV}^2)$ (10^{-4})	$\Delta\mathcal{B}(q^2 > 16 \text{ GeV}^2)$ (10^{-4})
CLEO untagged ^a	$1.38 \pm 0.15 \pm 0.11$	$0.69 \pm 0.12 \pm 0.07$	$0.41 \pm 0.08 \pm 0.04$
BABAR untagged 6 bins ^a	$1.41 \pm 0.05 \pm 0.08$	$0.88 \pm 0.04 \pm 0.05$	$0.32 \pm 0.02 \pm 0.03$
BABAR untagged 12 bins	$1.44 \pm 0.04 \pm 0.06$	$0.83 \pm 0.03 \pm 0.04$	$0.37 \pm 0.02 \pm 0.02$
Belle untagged	$1.48 \pm 0.04 \pm 0.07$	$0.82 \pm 0.03 \pm 0.04$	$0.40 \pm 0.02 \pm 0.02$
Belle hadronic tag	$1.49 \pm 0.09 \pm 0.07$	$0.81 \pm 0.06 \pm 0.04$	$0.45 \pm 0.05 \pm 0.02$
HFAG average	$1.45 \pm 0.02 \pm 0.04$	$0.81 \pm 0.02 \pm 0.02$	$0.38 \pm 0.01 \pm 0.01$

^aBased on a simultaneous measurement of $B^0 \rightarrow \pi^- \ell^+ \nu$ and $B^+ \rightarrow \pi^0 \ell^+ \nu$ decays using isospin symmetry.

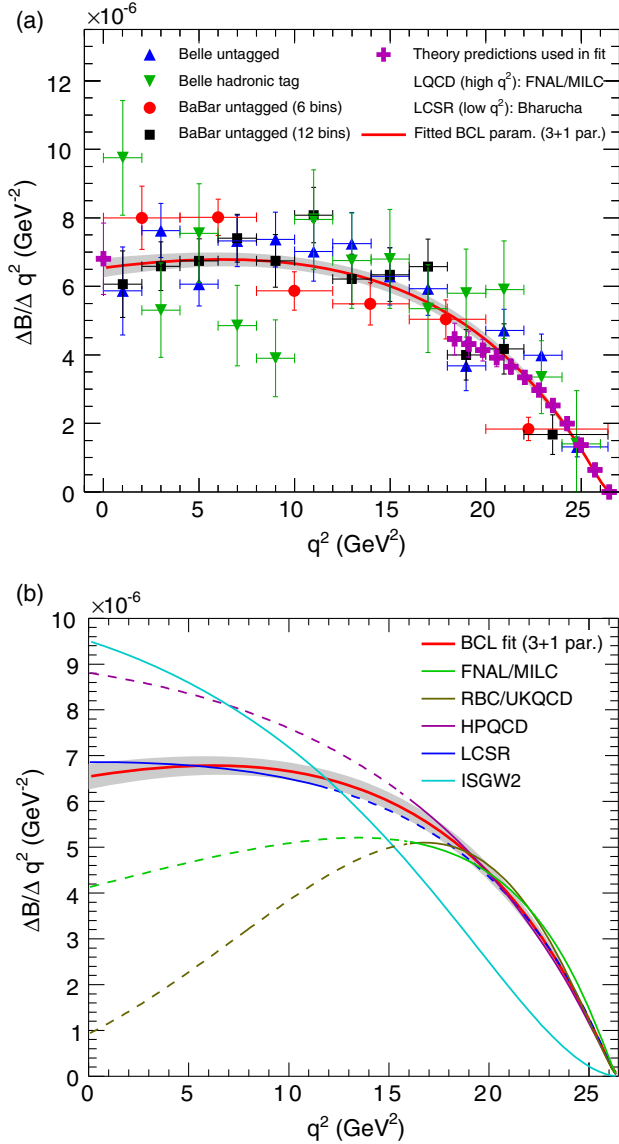


FIG. 31. Fit of the BCL parametrization to the $B \rightarrow \pi \ell \nu q^2$ spectrum: (a) Combined BCL fit to data and FNAL-MILC and LCSR predictions. The shaded band shows the fit uncertainty. The theoretical predictions are scaled according to the $|V_{ub}|$ value derived from the fit. (b) Shape comparison of the BCL fit with various form factor predictions, shown as solid lines in their regions of validity ($q^2 < 12 \text{ GeV}^2$ for LCSR, $q^2 > 16 \text{ GeV}^2$ for lattice QCD, all q^2 for ISGW2), where they have been normalized to the BCL fit. Extrapolations to the full q^2 range are shown as dashed lines and have large uncertainties (the corresponding uncertainty bands are not shown for a better visibility).

3. Determination of $|V_{ub}|$ from $B \rightarrow \pi \ell \nu$

The magnitude of the CKM parameter V_{ub} is determined from a comparison of the measured $B^0 \rightarrow \pi^- \ell^+ \nu$ branching fraction with the predicted decay rate from theory. Traditionally, $|V_{ub}|$ is calculated from

$$|V_{ub}| = \sqrt{\Delta\mathcal{B}(q_{\min}^2, q_{\max}^2) / \tau_{B^0} \Delta\zeta_{\text{th}}(q_{\min}^2, q_{\max}^2)}, \quad (111)$$

where τ_{B^0} is the mean B^0 lifetime, $\Delta\mathcal{B}(q_{\min}^2, q_{\max}^2)$ the measured partial branching fraction in the interval $[q_{\min}^2, q_{\max}^2]$, and $\Delta\zeta_{\text{th}}(q_{\min}^2, q_{\max}^2) = \Delta\Gamma_{\text{th}}(q_{\min}^2, q_{\max}^2) / |V_{ub}|^2$ denotes the normalized partial decay rate predicted by theory. The lattice calculations are used in the range $q^2 > 16 \text{ GeV}^2$ and the light-cone sum rules calculation in the range $q^2 < 12 \text{ GeV}^2$. Table XVII shows the $|V_{ub}|$ results obtained from the HFAG average of the $B^0 \rightarrow \pi^- \ell^+ \nu$ partial branching fractions combined with different form factor calculations. The uncertainty on $|V_{ub}|$ is dominated by the theoretical form factor uncertainty.

More recently, an alternative approach of determining $|V_{ub}|$ was used, which employs a combined fit of the BCL parametrization to the q^2 spectra from both experiment and theory. This method makes use of the full shape information from data over the whole q^2 range and both normalization and shape information from theory, resulting in a reduced uncertainty on $|V_{ub}|$. A combined fit to the FNAL, MILC, and LCSR calculations and the data from the BABAR and Belle measurements yields

$$|V_{ub}| = (3.59 \pm 0.12) \times 10^{-3} \quad (112)$$

and has a χ^2 probability of 10%. The fit result is shown in Fig. 31(a). The total uncertainty on $|V_{ub}|$ is 3.5%. The fit results for the BCL parameters are

$$\frac{b_1}{b_0} = -1.00 \pm 0.07, \quad \frac{b_2}{b_0} = -1.28 \pm 0.19. \quad (113)$$

They are very close to those obtained for the fit to data only [Eq. (109)] but have smaller uncertainties. From an extrapolation to $q^2 = 0$, we obtain

$$f_{B\pi}^+(0) |V_{ub}| = (0.920 \pm 0.019) \times 10^{-3}. \quad (114)$$

TABLE XVII. Results for $|V_{ub}|$ derived from the $B \rightarrow \pi \ell \nu$ partial branching fraction averages for different form factor calculations: LCSR (Khodjamirian *et al.*, 2011), HPQCD (Dalgic *et al.*, 2006), RBC and UKQCD (Flynn *et al.*, 2015), and FNAL and MILC (Bailey *et al.*, 2015a). The quoted uncertainties on $|V_{ub}|$ are experimental and theoretical ($\Delta\zeta_{\text{th}}$). The last column shows the $|V_{ub}|$ result of the combined fit to data and FNAL-MILC and LCSR predictions; the quoted uncertainty is the total (experimental and theoretical) uncertainty from the fit.

	LCSR	HPQCD	RBC and UKQCD	FNAL and MILC	Combined fit (data + theory)
q^2 range (GeV ²)	0–12	16–26.4	16–26.4	16–26.4	0–26.4
$\Delta\zeta_{\text{th}}$ (ps ⁻¹)	$4.59^{+1.00}_{-0.85}$	2.02 ± 0.55	1.77 ± 0.34	1.72 ± 0.14	...
$ V_{ub} $ (10 ⁻³)	$3.41 \pm 0.06^{+0.37}_{-0.32}$	$3.52 \pm 0.08^{+0.61}_{-0.40}$	$3.76 \pm 0.09^{+0.42}_{-0.32}$	$3.81 \pm 0.09^{+0.17}_{-0.15}$	3.59 ± 0.12

Using the HPQCD or RBC and UKQCD calculations instead of FNAL and MILC gives similar fit results, but with larger uncertainties.

BABAR has also extracted a value of $|V_{ub}|$ from $B \rightarrow \pi \ell \nu$ using information from their measurement of $D \rightarrow \pi \ell \nu$ decays (Lees *et al.*, 2015). The differential $B \rightarrow \pi \ell \nu$ branching fraction can be expressed as

$$\frac{dB}{dw_B}(B \rightarrow \pi \ell \nu) = \frac{dB}{dw_D}(D \rightarrow \pi \ell \nu) \frac{\tau_B m_B}{\tau_D m_D} \times \left(\frac{|V_{ub}|}{|V_{cd}|} \right)^2 \left| \frac{f_{B\pi}^+(w_B)}{f_{D\pi}^+(w_D)} \right|^2, \quad (115)$$

where $w_B = v_B v_\pi$ and $w_D = v_D v_\pi$. The $|V_{ub}|$ results obtained with this approach and using lattice QCD form factor predictions are consistent with the results in Table XVII,

but are still less precise. While they are based on predictions for the individual form factors, it is expected that lattice QCD will eventually provide a precise determination of the ratio $f_{B\pi}^+/f_{D\pi}^+$.

4. Other charmless semileptonic B decays

Semileptonic B decays to other charmless final states have been measured for the pseudoscalar mesons η and η' and the vector mesons ρ^\pm , ρ^0 , and ω . An overview of the most recent analyses of these decays is given in Table XVIII.

For $B^+ \rightarrow \omega \ell^+ \nu$, $B^+ \rightarrow \eta \ell^+ \nu$, and $B^+ \rightarrow \eta' \ell^+ \nu$ decays, the agreement between the different measurements is good. The $B \rightarrow \rho \ell \nu$ results, however, show sizable differences. The branching fraction results of the *BABAR* untagged analysis (del Amo Sanchez *et al.*, 2011) are lower than the ones of the Belle hadronic-tag analysis (Sibidanov *et al.*, 2013) by $\sim 2\sigma$

TABLE XVIII. Exclusive $B \rightarrow X_u \ell \nu$ measurements for $X_u = \rho^\pm$, ρ^0 , ω , η , and η' . For each measurement, the integrated luminosity, the number of selected signal events N_{sig} , and the measured total branching fraction are given. The uncertainties on the branching fractions are statistical and systematic.

Measurement	$\int \mathcal{L} dt$ (fb ⁻¹) $B^0 \rightarrow \rho^- \ell^+ \nu$	N_{sig}	\mathcal{B} (10 ⁻⁴)
CLEO untagged (Adam <i>et al.</i> , 2007) ^a	16	...	$2.93 \pm 0.37 \pm 0.37$
<i>BABAR</i> untagged (del Amo Sanchez <i>et al.</i> , 2011)	349	1577	$1.98 \pm 0.21 \pm 0.38$
Belle semileptonic tag (Hokuue <i>et al.</i> , 2007)	253	93	$2.24 \pm 0.54 \pm 0.31$
Belle hadronic tag (Sibidanov <i>et al.</i> , 2013)	711	343	$3.22 \pm 0.27 \pm 0.24$
$B^+ \rightarrow \rho^0 \ell^+ \nu$			
<i>BABAR</i> untagged (del Amo Sanchez <i>et al.</i> , 2011)	349	1970	$1.00 \pm 0.10 \pm 0.17$
Belle semileptonic tag (Hokuue <i>et al.</i> , 2007)	253	135	$1.33 \pm 0.23 \pm 0.18$
Belle hadronic tag (Sibidanov <i>et al.</i> , 2013)	711	622	$1.83 \pm 0.10 \pm 0.10$
$B^+ \rightarrow \omega \ell^+ \nu$			
<i>BABAR</i> untagged (Aubert <i>et al.</i> , 2009b)	347	802	$1.14 \pm 0.16 \pm 0.08$
<i>BABAR</i> untagged (Lees <i>et al.</i> , 2012b)	416	1861	$1.19 \pm 0.16 \pm 0.09$
<i>BABAR</i> untagged (Lees <i>et al.</i> , 2013a)	426	1125	$1.21 \pm 0.14 \pm 0.08$
<i>BABAR</i> semileptonic tag (Lees <i>et al.</i> , 2013d)	426	103	$1.35 \pm 0.21 \pm 0.11$
Belle hadronic tag (Sibidanov <i>et al.</i> , 2013)	711	106	$1.07 \pm 0.16 \pm 0.07$
$B^+ \rightarrow \eta \ell^+ \nu$			
CLEO untagged (Adam <i>et al.</i> , 2007)	16	...	$0.44 \pm 0.23 \pm 0.11$
<i>BABAR</i> untagged (Aubert <i>et al.</i> , 2009b)	347	554	$0.31 \pm 0.06 \pm 0.08$
<i>BABAR</i> untagged (Lees <i>et al.</i> , 2012b)	416	867	$0.38 \pm 0.05 \pm 0.05$
<i>BABAR</i> semileptonic tag (Aubert <i>et al.</i> , 2008e)	348	55	$0.64 \pm 0.20 \pm 0.03$
$B^+ \rightarrow \eta' \ell^+ \nu$			
CLEO untagged (Adam <i>et al.</i> , 2007)	16	...	$2.66 \pm 0.80 \pm 0.56$
<i>BABAR</i> untagged (Lees <i>et al.</i> , 2012b)	416	141	$0.24 \pm 0.08 \pm 0.03$
<i>BABAR</i> semileptonic tag (Aubert <i>et al.</i> , 2008e)	348	1	< 0.47 (90% C.L.)

^aThe branching fraction was determined in a simultaneous fit to both isospin states; the result in Adam *et al.* (2007) is quoted only in terms of the B^0 branching fraction.

for $B^0 \rightarrow \rho^- \ell^+ \nu$ decays and $\sim 3.5\sigma$ for $B^+ \rightarrow \rho^0 \ell^+ \nu$. As the ρ resonance is broad ($\Gamma_\rho \approx 149$ MeV), the backgrounds in $B \rightarrow \rho \ell \nu$ analyses are sizable, especially for untagged analyses, and it is difficult to control the background under the ρ mass peak. In particular, a potential contribution from non-resonant $\pi\pi$ states could not yet be experimentally constrained. Therefore, this decay mode benefits most from the clean environment in a hadronic-tag analysis. As seen in Table XVIII, the Belle hadronic-tag analysis (Sibidanov *et al.*, 2013) delivers the most precise $B \rightarrow \rho \ell \nu$ results. The M_{miss}^2 distributions from this analysis for various $B \rightarrow X_u \ell \nu$ decays ($X_u = \rho^\pm, \rho^0$, and ω) are shown in Figs. 30(c)–30(f).

Recently, Belle also reported the first indication of the decay $B^+ \rightarrow f_2 \ell^+ \nu$ in the $\pi^+ \pi^-$ invariant mass distribution around 1.3 GeV (Sibidanov *et al.*, 2013), but further studies are needed to consolidate this finding. In contrast to $B \rightarrow X_c \ell \nu$ decays, the observed exclusive decays make up only a small fraction, about 25%, of the total $B \rightarrow X_u \ell \nu$ branching fraction. Future measurements of semileptonic B decays to higher-mass charmless states would be important to improve our understanding of the composition of the charmless semileptonic decay rate.

The determination of $|V_{ub}|$ from non- π final states has not yet reached the level of precision as for $B \rightarrow \pi \ell \nu$ decays. Unquenched lattice QCD calculations are not available for these decays, since an unstable particle like the ρ meson is difficult to include in a lattice simulation as well as in a QCD sum rules estimate. Conversely, light-cone sum rule calculations exist for all of these decay modes (Ball and Braun, 1998; Ball and Jones, 2007; Ball and Zwicky, 2005a, 2005b), assuming stable final states, but even then the application of a light-cone sum rule remains questionable due to the large ρ mass. If we combine the light-cone sum rule predictions with the most recent $B \rightarrow \rho \ell \nu$ and $B^+ \rightarrow \omega \ell^+ \nu$ measurements (Sibidanov *et al.*, 2013), $|V_{ub}|$ values in the range $(3.0 - 3.6) \times 10^{-3}$ are obtained. However, these results have large uncertainties, mainly from the theoretical side. Nevertheless, they are compatible with the results from $B \rightarrow \pi \ell \nu$ decays.

5. $\Lambda_b \rightarrow p \mu \nu$

The LHCb experiment recently reported the first observation of $\Lambda_b \rightarrow p \mu \nu$ decays using a sample of 2.6×10^{11} $b\bar{b}$ pairs (Aaij *et al.*, 2015a). The decay $\Lambda_b \rightarrow p \mu \nu$ can be considered the baryonic correspondent of $B \rightarrow \pi \mu \nu$. Even though Λ_b baryons are produced only about half as often as B mesons at the LHC, the study of $\Lambda_b \rightarrow p \mu \nu$ decays at LHCb is more promising than $B \rightarrow \pi \mu \nu$, because protons are a rarer signature than pions. The key signature is a displaced vertex from the proton and the muon. Using kinematic constraints, q^2 can be reconstructed up to a twofold ambiguity. Only events with $q^2 > 15$ GeV² for both solutions are selected. The signal is extracted in a fit to the “corrected mass” m_{corr} , computed from the invariant $p\mu$ mass $m_{p\mu}$, and the momentum of the $p\mu$ system perpendicular to the Λ_b flight direction $p_{\perp, p\mu}$:

$$m_{\text{corr}} = \sqrt{p_{\perp, p\mu}^2 + m_{p\mu}^2} + p_{\perp, p\mu}. \quad (116)$$

The m_{corr} distribution exhibits a peak close to the Λ_b mass for signal events. The ratio of the partial branching fractions at high q^2 for $\Lambda_b \rightarrow p \mu \nu$ and $\Lambda_b \rightarrow \Lambda_c (\rightarrow p K \pi) \mu \nu$ decays is measured to reduce systematic uncertainties, for instance due to the production rate of Λ_b baryons. This ratio is proportional to $(|V_{ub}|/|V_{cb}|)^2$ and thus allows for a determination of $|V_{ub}|$, provided that $|V_{cb}|$ is known. Using lattice QCD predictions (Detmold, Lehner, and Meinel, 2015) of the form factors to calculate the ratio and the world average of $|V_{cb}|$ from exclusive decays (Olive *et al.*, 2014), LHCb obtains

$$|V_{ub}| = (3.27 \pm 0.15_{\text{exp}} \pm 0.17_{\text{th}} \pm 0.06_{|V_{cb}|}) \times 10^{-3} \quad (117)$$

with a total uncertainty of 7%.

6. Status of $|V_{ub}|$ from exclusive decays

The $|V_{ub}|$ result from LHCb is in agreement with the $B \rightarrow \pi \ell \nu$ result from the B factories obtained with the BCL fit. We combine these two results and derive an average for $|V_{ub}|$ from exclusive decays:

$$|V_{ub}| = (3.59 \pm 0.12) \times 10^{-3}. \quad (118)$$

As the $|V_{ub}|$ value derived by LHCb depends on $|V_{cb}|$, this average must still be taken with a grain of salt due to the difference in $|V_{cb}|$ between inclusive and exclusive measurements.

Improvements for $|V_{ub}|$ from exclusive decays will rely on further progress in form factor calculations based on lattice QCD or light-cone sum rules and on more precise experimental determinations of the q^2 spectrum. In particular, an improved precision in the high q^2 region, where lattice QCD predictions exist, would be important. This requires a better understanding of the composition and dynamics of $B \rightarrow X_u \ell \nu$ decays, which form the most problematic background at high q^2 , and significantly larger data samples to perform precision studies with tagged events.

The value of $|V_{ub}|$ from exclusive decays is significantly lower than that obtained from inclusive decays. The difference corresponds to 3.8σ . Nevertheless, we compute the weighted average of the exclusive and inclusive $|V_{ub}|$ determinations, assuming uncorrelated experimental and theoretical uncertainties, and obtain

$$|V_{ub}| = (3.70 \pm 0.38) \times 10^{-3}. \quad (119)$$

The χ^2 probability is only 0.01%. The uncertainty on the average has been scaled up by a factor of $\sqrt{\chi^2/\text{ndf}} = 3.8$ to account for the poor agreement.

7. New physics in $b \rightarrow u \ell \nu$

Although charged-current semileptonic decays are tree-level processes and thus are believed to be insensitive to physics beyond the SM, the tension between exclusive and inclusive $|V_{ub}|$ determinations has triggered speculations on possible right-handed admixtures to the $b \rightarrow u$ hadronic current.

In fact, such an admixture can in principle lead to a difference in exclusive and inclusive decays. Replacing the hadronic $b \rightarrow u$ current of the SM as follows:

$$\bar{b}_L \gamma_\mu u_L \rightarrow C_L (\bar{b}_L \gamma_\mu u_L) + C_R (\bar{b}_R \gamma_\mu u_R), \quad (120)$$

the inclusive $B \rightarrow X_u \ell \nu$ rate depends on the combination $|C_L|^2 + |C_R|^2$, while the exclusive decay $B \rightarrow \pi \ell \nu$ depends on the combination $|C_L + C_R|^2$. A recent analysis showed that one cannot get a consistent picture once the LHCb result from $\Lambda_b \rightarrow p \mu \nu$ decays is also included (Aaij *et al.*, 2015a).

IX. SEMILEPTONIC B DECAYS WITH A τ LEPTON

Similar to $B \rightarrow \tau \nu$ decays, semileptonic B decays with a τ lepton provide sensitivity to new charged particles that can be exchanged in place of the W boson in the diagram shown in Fig. 32. As there is a third-generation particle in both the initial and final state (b and τ), these decays are particularly sensitive to new particles that preferentially couple to heavy SM particles, such as charged Higgs bosons. As the semileptonic decay $B \rightarrow X \tau \nu$ is a three-body decay, it gives access to several observables that may provide constraints on extensions of the SM beyond what is possible with $B \rightarrow \tau \nu$, for instance through a study of τ polarization.

The SM prediction for the total $B \rightarrow X_c \tau \nu$ branching fraction is $(2.30 \pm 0.25)\%$ (Falk *et al.*, 1994), which is $\sim 25\%$ of that for the decays with electrons and muons, because of the larger τ mass. The first measurements of semileptonic b -hadron decays to τ leptons were performed at LEP (Acciarri *et al.*, 1994; Abreu *et al.*, 2000; Abbiendi *et al.*, 2001; Barate *et al.*, 2001). The b hadrons were produced in the fragmentation of b quarks from $Z \rightarrow b\bar{b}$ decays and their semileptonic decays were studied inclusively and semi-inclusively. Belle was the first experiment to observe an exclusive semileptonic B decay with a τ lepton $B^+ \rightarrow \bar{D}^{*0} \tau^+ \nu$ (Matyja *et al.*, 2007). In this section, we review the history of $B \rightarrow D^{(*)} \tau \nu$ measurements and discuss the most recent results in more detail, also in view of potential new physics interpretations.

A. Theory

For the light leptons e and μ from B decays, one may neglect the mass of the lepton, since both m_e^2/m_B^2 and m_μ^2/m_B^2 are small. The situation for the τ lepton is different, as the τ

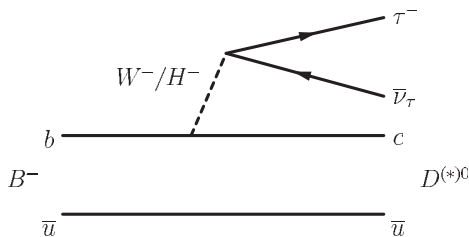


FIG. 32. A $B \rightarrow D^{(*)} \tau \nu$ decay. In models with an extended Higgs sector, the exchange of a charged Higgs boson instead of a W boson is also possible.

mass is too large to be neglected. Including the lepton mass forces us to include form factors (or form factor combinations) to which the massless case is insensitive. Since the leptonic $V - A$ current is conserved in the massless limit, all form factors related to the four-momentum transfer to the leptons q_μ do not appear in the expression for differential rates. Thus, in addition to the phase space effects in combination with the form factors known from the massless case, new hadronic quantities appear.

Without going into detail of the form factors, the structure of the decay rate for both $B \rightarrow D \tau \nu$ and $B \rightarrow D^* \tau \nu$ decays is given by

$$\begin{aligned} \frac{d\Gamma}{dq^2} &= \frac{G_F^2 |V_{cb}|^2 |\vec{p}_{D^{(*)}}|^2 q^2}{96\pi^3 m_B^2} \left(1 - \frac{m_\tau^2}{q^2}\right)^2 \\ &\times \left[(|H_+|^2 + |H_-|^2 + |H_0|^2) \left(1 + \frac{m_\tau^2}{2q^2}\right) \right. \\ &\left. + \frac{3m_\tau^2}{2q^2} |H_s|^2 \right], \end{aligned} \quad (121)$$

where H_\pm are the transverse helicity amplitudes, H_0 is the longitudinal helicity amplitude, and H_s is the scalar amplitude related to the form factors proportional to q_μ . From the massless case H_\pm and H_0 can be obtained, while the additional nonperturbative input goes into H_s .

Assuming that the c quark is heavy, the helicity amplitude H_s can be expressed in terms of the Isgur-Wise function, which means that heavy-quark symmetries relate the new form factors to the ones known from the massless case. Even if this may not yield a precise prediction for H_s , it still yields a good prediction of the decay rate, since the contribution of H_s to the rate is additionally suppressed by a factor of $m_\tau^2/m_B^2 \approx 0.11$. Given this, the SM prediction for $\ell = e, \mu$ (Fajfer, Kamenik, and Nisandzic, 2012) is

$$R(D) = \frac{\Gamma(B \rightarrow D \tau \bar{\nu})}{\Gamma(B \rightarrow D \ell \bar{\nu})} = 0.297 \pm 0.017, \quad (122)$$

$$R(D^*) = \frac{\Gamma(B \rightarrow D^* \tau \bar{\nu})}{\Gamma(B \rightarrow D^* \ell \bar{\nu})} = 0.252 \pm 0.003. \quad (123)$$

Becirevic, Kosnik, and Tayduganov (2012) found a slightly higher value for $R(D)$, which is still compatible with the result in Eq. (122), but has less tension with the measurements presented below. Recent lattice calculations by Bailey *et al.* (2015b) and Na *et al.* (2015) are consistent with Eq. (122) and have an improved precision.

Because of the mass of the τ lepton, $B \rightarrow D^{(*)} \tau \nu$ decays could be more sensitive to new physics effects than the decays into light leptons. In fact, all models involving an extended Higgs sector can significantly change the rates for $B \rightarrow D^{(*)} \tau \nu$ decays, while the semileptonic decays into e and μ remain practically unchanged, since Higgs couplings are proportional to the mass. Both BABAR and Belle have analyzed the data in terms of a type-II two-Higgs doublet model; the results are discussed in Sec. IX.C.

B. Measurements

The reconstruction of semileptonic decays with a τ lepton is complicated by the presence of several neutrinos in the final state: one primary neutrino from the semileptonic decay and one or two secondary neutrinos from the τ decay ($\tau^+ \rightarrow X^+ \bar{\nu}_\tau, \ell^+ \nu_\ell \bar{\nu}_\tau$). The undetected neutrinos make a complete reconstruction of the signal B meson impossible and call for additional kinematic constraints to reduce backgrounds. To reach a tolerable background level, the analysis of these decays has to rely on the reconstruction of the second B meson in the event.

In 2007 Belle reported the observation of the decay $B^0 \rightarrow D^{*-} \tau^+ \nu$ with a significance of 5.2σ in a data sample of 493 fb^{-1} (Matyja *et al.*, 2007). The analysis used an “inclusive” tagging method, which is based on reconstructing the B_{tag} from all particles other than the $D^{(*)}$ and lepton candidates from the signal decay, irrespective of any specific B_{tag} decay mode. The signal was extracted in a fit to the beam-constrained mass of the B_{tag} candidate. Subsequently, Belle published an analysis of the decay modes $B^+ \rightarrow \bar{D}^0 \tau^+ \nu$ and $B^+ \rightarrow \bar{D}^{*0} \tau^+ \nu$ using the same inclusive tagging method with a data sample of 605 fb^{-1} (Bozek *et al.*, 2010). The fit was extended to two dimensions by adding the momentum of the D^0 meson as a second variable, which helps to distinguish between the D^0 and D^{*0} signal modes. The signal significances were 8.1σ for $B^+ \rightarrow \bar{D}^{*0} \tau^+ \nu$ and 3.5σ for $B^+ \rightarrow \bar{D}^0 \tau^+ \nu$.

In 2009 both *BABAR* and Belle presented their first hadronic-tag measurements of the four decay modes $B^+ \rightarrow \bar{D}^0 \tau^+ \nu$, $B^+ \rightarrow \bar{D}^{*0} \tau^+ \nu$, $B^0 \rightarrow D^- \tau^+ \nu$, and $B^0 \rightarrow D^{*-} \tau^+ \nu$ (Adachi *et al.*, 2009; Aubert *et al.*, 2009c) with data samples of 209 and 605 fb^{-1} , respectively. The results of both experiments have by now been superseded by updates based on the full $\Upsilon(4S)$ data samples. The *BABAR* update was published in 2013 (Lees *et al.*, 2013c), and the new Belle result in 2015 (Huschle *et al.*, 2015). In addition to the statistical gain from the larger data samples, the new hadronic-tag analyses have a significantly improved signal efficiency due to improvements in the event selection and the B_{tag} reconstruction. Belle recently also published results for $B^0 \rightarrow D^{*-} \tau^+ \nu$ using semileptonic B tags (Sato *et al.*, 2016). First results on semileptonic B decays with τ leptons have also become available from the LHC. The LHCb experiment recently presented an analysis of $B \rightarrow D^* \tau \nu$ decays (Aaij *et al.*, 2015b), the first of this kind from a hadron collider.

In all these analyses, the ratios $R(D)$ and $R(D^*)$ [see Eqs. (122) and (123)] were measured. The results are summarized in Table XIX. We first describe the *BABAR* analysis in more detail and then compare with the results from Belle and LHCb.

A major challenge in $B \rightarrow D^{(*)} \tau \nu$ analyses is the separation of the $B \rightarrow D^{(*)} \tau \nu$ signal from $B \rightarrow D^{(*)} \ell \nu$ ($\ell = e, \mu$). As the main quantities to be measured are the ratios $R(D)$ and $R(D^*)$, the decays $B \rightarrow D^{(*)} \ell \nu$ serve to normalize the corresponding signal branching fractions. We thus refer to them as “normalization decays” in the following. In the *BABAR* analysis signal D^0 candidates are reconstructed in five decay modes, D^- in six, and D^* candidates in four decay modes (see Table III). The τ lepton is reconstructed only in its

TABLE XIX. Measurements of $R(D^{(*)})$. The uncertainties are statistical and systematic. For *BABAR* and Belle the B^0 and B^+ results have been combined using isospin relations.

Decay mode	N_{sig}	$R(D^{(*)})$
	<i>BABAR</i> hadronic tag (426 fb^{-1})	
$B \rightarrow D \tau \nu$	489	$0.440 \pm 0.058 \pm 0.042$
$B \rightarrow D^* \tau \nu$	888	$0.332 \pm 0.024 \pm 0.018$
	Belle hadronic tag (711 fb^{-1})	
$B \rightarrow D \tau \nu$	320	$0.375 \pm 0.064 \pm 0.026$
$B \rightarrow D^* \tau \nu$	503	$0.293 \pm 0.038 \pm 0.015$
	Belle semileptonic tag (711 fb^{-1})	
$B \rightarrow D^* \tau \nu$	231	$0.302 \pm 0.030 \pm 0.011$
	LHCb (3.0 fb^{-1})	
$B \rightarrow D^* \tau \nu$...	$0.336 \pm 0.027 \pm 0.030$

leptonic decays $\tau^+ \rightarrow e^+ \nu_e \bar{\nu}_\tau, \mu^+ \nu_\mu \bar{\nu}_\tau$. With this choice, the $B \rightarrow D^{(*)} \tau \nu$ signal and the $B \rightarrow D^{(*)} \ell \nu$ normalization decays have the same final state $D^{(*)} \ell$ and differ only in kinematics. Consequently, many of the experimental uncertainties, such as lepton and hadron identification or track uncertainties, cancel in the ratio $R(D^{(*)})$. Four signal channels corresponding to the final states $D^0 \ell, D^{*0} \ell, D^- \ell,$ and $D^{*-} \ell$ are analyzed. After reconstructing the $B_{\text{tag}}, D^{(*)}$, and lepton candidates, no additional tracks are allowed in the event. In case of multiple $D^{(*)} \ell$ candidates, the one with the lowest remaining energy in the calorimeter $E_{\text{extra}}^{\text{ECL}}$ is chosen.

The signal is extracted in a fit to the joint distribution of p_ℓ^* and M_{miss}^2 . These two variables serve to distinguish $B \rightarrow D^{(*)} \tau \nu$ signal from normalization decays and other backgrounds. Semileptonic decays with a leptonic τ decay involve three neutrinos and thus have large M_{miss}^2 . As the signal electron or muon is a secondary lepton from the τ decay, its p_ℓ^* distribution is softer than for the primary lepton from normalization decays. The fit is performed simultaneously on the four $D^{(*)} \ell$ samples and four additional $D^{(*)} \pi^0 \ell$ control samples. The $D^{(*)} \pi^0 \ell$ samples have an enhanced D^{**} contribution and allow the $B \rightarrow D^{**} \ell \nu$ and $B \rightarrow D^{**} \tau \nu$ backgrounds to be constrained with data. This leads to a significantly reduced dependence on simulation for these rather poorly known decays.

Figure 33(a) shows the fit projections in M_{miss}^2 and p_ℓ^* for the four signal samples. The resulting $R(D^{(*)})$ values and branching fractions are listed in Table XIX. In addition to the results for the individual signal modes, *BABAR* provides results of a fit using isospin relations to link B^0 and B^+ decays. The signal significances obtained in the isospin-constrained fit are 13.2σ for $B \rightarrow D^* \tau \nu$ and 6.8σ for $B \rightarrow D \tau \nu$. For $B \rightarrow D \tau \nu$ decays, this result represents the first observation with a significance higher than 5σ . The $B \rightarrow D^{(*)} \tau \nu$ branching fractions are calculated from the $R(D^{(*)})$ results and the known $B \rightarrow D^{(*)} \ell \nu$ branching fractions (Aubert *et al.*, 2008b, 2009d, 2010c). For the isospin-constrained fit they are

$$\mathcal{B}(B^+ \rightarrow \bar{D}^0 \tau^+ \nu) = (1.02 \pm 0.13_{\text{stat}} \pm 0.10_{R(D)} \pm 0.04_{\mathcal{B}(B \rightarrow D \ell \nu)})\%, \quad (124)$$

$$\mathcal{B}(B^+ \rightarrow \bar{D}^{*0} \tau^+ \nu) = (1.76 \pm 0.13_{\text{stat}} \pm 0.10_{R(D^*)} \pm 0.06_{\mathcal{B}(B \rightarrow D^* \ell \nu)})\%, \quad (125)$$

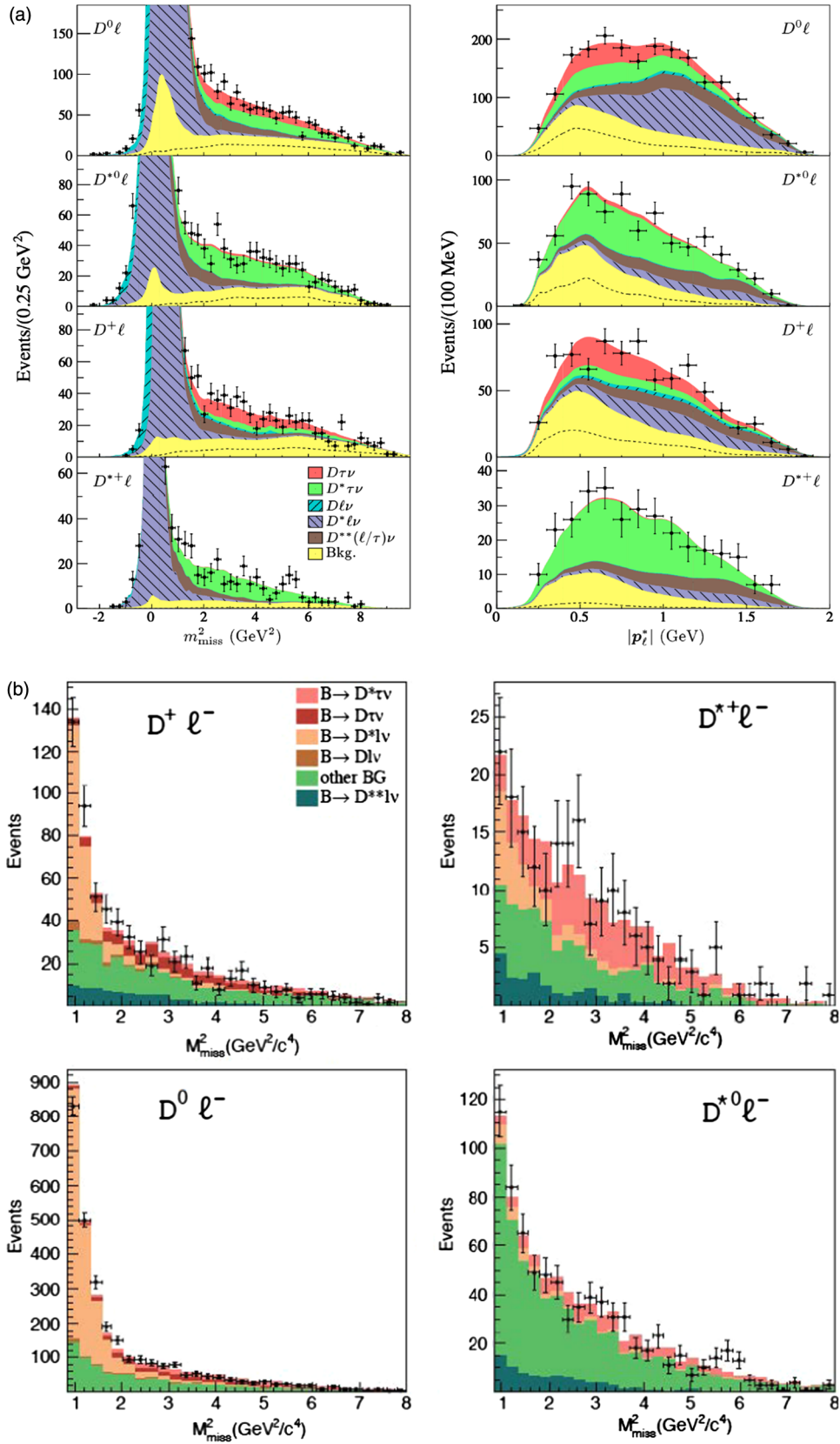


FIG. 33. Fit projections for the $D^{(*)}\ell$ samples in the $B \rightarrow D^{(*)}\tau\nu$ analysis of (a) BABAR (Lees *et al.*, 2013c) and (b) Belle (Huschle *et al.*, 2015). For the BABAR analysis, the distributions of the two fit variables M_{miss}^2 and p_ℓ^* after the fit are shown. For the Belle analysis, the M_{miss}^2 distribution is shown for $M_{\text{miss}}^2 > 0.85$ GeV².

where the first uncertainty is statistical and the second and third are systematic uncertainties from the $R(D^*)$ measurement and the branching fractions of the normalization decays. The measured values of $R(D^{(*)})$,

$$\begin{aligned} R(D) &= 0.440 \pm 0.072, \\ R(D^*) &= 0.332 \pm 0.030, \end{aligned} \quad (126)$$

can be compared with the SM predictions given in Eqs. (122) and (123). Deviations of 2σ and 2.7σ from the SM are observed for $R(D)$ and $R(D^*)$, respectively. The probability that the $R(D)$ and $R(D^*)$ results both agree with the SM expectation is calculated to be 6.9×10^{-4} (Lees *et al.*, 2013c), taking the correlation between the two results into account. The $B \rightarrow D\tau\nu$ and $B \rightarrow D^*\tau\nu$ results thus agree only at the 3.4σ level.

The new hadronic-tag analysis from Belle (Huschle *et al.*, 2015) uses a modified fitting approach. A fit to M_{miss}^2 is used only in the low- M_{miss}^2 region, where the background from normalization decays dominates, which can be well separated from the signal. In the high- M_{miss}^2 region, where backgrounds with multiple unreconstructed particles (e.g., from D^{**} decays) become more relevant that are harder to discriminate from the signal, a neural network is trained for each of the four signal channels to achieve a more effective background suppression. The inputs to the neural network include M_{miss}^2 , p_e^* , q^2 , $E_{\text{extra}}^{\text{ECL}}$, and several other discriminating variables. The sample is split at $M_{\text{miss}}^2 = 0.85 \text{ GeV}^2$ and both subsamples are fitted simultaneously, using M_{miss}^2 in the low- M_{miss}^2 and the neural-network output in the high- M_{miss}^2 region. The M_{miss}^2 distribution is shown in Fig. 33(b). The results for $R(D)$ and $R(D^*)$ are given in Table XIX. Because of the different fitting approach the statistical uncertainty is larger than for the *BABAR* analysis in spite of the larger analyzed data sample, but the systematic uncertainty is smaller. The total uncertainties are comparable for the two experiments.

In the Belle semileptonic-tag analysis (Sato *et al.*, 2016), both B mesons are reconstructed in semileptonic decays with a D^* meson. The signal is extracted in a two-dimensional fit to $E_{\text{extra}}^{\text{ECL}}$ and the output of a neural network trained to separate signal and normalization events. The $R(D^*)$ result (see Table XIX) is in good agreement with previous measurements.

In the LHCb analysis of $B \rightarrow D^*\tau\nu$ decays (Aaij *et al.*, 2015b) only the decay $\tau^+ \rightarrow \mu^+ \nu_\mu \bar{\nu}_\tau$ has been considered. The yields of the signal and normalization decays are determined in a three-dimensional fit to the distributions of M_{miss}^2 , p_μ , and q^2 . Backgrounds from $B \rightarrow D^{**}\mu\nu$ and $B \rightarrow D^*DX$ decays as well as combinatorial background are constrained from data using dedicated control samples. The $R(D^*)$ result lies 2.1σ above the SM prediction (see Table XIX) and is in good agreement with the *BABAR* measurement of $B \rightarrow D^*\tau\nu$.

All measurements of $R(D)$ and $R(D^*)$ have consistently yielded values larger than the SM prediction, as illustrated in Fig. 34. However, as the new $B \rightarrow D\tau\nu$ and $B \rightarrow D^*\tau\nu$ results from Belle are consistent with both the SM prediction and the *BABAR* result, the situation remains unclear. Combining the latest hadronic-tag results from *BABAR* and Belle and the

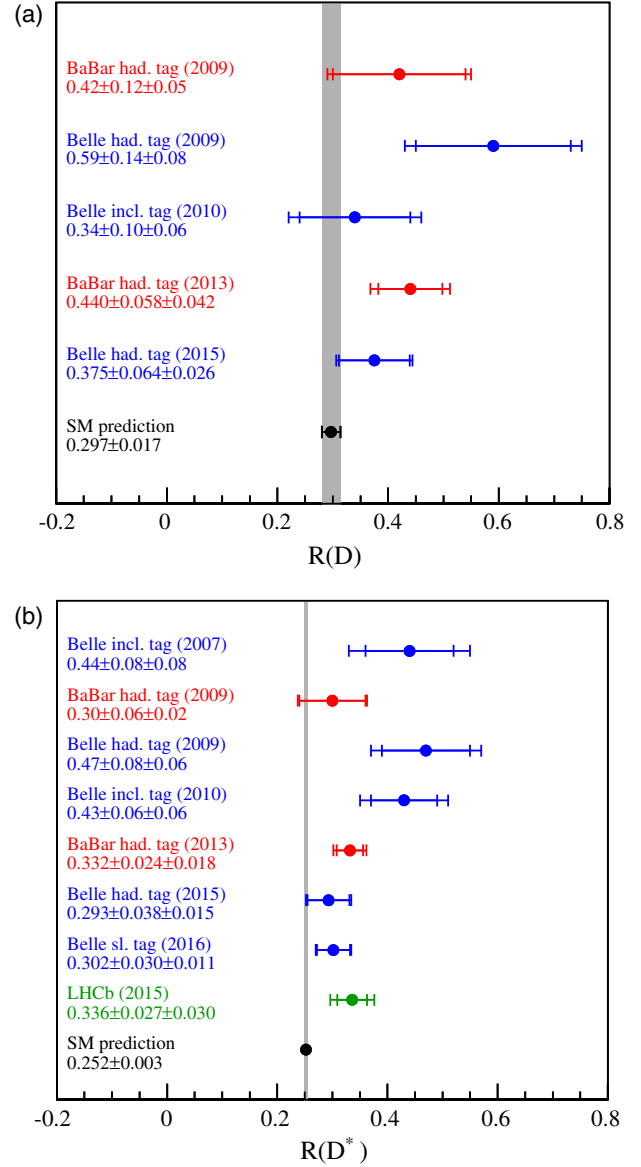


FIG. 34. History of (a) $R(D)$ and (b) $R(D^*)$ measurements. The gray bands indicate the SM predictions.

LHCb result (for $B \rightarrow D^*\tau\nu$ only) gives the following averages computed by HFAG (Amhis *et al.*, 2016):

$$\begin{aligned} R(D) &= 0.397 \pm 0.049, \\ R(D^*) &= 0.316 \pm 0.019. \end{aligned} \quad (127)$$

$R(D)$ and $R(D^*)$ exceed the SM predictions (Fajfer, Kamenik, and Nisandzic, 2012) by 1.9σ and 3.3σ , respectively. The probability of the combination is 5.2×10^{-5} , considering the correlation between $R(D)$ and $R(D^*)$, and the total deviation from the SM prediction corresponds to 4.0σ . More data from Belle II are needed to conclude if the observed excess from the SM is a sign of new physics or not.

C. Charged Higgs and new physics interpretation

One possible interpretation of the observed excess of $B \rightarrow D\tau\nu$ and $B \rightarrow D^*\tau\nu$ decays could be a contribution from

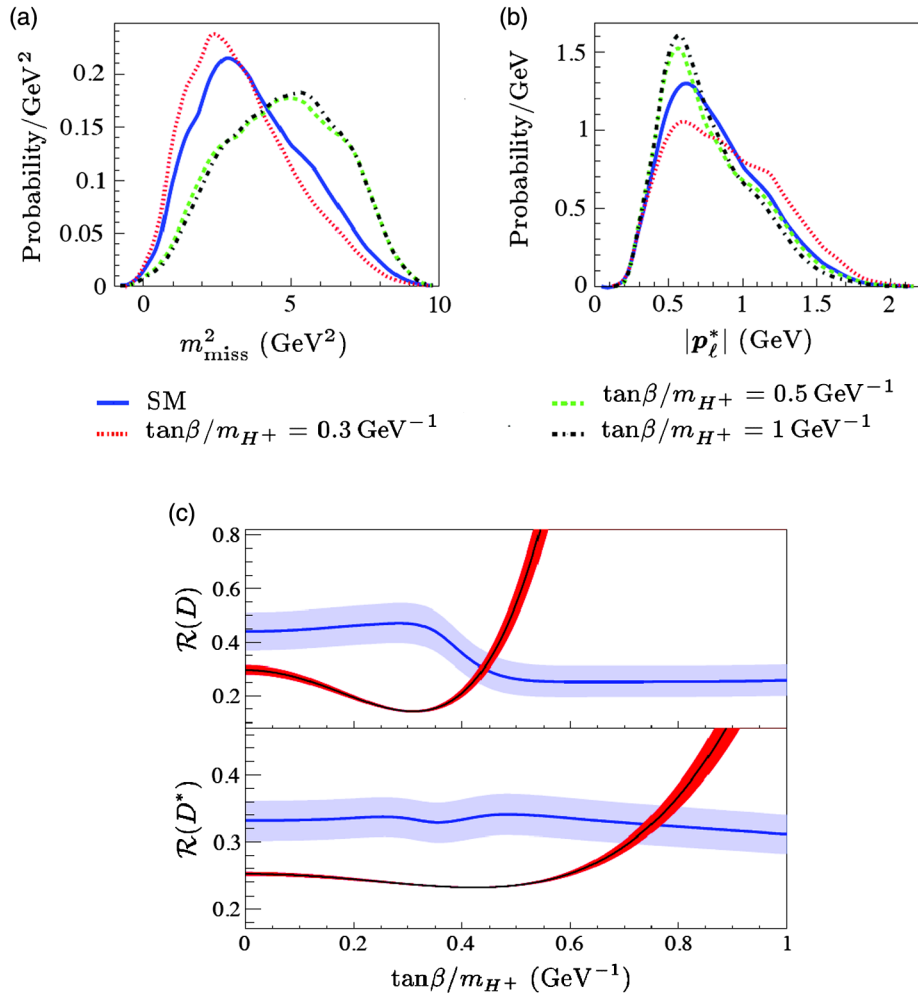


FIG. 35. Expected shapes of the (a) M_{miss}^2 and (b) p_ℓ^* distributions in $B \rightarrow D\tau\nu$ decays for four values of $\tan\beta/m_{H^\pm}$. (c) The $R(D)$ and $R(D^*)$ results for the *BABAR* measurement reweighted to different $\tan\beta/m_{H^\pm}$ values (light-shaded, blue band) is compared with the type-II 2HDM prediction (dark-shaded, red band). The bands indicate the 1σ uncertainty. From *Lees et al., 2013c*.

charged Higgs bosons in 2HDMs. Two versions of these models are considered in the following. In the type-II 2HDM, one Higgs doublet couples only to down-type quarks, and the other only to up-type quarks. For instance, the minimal supersymmetric standard model (MSSM) is a type-II 2HDM. At tree level, the type-II 2HDM is fully determined by two parameters, which can be chosen to be the ratio of the vacuum expectation values of the two Higgs doublets $\tan\beta$ and the mass of the charged Higgs boson m_{H^\pm} (see Sec. IV.A). A more general model is the type-III 2HDM, where both Higgs doublets couple to up- and down-type quarks.

BABAR and Belle reweighted their signal distributions to include the effect of charged Higgs exchange in the type-II 2HDM for various values of the ratio $\tan\beta/m_{H^\pm}$ and studied the dependence of the fit result on this ratio. As the decay kinematics are modified by the charged Higgs contribution, the signal efficiencies and hence the $R(D^{(*)})$ results also change. Figures 35(a) and 35(b) illustrate how the M_{miss}^2 and p_ℓ^* distributions change for different values of $\tan\beta/m_{H^\pm}$. Figure 35(c) shows a comparison of the $R(D^{(*)})$ results obtained for the reweighted signal distributions with the prediction of the type-II 2HDM in dependence of $\tan\beta/m_{H^\pm}$.

The *BABAR* measurements and the type-II 2HDM predictions agree best for $\tan\beta/m_{H^\pm} = 0.44 \pm 0.02 \text{ GeV}^{-1}$ ($B \rightarrow D\tau\nu$) and $\tan\beta/m_{H^\pm} = 0.75 \pm 0.04 \text{ GeV}^{-1}$ ($B \rightarrow D^*\tau\nu$). It is interesting to see that these $\tan\beta/m_{H^\pm}$ values differ significantly for the two decay modes. As a consequence, the combination of $R(D)$ and $R(D^*)$ measurements disfavors the type-II 2HDM with at least 99.8% confidence level for all values of $\tan\beta/m_{H^\pm}$.⁸ The $B \rightarrow D^{(*)}\tau\nu$ results from *BABAR* thus also disfavor the MSSM and provide interesting information for the search for supersymmetry at the high-energy frontier with the LHC. The Belle results are, however, not in conflict with a type-II 2HDM interpretation.

BABAR also interpreted their results in the context of the more general type-III 2HDM. Even though the type-III 2HDM cannot be ruled out, the measurement of $R(D^{(*)})$ combined with a study of the q^2 distributions measured in $B \rightarrow D^{(*)}\ell\nu$ decays excludes a significant part of the parameter space of this model. In general, the study of the q^2 spectra showed that

⁸The region $\tan\beta/m_{H^\pm} < 15 \text{ GeV}^{-1}$ has already been excluded by $B \rightarrow X_s\gamma$ decays.

interpretations of the results based on new physics models with a spin-1 particle are favored over models with a spin-0 particle.

Overall, the $B \rightarrow D^{(*)}\tau\nu$ results seem to be hard to accommodate in a well-motivated model of new physics. Many attempts have been made, for instance, in the context of R -parity violating supersymmetry, left-right-symmetric models and models with leptoquarks or sterile neutrinos, but they all seem to be more or less contrived.

X. ISOSPIN AND FLAVOR SYMMETRY

In this section, we briefly look at the results of the previously discussed semileptonic B -decay analyses in view of isospin symmetry. Weak annihilation is discussed as a special case of an isospin-symmetry-breaking effect that shows up at large momentum transfers. We also compare the inclusive semileptonic B decay rate with a measurement for B_s decays as a test of flavor symmetry.

A. Isospin symmetry

Isospin relations have been used to link B^0 and B^+ decays and to derive a combined result for the two isospin-conjugate decay modes in many of the analyses of semileptonic decays presented in the previous sections. It is important to experimentally confirm that the assumed isospin relations indeed hold.

If isospin-symmetry-breaking effects are neglected, the following relation between B^0 and B^+ decays is expected for inclusive semileptonic decays:

$$\mathcal{B}(B^0 \rightarrow X^-\ell^+\nu) = \frac{\tau_{B^0}}{\tau_{B^+}} \mathcal{B}(B^+ \rightarrow X^0\ell^+\nu). \quad (128)$$

For exclusive semileptonic decays one obtains

$$\mathcal{B}(B^0 \rightarrow D^{(*)-}\ell^+\nu) = \frac{\tau_{B^0}}{\tau_{B^+}} \mathcal{B}(B^+ \rightarrow D^{(*)0}\ell^+\nu), \quad (129)$$

$$\mathcal{B}(B^0 \rightarrow \pi^-\ell^+\nu) = 2 \frac{\tau_{B^0}}{\tau_{B^+}} \mathcal{B}(B^+ \rightarrow \pi^0\ell^+\nu), \quad (130)$$

$$\mathcal{B}(B^0 \rightarrow \rho^-\ell^+\nu) = 2 \frac{\tau_{B^0}}{\tau_{B^+}} \mathcal{B}(B^+ \rightarrow \rho^0\ell^+\nu). \quad (131)$$

Isospin breaking is due to the mass difference $m_u - m_d$ and electromagnetic interactions. However, for heavy-hadron processes involving energy scales of the order of the heavy-quark masses, such effects are expected to be small.

Table XX shows the isospin ratio $R_{0/+}$ [defined as the ratio of the left and right sides of Eqs. (128)–(131)], for some of the more recent inclusive and exclusive $B \rightarrow X_u\ell\nu$ and $B \rightarrow X_c\ell\nu$ analyses, for which results on both B^0 and B^+ decays are quoted in the publications. The $R_{0/+}$ values for all decay modes are consistent with unity and demonstrate that within the current experimental precision all measurements are in good agreement with isospin symmetry.

B. Weak annihilation

The process of *weak annihilation* leads to a difference between the B^+ and B^0 semileptonic decay rates at high four-momentum transfers.

TABLE XX. Isospin ratios $R_{0/+} = [\mathcal{B}(B^0)/\mathcal{B}(B^+)] \times (\tau_{B^+}/\tau_{B^0}) \times (1/n)$, where $n = 2$ for $B \rightarrow \pi\ell\nu$ and $B \rightarrow \rho\ell\nu$ decays and $n = 1$ otherwise. The uncertainties are statistical and systematic.

Measurement	$R_{0/+}$
Inclusive $B \rightarrow X_u\ell\nu$ hadronic tag (BABAR)	$1.03 \pm 0.15 \pm 0.18$
Inclusive $B \rightarrow X_c\ell\nu$ (Belle)	$1.01 \pm 0.04 \pm 0.03$
$B \rightarrow D\ell\nu$ hadronic tag (BABAR)	$1.04 \pm 0.06 \pm 0.06$
$B \rightarrow D^*\ell\nu$ untagged (BABAR)	$0.91 \pm 0.02 \pm 0.09$
$B \rightarrow \pi\ell\nu$ hadronic tag (Belle)	$1.00 \pm 0.12 \pm 0.07$
$B \rightarrow \pi\ell\nu$ untagged (BABAR, 12 bins)	$1.03 \pm 0.06 \pm 0.06$
$B \rightarrow \pi\ell\nu$ untagged (BABAR, 6 bins)	$1.03 \pm 0.09 \pm 0.06$
$B \rightarrow \rho\ell\nu$ hadronic tag (Belle)	$0.95 \pm 0.10 \pm 0.09$
$B \rightarrow \rho\ell\nu$ untagged (BABAR)	$1.06 \pm 0.16 \pm 0.08$

Weak annihilation refers to the annihilation of the two quarks inside a charged B meson into a virtual W boson ($u\bar{b} \rightarrow W^+X \rightarrow \ell^+\nu_\ell X$), producing final states with a lepton-neutrino pair from the W boson and a hadronic system created by the emission of low-energy gluons. This process enhances the charmless B^+ semileptonic decay rate at high q^2 as the lepton-neutrino pair carries most of the energy ($q^2 \approx m_B^2$). The enhancement in semileptonic B decays has been estimated from leptonic and semileptonic D and D_s decays to be at most 2%–3% (Bigi and Uraltsev, 1994; Voloshin, 2001; Gambino and Kamenik, 2010; Ligeti, Luke, and Manohar, 2010). Experimental investigations of weak annihilation based on studies of the q^2 spectra and comparisons of B^+ and B^0 partial decay rates at high q^2 in $B \rightarrow X_u\ell\nu$ decays have so far provided only weaker limits. CLEO constrains the contribution from weak annihilation (WA) to $\Gamma_{\text{WA}}/\Gamma(B^+ \rightarrow X_u^0\ell^+\nu) < 7.4\%$ at the 90% confidence level (Rosner *et al.*, 2006). From the inclusive hadronic-tag $B \rightarrow X_u\ell\nu$ analysis by BABAR (Lees *et al.*, 2012c), the limit $-13\% < \Gamma_{\text{WA}}/\Gamma(B^+ \rightarrow X_u^0\ell^+\nu) < 9\%$ at the 90% confidence level is obtained.

C. Semileptonic B_s decays and flavor symmetry

The decays of B_u ($= B^+$) and B_d ($= B^0$) mesons have been studied precisely at the B factories, but our knowledge of B_s mesons, which contain a \bar{b} and an s quark, is still fairly limited. Semileptonic decays of B and B_s mesons differ from one another only by the flavor of the spectator quark (d or s). A study of semileptonic B_s decays allows for a test of SU(3) flavor symmetry, which predicts for the total semileptonic B_s branching fraction:

$$\begin{aligned} \mathcal{B}(B_s \rightarrow X^-\ell^+\nu) &= \frac{\tau_{B_s}}{\tau_{B_d}} \mathcal{B}(B_d \rightarrow X^-\ell^+\nu) \\ &= (10.28 \pm 0.28)\%, \end{aligned} \quad (132)$$

where the B_s and B_d mean lifetimes $\tau_{B_s} = 1.512 \pm 0.007$ and $\tau_{B_d} = 1.519 \pm 0.005$ ps (Olive *et al.*, 2014) and the branching fraction $\mathcal{B}(B_d \rightarrow X^-\ell^+\nu) = (10.33 \pm 0.28)\%$ (Olive *et al.*, 2014) have been used. Theoretical calculations predict that the relation in Eq. (132) holds at the percent level (Bigi, Mannel, and Uraltsev, 2011; Gronau and Rosner, 2011), but this must be confirmed experimentally. Semileptonic B_s decays are also interesting for the determination of $|V_{ub}|$ and $|V_{cb}|$, as lattice

QCD calculations for heavier quarks (here s instead of u , d) have smaller theoretical uncertainties.

Exclusive semileptonic B_s decays can be studied well with the large B_s samples collected in hadron collisions at the Tevatron and more recently at the LHC. The D0 and LHCb experiments observed semileptonic B_s decays to orbitally excited (P -wave) D_s^{**} mesons. B_s decays to higher-mass D_s states contain valuable information for tests of HQET, as they provide access to the regime of low hadronic recoil and may help to understand the $j_{\text{light}} = 1/2$ vs $j_{\text{light}} = 3/2$ puzzle in $B \rightarrow D^{**} \ell \nu$ decays. In contrast to the broad D^{**} states that appear in B decays, the D_s^{**} states are all relatively narrow and can thus be more effectively separated from the background and more precisely measured. The D0 experiment observed the decay $B_s \rightarrow D_{s1}^- \mu^+ \nu X$ with the subsequent decay chain $D_{s1}^- \rightarrow D^{*-} K_S^0$, $D^{*-} \rightarrow \bar{D}^0 \pi^-$, $\bar{D}^0 \rightarrow K^+ \pi^-$, $K_S^0 \rightarrow \pi^+ \pi^-$ and determined its branching fraction (Abazov *et al.*, 2009). LHCb measured the branching fractions of $B_s \rightarrow D_{s1}^- \mu \nu X$ and $B_s \rightarrow D_{s2}^- \mu \nu X$ decays (Aaij *et al.*, 2011); the latter represents the first observation of the D_{s2}^- state in B_s decays.

Inclusive semileptonic B_s decays can be studied only at the B factories. BABAR recorded a data sample of 4.25 fb^{-1} during an energy scan above the $\Upsilon(4S)$ resonance with center-of-mass energies between 10.45 and 11.20 GeV, including the region near the $B_s \bar{B}_s$ threshold. Belle recorded a significantly larger data sample of 121 fb^{-1} at the $\Upsilon(5S)$ resonance with a center-of-mass energy of about 10.87 GeV. As the $e^+ e^- \rightarrow \Upsilon(5S)$ cross section amounts to $\sim 30\%$ of the $e^+ e^- \rightarrow \Upsilon(4S)$ cross section and the $\Upsilon(5S)$ decays into B_s pairs only about 20% of the time, the B_s samples available at the B factories are significantly smaller than the samples of B mesons, limiting the statistical precision of the B_s measurements.

BABAR performed the first measurement of the inclusive $B_s \rightarrow X^- \ell^+ \nu$ branching fraction, $\mathcal{B}(B_s \rightarrow X^- \ell^+ \nu) = (9.5^{+2.5}_{-2.0} \text{stat} \text{ } ^{+1.1}_{-1.9} \text{syst})\%$ (Lees *et al.*, 2012a). Belle subsequently published a measurement of this branching fraction (Oswald *et al.*, 2013) with a significantly improved precision due to the larger B_s sample. In this analysis, the fraction of $B_s \bar{B}_s$ events is enhanced from $\sim 20\%$ to $\sim 70\%$ by reconstructing a tag D_s^+ candidate from the decay $B_s \rightarrow D_s X$, which has a large branching fraction of $(93 \pm 25)\%$. The D_s^+ candidates are reconstructed in the decay mode $D_s^+ \rightarrow \phi \pi^+$, $\phi \rightarrow K^+ K^-$. The signal lepton and the tag D_s^+ candidates are required to have same-sign charges to ensure that they come from different B_s mesons. A sketch of the selection strategy is shown in Fig. 36(a). Two samples are selected, one with D_s^+ and the other with $D_s^+ \ell^+$ candidates, representing a subsample of the former. The yield of correctly reconstructed D_s^+ candidates is determined from fits to the invariant $K^+ K^- \pi^+$ mass. The $D_s^+ \ell^+$ sample contains not only primary leptons, but also secondary leptons from $B_{(s)}$ decays and misidentified lepton candidates, which have softer momentum spectra. The yield of events with primary leptons is obtained from a fit of the simulated signal and background shapes to the lepton momentum spectrum; see Fig. 36(b). The $B_s \rightarrow X^- \ell^+ \nu$ branching fraction is calculated from the efficiency-corrected D_s^+ and $D_s^+ \ell^+$ yields. As these yields include contributions from B^0 and B^+ decays ($B \rightarrow D_s X$ and $B \rightarrow X \ell \nu$), the

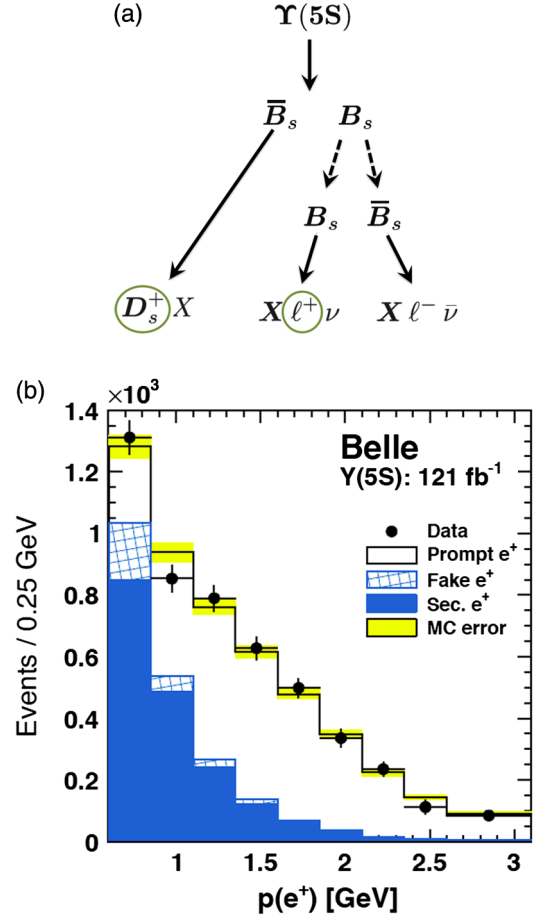


FIG. 36. (a) The selection strategy and (b) the lepton momentum spectrum in the Belle analysis of $B_s \rightarrow X^- \ell^+ \nu$ decays. In (a), the dashed lines indicate $B_s \bar{B}_s$ oscillations. The spectrum in (b) is obtained from $K^+ K^- \pi^+$ mass fits in bins of lepton momentum. The signal is the topmost, white histogram. From Oswald *et al.*, 2013.

fraction of $B_s \bar{B}_s$ events in the two samples is estimated using parameters from external measurements [e.g., the probability of $B_s \bar{B}_s$ production in $\Upsilon(5S)$ decays f_s or the $B_s \bar{B}_s$ mixing probability]. The resulting inclusive semileptonic B_s branching fraction is

$$\mathcal{B}(B_s \rightarrow X^- \ell^+ \nu) = (9.6 \pm 0.4_{\text{stat}} \pm 0.7_{\text{syst}})\%. \quad (133)$$

It agrees with the theoretical prediction based on SU(3) flavor symmetry. A review of Belle results with $\Upsilon(5S)$ data can be found in Oswald and Pedlar (2013).

XI. CONCLUSIONS AND OUTLOOK

The field of charged-current leptonic and semileptonic B decays has greatly developed over the last 15 years. On the one hand, there have been large-scale experimental efforts, resulting in a large number of measurements of semileptonic decays and in first measurements of purely leptonic decays. On the other hand, the heavy-quark expansion in combination with improved lattice QCD calculations and QCD sum rule estimates brought a breakthrough in the theoretical

description, providing QCD-based predictions with controllable uncertainties. In the framework of the SM, experimental data combined with theoretical predictions yield relative uncertainties of about 2% on $|V_{cb}|$ and 4%–5% on $|V_{ub}|$. Figure 37 summarizes the current status of $|V_{cb}|$ and $|V_{ub}|$ determinations.

The values of $|V_{cb}|$ extracted from exclusive and inclusive decays are consistent only at the level of 2.8σ . The inclusive determination of $|V_{cb}|$ is based on the HQE derived from the local OPE and hence is believed to be theoretically very clean.

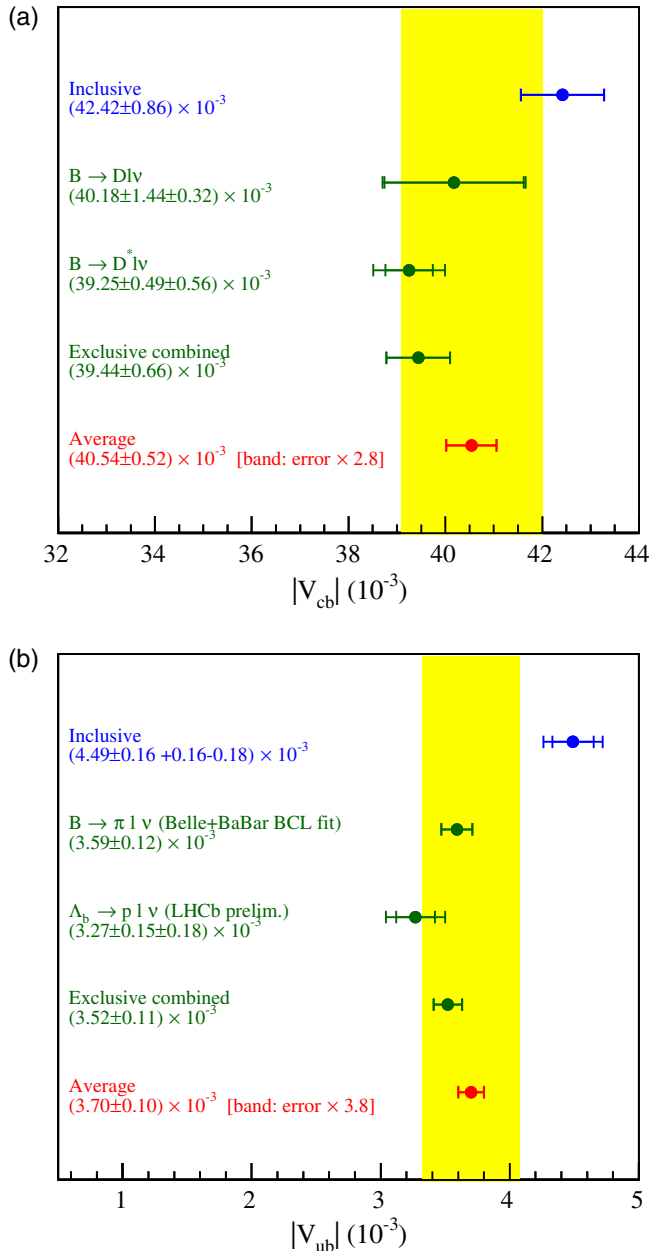


FIG. 37. Comparison of the determinations of (a) $|V_{cb}|$ and (b) $|V_{ub}|$ based on exclusive and inclusive decays. Because of the marginal compatibility of the exclusive and inclusive results, the uncertainty on the average has been scaled by a factor of $\sqrt{\chi^2/\text{ndf}} = 2.8$ for $|V_{cb}|$ and 3.8 for $|V_{ub}|$. The error bars on the average correspond to the unscaled uncertainties, while the bands represent the scaled uncertainties.

The value obtained from $B \rightarrow D^* \ell \nu$ decays relies on the lattice QCD calculations performed by one group. It is interesting to note that a QCD sum rules estimate, although much less precise, yields a central value that is compatible with the inclusive determination. This may indicate that further scrutiny might solve this tension within the SM.

The difference between the inclusive and exclusive determinations of $|V_{ub}|$ seems to be more serious. The level of agreement is 3.8σ . The determination of $|V_{ub}|$ from inclusive decays has a precision of $\sim 5\%$, with about equal contributions from statistical, experimental systematic, and theoretical uncertainties. The results obtained in different phase space regions and for different QCD calculations of partial rates show a high level of consistency. However, the HQE is much more uncertain than in the $b \rightarrow c$ case. The $|V_{ub}|$ extraction from exclusive decays relies mainly on $B \rightarrow \pi \ell \nu$ decays, where good theoretical methods as well as precise measurements are available. A simultaneous fit of a form factor parametrization to the measured q^2 spectrum and predictions from lattice QCD and QCD sum rules yields a precision of about 4%. In this approach, the form factor shape is determined from data, allowing for an extraction of $|V_{ub}|$ over the entire q^2 range.

To resolve the puzzle of the difference between $|V_{ub}|$ (and possibly also $|V_{cb}|$) from inclusive and exclusive decays, major experimental and theoretical efforts are necessary. On the experimental side, significantly larger data samples that allow for precise hadronic-tag measurements and a more detailed understanding of backgrounds and the composition of the semileptonic decay rate are needed. In particular, both $B \rightarrow X_u \ell \nu$ and $B \rightarrow X_c \ell \nu$ analyses will benefit from a more precise measurement of $B \rightarrow D^{**} \ell \nu$ decays and decays to higher charm resonances, which may also be the key to understanding the missing part of the inclusive semileptonic decay rate. On the theory side, further progress in the description of exclusive decays will result in a better understanding of the form factors, which might come from further advancements in lattice QCD calculations. An improvement of the inclusive predictions would require a better control over leading and subleading shape functions to improve the HQE for $b \rightarrow u$ transitions.

Eventually, the purely leptonic decays will also contribute significantly to the $|V_{ub}|$ determination. With much larger data samples, a precise determination of $|V_{ub}|$ will be possible with $B \rightarrow \tau \nu$ decays, assuming SM interactions only. These decays are theoretically simpler, since the main hadronic input is the B -meson decay constant f_B for which precise predictions from lattice QCD already exist. The extraction of $|V_{ub}|$ from this decay is statistically limited, but the $|V_{ub}|$ result obtained from the combination of all $B \rightarrow \tau \nu$ measurements combined with the most precise f_B prediction is already approaching a precision of $\sim 10\%$.

Among the purely leptonic charged-current B decays, only $B \rightarrow \tau \nu$ has been observed so far. The decay $B \rightarrow \mu \nu$ is still beyond the experimental reach with the available data samples. Even though for several years all $B \rightarrow \tau \nu$ measurements yielded branching fractions that were consistently—but not very significantly—above the SM expectation, the latest measurement by Belle resulted in a lower branching fraction, so the world average is now in agreement with the SM

expectation. Larger data samples will be needed for an improved understanding of leptonic B decays.

One of the most interesting results in B physics comes from the measurement of $B \rightarrow D^{(*)}\tau\nu$ decays. The current data suggest that the decays $B \rightarrow D\tau\nu$ and $B \rightarrow D^*\tau\nu$ have a larger rate than predicted by the SM. If this finding persists, it could be interpreted as a hint of physics beyond the SM. While the deviation from the SM is significant for the $BABAR$ measurement, the Belle results are not in disagreement with the SM prediction, so the situation remains unclear. Further insight into possible new physics interpretations can be obtained by precision measurements of the kinematic spectra and angular distributions of these decays. With larger data samples it will also be interesting to study the rarer decay $B \rightarrow \pi\tau\nu$; a first search for this decay by Belle yielded a signal significance of only 2.4σ (Hamer *et al.*, 2015).

It is generally believed that charged-current interactions are less sensitive to physics beyond the SM, since the dominating contribution is at tree level. An exception is extensions of the Higgs sector with additional charged scalars that can mediate charged-current interactions, such as the type-II two-Higgs-doublet model. One may speculate if the tension in $|V_{ub}|$ (and maybe also $|V_{cb}|$) as well as the findings in $B \rightarrow D\tau\nu$ and $B \rightarrow D^*\tau\nu$ can be interpreted in terms of new physics. However, the simplest version of the type-II two-Higgs-doublet model is disfavored by the $BABAR$ data, which seem to require more sophisticated models of new physics.

Since 2009, the LHC experiments have recorded large samples of b hadrons in proton-proton collisions. Over the last few years, in particular, the dedicated b -hadron experiment LHCb has produced an impressive number of results. Because of the neutrino in $B \rightarrow \ell\nu$ and $B \rightarrow X\ell\nu$ decays, measurements of these decays in hadron collisions are challenging. Likewise, measurements of inclusive decays are not feasible at a hadron collider. LHCb has used semileptonic b -hadron decays to measure the $b\bar{b}$ production cross section, b -hadron production fractions, and CP violation in B -meson mixing. Dedicated measurements of exclusive semileptonic decay modes have also started to appear and a first, precise determination of $|V_{ub}|$ has recently been performed. It will be interesting to see further measurements of semileptonic b -hadron decays from LHCb in the future.

The next-generation high-luminosity B factory, SuperKEKB in Japan, is scheduled to start operation in 2018 and is supposed to deliver about 50 times more data than its predecessor KEKB. The Belle detector is currently being upgraded to the Belle II detector, which will be able to cope with the higher interaction rate and radiation levels. With the data sample expected at Belle II, precision measurements of leptonic B decays will become feasible, in particular, through the use of hadronic-tag measurements. The leptonic decay $B \rightarrow \mu\nu$ is expected to be observed with the first $\sim 5 \text{ ab}^{-1}$ of data, probably already within the first 2 years after the start of data taking. The study of semileptonic B decays will benefit from the larger data samples in terms of an improved precision for form factor shape measurements and the possibility to precisely study angular distributions in decays to vector mesons. In combination with progress in form factor calculations, this should lead to a significant

improvement in our knowledge of the CKM matrix elements, in particular, $|V_{ub}|$.

With the new data delivered by the LHC and the next-generation B factory on the horizon, interesting times for research in flavor physics lie ahead of us.

ACKNOWLEDGMENTS

We thank Florian Bernlochner, Bob Kowalewski, Vera Lüth, Marcello Rotondo, Christoph Schwanda, and Phillip Urquijo for their valuable comments and an excellent collaboration over many years. We also express our gratitude to Daping Du for providing helpful information on the Fermilab/MILC form factor results and to Will Davey for a careful proofreading of the article.

REFERENCES

- Aaij, R., *et al.* (LHCb Collaboration), 2011, “First observation of $\bar{B}_s^0 \rightarrow D_{s2}^{*+} X \mu^- \bar{\nu}$ decays,” *Phys. Lett. B* **698**, 14–20.
- Aaij, Roel, *et al.* (LHCb Collaboration), 2015a, “Determination of the quark coupling strength $|V_{ub}|$ using baryonic decays,” *arXiv: 1504.01568*.
- Aaij, Roel, *et al.* (LHCb Collaboration), 2015b, “Measurement of the ratio of branching fractions $\mathcal{B}(\bar{B}^0 \rightarrow D^{*+} \tau^- \bar{\nu}_\tau) / \mathcal{B}(\bar{B}^0 \rightarrow D^{*+} \mu^- \bar{\nu}_\mu)$,” *Phys. Rev. Lett.* **115**, 111803 [**115**, 159901(E) (2015)].
- Abashian, A., *et al.*, 2002, “The Belle Detector,” *Nucl. Instrum. Methods Phys. Res., Sect. A* **479**, 117–232.
- Abazov, V. M., *et al.* (D0 Collaboration), 2005, “Measurement of semileptonic branching fractions of B mesons to narrow D^{**} states,” *Phys. Rev. Lett.* **95**, 171803.
- Abazov, V. M., *et al.* (D0 Collaboration), 2009, “Measurement of the B_s^0 semileptonic branching ratio to an orbitally excited D_s state, $\text{Br}(B_s^0 \rightarrow D_{s1}^-(2536)\mu^+\nu X)$,” *Phys. Rev. Lett.* **102**, 051801.
- Abbiendi, G., *et al.* (OPAL Collaboration), 2000, “Measurement of $|V_{cb}|$ using anti- $B^0 \rightarrow D^{*+}$ lepton $^-$ anti-neutrino decays,” *Phys. Lett. B* **482**, 15–30.
- Abbiendi, G., *et al.* (OPAL Collaboration), 2001, “Measurement of the branching ratio for the process $b \rightarrow \text{tau}^-$ anti-nu(tau) X,” *Phys. Lett. B* **520**, 1–10.
- Abbiendi, G., *et al.* (OPAL Collaboration), 2003, “A Measurement of semileptonic B decays to narrow orbitally excited charm mesons,” *Eur. Phys. J. C* **30**, 467–475.
- Abdallah, J., *et al.* (DELPHI Collaboration), 2004, “Measurement of $|V_{cb}|$ using the semileptonic decay anti- $B^0(d) \rightarrow D^{*+} \ell^-$ anti-nu(ℓ),” *Eur. Phys. J. C* **33**, 213–232.
- Abdallah, J., *et al.* (DELPHI Collaboration), 2006, “Determination of heavy quark non-perturbative parameters from spectral moments in semileptonic B decays,” *Eur. Phys. J. C* **45**, 35.
- Abe, K., *et al.* (Belle Collaboration), 2002, “Measurement of $\mathcal{B}(\text{anti-}B^0 \rightarrow D^+ \ell^- \text{anti-nu})$ and determination of $|V_{cb}|$,” *Phys. Lett. B* **526**, 258–268.
- Abreu, P., *et al.* (DELPHI Collaboration), 2000, “Upper limit for the decay $B^- \rightarrow \tau^-$ anti-neutrino(τ) and measurement of the $b \rightarrow \tau$ anti-neutrino(τ) X branching ratio,” *Phys. Lett. B* **496**, 43–58.
- Abreu, P., *et al.* (DELPHI Collaboration), 2001, “Measurement of $|V_{cb}|$ from the decay process anti- $B^0 \rightarrow D^{*+}$ lepton $^-$ anti-neutrino,” *Phys. Lett. B* **510**, 55–74.
- Acciarri, M., *et al.* (L3 Collaboration), 1994, “Measurement of the inclusive $B \rightarrow \text{tau-neutrino X}$ branching ratio,” *Phys. Lett. B* **332**, 201–208.

- Acciarri, M., *et al.* (L3 Collaboration), 1997, “Measurement of $D(s)^- \rightarrow \tau^- \text{ anti-}\tau\text{-neutrino}$ and a new limit for $B^- \rightarrow \tau^- \text{ anti-}\tau\text{-neutrino}$,” *Phys. Lett. B* **396**, 327–337.
- Acosta, D., *et al.* (CDF Collaboration), 2005, “Measurement of the moments of the hadronic invariant mass distribution in semileptonic B decays,” *Phys. Rev. D* **71**, 051103.
- Adachi, I., *et al.* (Belle Collaboration), 2009, “Measurement of $B \rightarrow D^{(*)} \tau \nu$ using full reconstruction tags,” [arXiv:0910.4301](https://arxiv.org/abs/0910.4301).
- Adachi, I., *et al.* (Belle Collaboration), 2013, “Evidence for $B^- \rightarrow \tau^- \bar{\nu}_\tau$ with a Hadronic Tagging Method Using the Full Data Sample of Belle,” *Phys. Rev. Lett.* **110**, 131801.
- Adam, N.E., *et al.* (CLEO Collaboration), 2007, “A Study of Exclusive Charmless Semileptonic B Decays and $|V_{ub}|$,” *Phys. Rev. Lett.* **99**, 041802.
- Ademollo, M., and Raoul Gatto, 1964, “Nonrenormalization Theorem for the Strangeness Violating Vector Currents,” *Phys. Rev. Lett.* **13**, 264–265.
- Alberti, Andrea, Paolo Gambino, and Soumitra Nandi, **2014**, “Perturbative corrections to power suppressed effects in semileptonic B decays,” *J. High Energy Phys.* **01**, 147.
- Albrecht, H., *et al.* (ARGUS Collaboration), 1995, “Search for rare B decays,” *Phys. Lett. B* **353**, 554–562.
- Alexander, J. P., *et al.* (CLEO Collaboration), 1996, “First measurement of the $B \rightarrow \pi$ lepton neutrino and $B \rightarrow \rho$ (omega) lepton neutrino branching fractions,” *Phys. Rev. Lett.* **77**, 5000–5004.
- Allison, I., *et al.* (HPQCD Collaboration), 2008, “High-Precision Charm-Quark Mass from Current-Current Correlators in Lattice and Continuum QCD,” *Phys. Rev. D* **78**, 054513.
- Amhis, Y., *et al.* (Heavy Flavor Averaging Group (HFAG)), 2014, “Averages of b -hadron, c -hadron, and τ -lepton properties as of summer 2014,” [arXiv:1412.7515](https://arxiv.org/abs/1412.7515).
- Amhis, Y., *et al.* (Heavy Flavor Averaging Group (HFAG)), 2016, “Average of $R(D)$ and $R(D^*)$ for Winter 2016,” http://www.slac.stanford.edu/xorg/hfag/semi/winter16/winter16_dtaunu.html.
- Anastassov, A., *et al.* (CLEO Collaboration), 1998, “Investigation of semileptonic B meson decay to P wave charm mesons,” *Phys. Rev. Lett.* **80**, 4127–4131.
- Andersen, Jeppe R., and Einan Gardi, **2006**, “Inclusive spectra in charmless semileptonic B decays by dressed gluon exponentiation,” *J. High Energy Phys.* **01**, 097.
- Artuso, M., *et al.* (CLEO Collaboration), 1995, “A Search for $B \rightarrow \text{lepton anti-lepton-neutrino}$,” *Phys. Rev. Lett.* **75**, 785–789.
- Athar, S.B., *et al.* (CLEO Collaboration), 2003, “Study of the q^2 dependence of $B \rightarrow \pi$ l nu and $B \rightarrow \rho$ (omega) l nu decay and extraction of $|V_{ub}|$,” *Phys. Rev. D* **68**, 072003.
- Aubert, B., *et al.* (BABAR Collaboration), 2013, “The BABAR Detector: Upgrades, Operation and Performance,” *Nucl. Instrum. Methods Phys. Res., Sect. A* **729**, 615–701.
- Aubert, Bernard, *et al.* (BABAR Collaboration), 2002, “The BABAR detector,” *Nucl. Instrum. Methods Phys. Res., Sect. A* **479**, 1–116.
- Aubert, Bernard, *et al.* (BABAR Collaboration), 2004a, “Measurement of the electron energy spectrum and its moments in inclusive $B \rightarrow X e \nu$ decays,” *Phys. Rev. D* **69**, 111104.
- Aubert, Bernard, *et al.* (BABAR Collaboration), 2004b, “Measurements of moments of the hadronic mass distribution in semileptonic B decays,” *Phys. Rev. D* **69**, 111103.
- Aubert, Bernard, *et al.* (BABAR Collaboration), 2005, “Determination of $|V_{ub}|$ from measurements of the electron and neutrino momenta in inclusive semileptonic B decays,” *Phys. Rev. Lett.* **95**, 111801.
- Aubert, Bernard, *et al.* (BABAR Collaboration), 2006a, “Determinations of $|V_{ub}|$ from inclusive semileptonic B decays with reduced model dependence,” *Phys. Rev. Lett.* **96**, 221801.
- Aubert, Bernard, *et al.* (BABAR Collaboration), 2006b, “Measurement of the $B \rightarrow \pi \ell \nu$ Branching Fraction and Determination of $|V_{ub}|$ with Tagged B Mesons,” *Phys. Rev. Lett.* **97**, 211801.
- Aubert, Bernard, *et al.* (BABAR Collaboration), 2006c, “Measurement of the inclusive electron spectrum in charmless semileptonic B decays near the kinematic endpoint and determination of $|V_{ub}|$,” *Phys. Rev. D* **73**, 012006.
- Aubert, Bernard, *et al.* (BABAR Collaboration), 2006d, “Measurements of the $B \rightarrow D^*$ form-factors using the decay $\bar{B}^0 \rightarrow D^{*+} e^- e^- \text{ neutrino}$,” *Phys. Rev. D* **74**, 092004.
- Aubert, Bernard, *et al.* (BABAR Collaboration), 2008a, “A Search for $B^+ \rightarrow \tau^+ \nu$ with Hadronic B tags,” *Phys. Rev. D* **77**, 011107.
- Aubert, Bernard, *et al.* (BABAR Collaboration), 2008b, “Determination of the form-factors for the decay $B^0 \rightarrow D^{*-} \ell^+ \nu_\ell$ and of the CKM matrix element $|V_{cb}|$,” *Phys. Rev. D* **77**, 032002.
- Aubert, Bernard, *et al.* (BABAR Collaboration), 2008c, “Measurement of the Branching Fractions of anti- $B \rightarrow D^{*+} \ell^- \text{ anti-}\nu(\ell)$ Decays in Events Tagged by a Fully Reconstructed B Meson,” *Phys. Rev. Lett.* **101**, 261802.
- Aubert, Bernard, *et al.* (BABAR Collaboration), 2008d, “Measurement of the Decay $B^- \rightarrow D^{*0} e^- \bar{\nu}(e)$,” *Phys. Rev. Lett.* **100**, 231803.
- Aubert, Bernard, *et al.* (BABAR Collaboration), 2008e, “Measurements of $B \rightarrow \{\pi, \eta, \eta'\} \ell \nu_\ell$ Branching Fractions and Determination of $|V_{ub}|$ with Semileptonically Tagged B Mesons,” *Phys. Rev. Lett.* **101**, 081801.
- Aubert, Bernard, *et al.* (BABAR Collaboration), 2008f, “Observation of $B^+ \rightarrow b(1)^+ K^0$ and search for B -meson decays to $b(1)^0 K^0$ and $b(1)^0 \pi^0$,” *Phys. Rev. D* **78**, 011104.
- Aubert, Bernard, *et al.* (BABAR Collaboration), 2008g, “Searches for the decays $B^0 \rightarrow \ell^\pm \tau^\mp$ and $B^+ \rightarrow \ell^+ \nu$ ($\ell = e, \mu$) using hadronic tag reconstruction,” *Phys. Rev. D* **77**, 091104.
- Aubert, Bernard, *et al.* (BABAR Collaboration), 2009a, “Measurement of Semileptonic B Decays into Orbitally-Excited Charmed Mesons,” *Phys. Rev. Lett.* **103**, 051803.
- Aubert, Bernard, *et al.* (BABAR Collaboration), 2009b, “Measurement of the $B^+ \rightarrow \omega \ell^+ \nu$ and $B^+ \rightarrow \eta \ell^+ \nu$ Branching Fractions,” *Phys. Rev. D* **79**, 052011.
- Aubert, Bernard, *et al.* (BABAR Collaboration), 2009c, “Measurement of the Semileptonic Decays $B \rightarrow D \tau^- \text{ anti-}\nu(\tau)$ and $B \rightarrow D^* \tau^- \text{ anti-}\nu(\tau)$,” *Phys. Rev. D* **79**, 092002.
- Aubert, Bernard, *et al.* (BABAR Collaboration), 2009d, “Measurements of the Semileptonic Decays anti- $B \rightarrow D \ell^- \text{ anti-}\nu$ and anti- $B \rightarrow D^* \ell^- \text{ anti-}\nu$ Using a Global Fit to $D X \ell^- \text{ anti-}\nu$ Final States,” *Phys. Rev. D* **79**, 012002.
- Aubert, Bernard, *et al.* (BABAR Collaboration), 2009e, “Search for the Rare Leptonic Decays $B^+ \rightarrow \ell^+ \nu(\ell)$ ($\ell = e, \mu$),” *Phys. Rev. D* **79**, 091101.
- Aubert, Bernard, *et al.* (BABAR Collaboration), 2010a, “A Search for $B^+ \rightarrow \ell^+ \nu_\ell$ Recoiling Against $B^- \rightarrow D^0 \ell^- \bar{\nu} X$,” *Phys. Rev. D* **81**, 051101.
- Aubert, Bernard, *et al.* (BABAR Collaboration), 2010b, “Measurement and interpretation of moments in inclusive semileptonic decays anti- $B \rightarrow X(c) \ell^- \text{ anti-}\nu$,” *Phys. Rev. D* **81**, 032003.
- Aubert, Bernard, *et al.* (BABAR Collaboration), 2010c, “Measurement of $|V_{cb}|$ and the Form-Factor Slope in anti- $B \rightarrow D \ell^- \text{ anti-}\nu$ Decays in Events Tagged by a Fully Reconstructed B Meson,” *Phys. Rev. Lett.* **104**, 011802.
- Bailey, Jon A., *et al.* (Fermilab Lattice and MILC Collaborations), 2009, “ $B \rightarrow \pi \nu_\ell$,” *Phys. Rev. D* **79**, 054507.
- Bailey, Jon A., *et al.* (Fermilab Lattice and MILC Collaborations), 2014, “Update of $|V_{cb}|$ from the $\bar{B} \rightarrow D^* \ell^- \bar{\nu}$ form factor at zero recoil with three-flavor lattice QCD,” *Phys. Rev. D* **89**, 114504.

- Bailey, Jon A., *et al.* (Fermilab Lattice and MILC Collaborations), 2015a, “ $|V_{ub}|$ from $B \rightarrow \pi \ell \nu$ decays and $(2+1)$ -flavor lattice QCD,” [arXiv:1503.07839](https://arxiv.org/abs/1503.07839).
- Bailey, Jon A., *et al.* (Fermilab Lattice and MILC Collaborations), 2015b, “ $B \rightarrow D \ell \nu$ form factors at nonzero recoil and $|V_{cb}|$ from $2+1$ -flavor lattice QCD,” *Phys. Rev. D* **92**, 034506.
- Ball, Patricia, and Vladimir M. Braun, 1998, “Exclusive semileptonic and rare B meson decays in QCD,” *Phys. Rev. D* **58**, 094016.
- Ball, Patricia, and G. W. Jones, 2007, “ $B \rightarrow \eta^-(\text{prime})$ Form Factors in QCD,” *J. High Energy Phys.* **08**, 025.
- Ball, Patricia, and Roman Zwicky, 2005a, “ $B(d,s) \rightarrow \rho, \omega, K^*, \phi$ decay form-factors from light-cone sum rules revisited,” *Phys. Rev. D* **71**, 014029.
- Ball, Patricia, and Roman Zwicky, 2005b, “New results on $B \rightarrow \pi, K, \eta$ decay form factors from light-cone sum rules,” *Phys. Rev. D* **71**, 014015.
- Barate, R., *et al.* (ALEPH Collaboration), 2001, “Measurements of $\text{BR}(b \rightarrow \tau^- \text{anti-}\nu(\tau) X)$ and $\text{BR}(b \rightarrow \tau^- \text{anti-}\nu(\tau) D^{*\pm} X)$ and upper limits on $\text{BR}(B^- \rightarrow \tau^- \text{anti-}\nu(\tau))$ and $\text{BR}(b \rightarrow s \nu \text{ anti-}\nu)$,” *Eur. Phys. J. C* **19**, 213–227.
- Bardeen, W. A., A. J. Buras, D. W. Duke, and T. Muta, 1978, “Deep Inelastic Scattering Beyond the Leading Order in Asymptotically Free Gauge Theories,” *Phys. Rev. D* **18**, 3998.
- Bartelt, John E., *et al.* (CLEO Collaboration), 1993, “Measurement of charmless semileptonic decays of B mesons,” *Phys. Rev. Lett.* **71**, 4111–4115.
- Bartelt, John E., *et al.* (CLEO Collaboration), 1999, “Measurement of the $B \rightarrow D$ lepton neutrino branching fractions and form-factor,” *Phys. Rev. Lett.* **82**, 3746.
- Bauer, Christian W., Zoltan Ligeti, Michael Luke, Aneesh V. Manohar, and Michael Trott, 2004, “Global analysis of inclusive B decays,” *Phys. Rev. D* **70**, 094017.
- Bauer, Christian W., Zoltan Ligeti, and Michael E. Luke, 2001, “Precision determination of $|V_{ub}|$ from inclusive decays,” *Phys. Rev. D* **64**, 113004.
- Bauer, Christian W., Michael Luke, and Thomas Mannel, 2002, “Subleading shape functions in $B \rightarrow X(u)$ lepton anti- ν and the determination of $|V_{ub}|$,” *Phys. Lett. B* **543**, 261–268.
- Bauer, Christian W., Michael E. Luke, and Thomas Mannel, 2003, “Light cone distribution functions for B decays at subleading order in $1/m(b)$,” *Phys. Rev. D* **68**, 094001.
- Becher, Thomas, Heike Boos, and Enrico Lunghi, 2007, “Kinetic corrections to $B \rightarrow X_c \ell \bar{\nu}$ at one loop,” *J. High Energy Phys.* **12**, 062.
- Becirevic, Damir, and Alexei B. Kaidalov, 2000, “Comment on the heavy \rightarrow light form-factors,” *Phys. Lett. B* **478**, 417–423.
- Becirevic, Damir, Nejc Kosnik, and Andrey Tayduganov, 2012, “ $\bar{B} \rightarrow D \tau \bar{\nu}_\tau$ vs. $\bar{B} \rightarrow D \mu \bar{\nu}_\mu$,” *Phys. Lett. B* **716**, 208–213.
- Beneke, M., F. Campanario, T. Mannel, and B. D. Pecjak, 2005, “Power corrections to anti- $B \rightarrow X(u) \ell^- \text{ anti-}\nu(X(s) \gamma)$ decay spectra in the ‘shape-function’ region,” *J. High Energy Phys.* **06**, 071.
- Beneke, M., and J. Rohrwild, 2011, “ B meson distribution amplitude from $B \rightarrow \gamma \ell \nu$,” *Eur. Phys. J. C* **71**, 1818.
- Benson, D., I. I. Bigi, T. Mannel, and N. Uraltsev, 2003, “Imprecated, yet impeccable: On the theoretical evaluation of $\Gamma(B \rightarrow X(c) \ell \text{ nu})$,” *Nucl. Phys.* **B665**, 367–401.
- Bernlochner, Florian U., Zoltan Ligeti, and Sascha Turczyk, 2012, “A Proposal to solve some puzzles in semileptonic B decays,” *Phys. Rev. D* **85**, 094033.
- Bernlochner, Florian U., *et al.* (SIMBA Collaboration), 2013, “A model independent determination of the $B \rightarrow X_s \gamma$ decay rate,” *PoS ICHEP2012*, 370.
- Bevan, A. J., *et al.* (BABAR Collaboration, Belle Collaboration), 2014, “The Physics of the B Factories,” *Eur. Phys. J. C* **74**, 3026.
- Bharucha, Aoife, 2012, “Two-loop Corrections to the $B \rightarrow \pi$ Form Factor from QCD Sum Rules on the Light-Cone and $|V_{ub}|$,” *J. High Energy Phys.* **05**, 092.
- Bigi, I. I., Th. Mannel, and N. Uraltsev, 2011, “Semileptonic width ratios among beauty hadrons,” *J. High Energy Phys.* **09**, 012.
- Bigi, I. I., *et al.*, 2007, “Memorino on the ‘1/2 vs. 3/2 Puzzle’ in anti- $B \rightarrow \ell^- \text{ anti-}\nu X(c)$: A Year Later and a Bit Wiser,” *Eur. Phys. J. C* **52**, 975–985.
- Bigi, Ikaros I., and Thomas Mannel, 2002, “Parton hadron duality in B meson decays,” [arXiv:hep-ph/0212021](https://arxiv.org/abs/hep-ph/0212021).
- Bigi, Ikaros I. Y., Mikhail A. Shifman, N. Uraltsev, and Arkady I. Vainshtein, 1997, “High power n of $m(b)$ in beauty widths and $n = 5 \rightarrow \text{infinity}$ limit,” *Phys. Rev. D* **56**, 4017–4030.
- Bigi, Ikaros I. Y., Mikhail A. Shifman, N. G. Uraltsev, and A. I. Vainshtein, 1994a, “On the motion of heavy quarks inside hadrons: Universal distributions and inclusive decays,” *Int. J. Mod. Phys. A* **09**, 2467–2504.
- Bigi, Ikaros I. Y., Mikhail A. Shifman, N. G. Uraltsev, and A. I. Vainshtein, 1994b, “The pole mass of the heavy quark. Perturbation theory and beyond,” *Phys. Rev. D* **50**, 2234–2246.
- Bigi, Ikaros I. Y., Mikhail A. Shifman, N. G. Uraltsev, and Arkady I. Vainshtein, 1993, “QCD predictions for lepton spectra in inclusive heavy flavor decays,” *Phys. Rev. Lett.* **71**, 496–499.
- Bigi, Ikaros I. Y., and N. G. Uraltsev, 1994, “Weak annihilation and the endpoint spectrum in semileptonic B decays,” *Nucl. Phys.* **B423**, 33–55.
- Bigi, Ikaros I. Y., and Nikolai Uraltsev, 2001, “A Vademecum on quark hadron duality,” *Int. J. Mod. Phys. A* **16**, 5201–5248.
- Bloch, F., and A. Nordsieck, 1937, “Note on the Radiation Field of the electron,” *Phys. Rev.* **52**, 54–59.
- Bornheim, A., *et al.* (CLEO Collaboration), 2002, “Improved measurement of $|V_{ub}|$ with inclusive semileptonic B decays,” *Phys. Rev. Lett.* **88**, 231803.
- Bosch, S. W., B. O. Lange, M. Neubert, and Gil Paz, 2004, “Factorization and shape function effects in inclusive B meson decays,” *Nucl. Phys.* **B699**, 335–386.
- Bourrely, Claude, Irinel Caprini, and Laurent Lellouch, 2009, “Model-independent description of $B \rightarrow \pi \ell^- \text{ nu}$ decays and a determination of $|V_{ub}|$,” *Phys. Rev. D* **79**, 013008.
- Boyd, C. Glenn, Benjamin Grinstein, and Richard F. Lebed, 1995, “Model independent extraction of $|V_{cb}|$ using dispersion relations,” *Phys. Lett. B* **353**, 306–312.
- Bozek, A., *et al.* (Belle Collaboration), 2010, “Observation of $B^+ \rightarrow \bar{D}^{*0} \tau^+ \nu(\tau)$ and Evidence for $B^+ \rightarrow \bar{D}^0 \tau^+ \nu(\tau)$ at Belle,” *Phys. Rev. D* **82**, 072005.
- Brandenburg, G., *et al.* (CLEO Collaboration), 2000, “Charged track multiplicity in B meson decay,” *Phys. Rev. D* **61**, 072002.
- Brandt, S., 2009, “The Harvest of a Century,” Oxford University Press, New York.
- Breidenbach, C., T. Feldmann, T. Mannel, and S. Turczyk, 2008, “On the Role of ‘Intrinsic Charm’ in Semi-Leptonic B -Meson Decays,” *Phys. Rev. D* **78**, 014022.
- Briere, Roy A., *et al.* (CLEO Collaboration), 2002, “Improved measurement of $|V_{cb}|$ using anti- $B \rightarrow D^* \ell^- \text{ nu}$ decays,” *Phys. Rev. Lett.* **89**, 081803.
- Browder, T. E., *et al.* (CLEO Collaboration), 2001, “A Search for $B \rightarrow \tau \text{ nu}$,” *Phys. Rev. Lett.* **86**, 2950–2954.
- Brucherseifer, Mathias, Fabrizio Caola, and Kirill Melnikov, 2013, “On the $O(\alpha_s^2)$ corrections to $b \rightarrow X_u e \bar{\nu}$ inclusive decays,” *Phys. Lett. B* **721**, 107–110.

- Buchmüller, Oliver, and Henning Flücher, 2006, “Fit to moment from $B \rightarrow X(c)\ell$ anti-nu and $B \rightarrow X(s)$ gamma decays using heavy quark expansions in the kinetic scheme,” *Phys. Rev. D* **73**, 073008.
- Buskulic, D., *et al.* (ALEPH Collaboration), 1997a, “Measurements of $|V_{cb}|$, form-factors and branching fractions in the decays anti- $B^0 \rightarrow D^{*+}$ lepton $^-$ anti-lepton-neutrino and anti- $B^0 \rightarrow D^+$ lepton $^-$ anti-lepton-neutrino,” *Phys. Lett. B* **395**, 373–387.
- Buskulic, D., *et al.* (ALEPH Collaboration), 1997b, “Production of orbitally excited charm mesons in semileptonic B decays,” *Z. Phys. C* **73**, 601–612.
- Caprini, Irinel, Laurent Lellouch, and Matthias Neubert, 1998, “Dispersive bounds on the shape of anti- $B \rightarrow D^{(*)}$ lepton anti-neutrino form-factors,” *Nucl. Phys.* **B530**, 153–181.
- Caprini, Irinel, and Matthias Neubert, 1996, “Improved bounds for the slope and curvature of anti- $B \rightarrow D^{(*)}$ lepton anti-neutrino form-factors,” *Phys. Lett. B* **380**, 376–384.
- Chay, Junegone, Howard Georgi, and Benjamin Grinstein, 1990, “Lepton energy distributions in heavy meson decays from QCD,” *Phys. Lett. B* **247**, 399–405.
- Chetyrkin, K. G., *et al.*, 2009, “Charm and Bottom Quark Masses: An Update,” *Phys. Rev. D* **80**, 074010.
- Colangelo, Pietro, Giuseppe Nardulli, and Nello Paver, 1992, “Semileptonic B decays into charmed p wave mesons and the heavy quark symmetry,” *Phys. Lett. B* **293**, 207–215.
- Cronin-Hennessy, D., *et al.* (CLEO Collaboration), 2001, “Hadronic mass moments in inclusive semileptonic B meson decays,” *Phys. Rev. Lett.* **87**, 251808.
- Csorna, S. E., *et al.* (CLEO Collaboration), 2004, “Moments of the B meson inclusive semileptonic decay rate using neutrino reconstruction,” *Phys. Rev. D* **70**, 032002.
- Dalgic, Emel, *et al.*, 2006, “ B meson semileptonic form-factors from unquenched lattice QCD,” *Phys. Rev. D* **73**, 074502.
- Dassinger, Benjamin M., Thomas Mannel, and Sascha Turczyk, 2007, “Inclusive semi-leptonic B decays to order $1/m(b)^4$,” *J. High Energy Phys.* **03**, 087.
- De Fazio, Fulvia, and Matthias Neubert, 1999, “ $B \rightarrow X(u)$ lepton anti-neutrino lepton decay distributions to order $\alpha(s)$,” *J. High Energy Phys.* **06**, 017.
- Dehnadi, Bahman, Andre H. Hoang, Vicent Mateu, and S. Mohammad Zebarjad, 2013, “Charm Mass Determination from QCD Charmonium Sum Rules at Order α_s^3 ,” *J. High Energy Phys.* **09**, 103.
- del Amo Sanchez, P., *et al.* (BABAR Collaboration), 2011, “Study of $B \rightarrow \pi\ell\nu$ and $B \rightarrow \rho\ell\nu$ Decays and Determination of $|V_{ub}|$,” *Phys. Rev. D* **83**, 032007.
- Detmold, William, Christoph Lehner, and Stefan Meinel, 2015, “ $\Lambda_b \rightarrow p\ell^-\bar{\nu}_\ell$ and $\Lambda_b \rightarrow \Lambda_c\ell^-\bar{\nu}_\ell$ form factors from lattice QCD with relativistic heavy quarks,” [arXiv:1503.01421](https://arxiv.org/abs/1503.01421).
- Dowdall, R. J., C. T. H. Davies, R. R. Horgan, C. J. Monahan, and J. Shigemitsu (HPQCD Collaboration), 2013, “ B -Meson Decay Constants from Improved Lattice Nonrelativistic QCD with Physical u , d , s , and c Quarks,” *Phys. Rev. Lett.* **110**, 222003.
- Duboscq, J. E., *et al.* (CLEO Collaboration), 1996, “Measurement of the form-factors for $\bar{B}^0 \rightarrow D^{*+}\ell^+\nu$,” *Phys. Rev. Lett.* **76**, 3898–3902.
- Dungel, W., *et al.* (Belle Collaboration), 2010, “Measurement of the form factors of the decay $B^0 \rightarrow D^{*+}\ell^+\nu$ and determination of the CKM matrix element $|V_{cb}|$,” *Phys. Rev. D* **82**, 112007.
- Fajfer, Sveltjana, Jernej F. Kamenik, and Ivan Nisandzic, 2012, “On the $B \rightarrow D^{*+}\tau^+\nu_\tau$ Sensitivity to New Physics,” *Phys. Rev. D* **85**, 094025.
- Falk, Adam F., Zoltan Ligeti, Matthias Neubert, and Yosef Nir, 1994, “Heavy quark expansion for the inclusive decay anti- $B \rightarrow$ tau anti-neutrino X ,” *Phys. Lett. B* **326**, 145–153.
- Faller, Sven, Thorsten Feldmann, Alexander Khodjamirian, Thomas Mannel, and Danny van Dyk, 2014, “Disentangling the Decay Observables in $B^- \rightarrow \pi^+\pi^-\ell^-\bar{\nu}_\ell$,” *Phys. Rev. D* **89**, 014015.
- Feindt, Michael, 2004, “A Neural Bayesian Estimator for Conditional Probability Densities,” [arXiv:physics/0402093](https://arxiv.org/abs/physics/0402093).
- Feindt, Michael, *et al.*, 2011, “A Hierarchical NeuroBayes-based Algorithm for Full Reconstruction of B Mesons at B Factories,” *Nucl. Instrum. Methods Phys. Res., Sect. A* **654**, 432–440.
- Flynn, J. M., *et al.*, 2015, “ $B \rightarrow \pi\ell\nu$ and $B_s \rightarrow K\ell\nu$ form factors and $|V_{ub}|$ from 2 + 1-flavor lattice QCD with domain-wall light quarks and relativistic heavy quarks,” *Phys. Rev. D* **91**, 074510.
- Fox, Geoffrey C., and Stephen Wolfram, 1979, “Event Shapes in e^+e^- Annihilation,” *Nucl. Phys.* **B149**, 413.
- Gambino, P., P. Giordano, G. Ossola, and N. Uraltsev, 2007, “Inclusive semileptonic B decays and the determination of $|V_{ub}|$,” *J. High Energy Phys.* **10**, 058.
- Gambino, Paolo, 2011, “ B semileptonic moments at NNLO,” *J. High Energy Phys.* **09**, 055.
- Gambino, Paolo, and Jernej F. Kamenik, 2010, “Lepton energy moments in semileptonic charm decays,” *Nucl. Phys.* **B840**, 424–437.
- Gambino, Paolo, Thomas Mannel, and Nikolai Uraltsev, 2010, “ $B \rightarrow D^*$ at zero recoil revisited,” *Phys. Rev. D* **81**, 113002.
- Gambino, Paolo, Thomas Mannel, and Nikolai Uraltsev, 2012, “ $B^- \rightarrow D^*$ Zero-Recoil Formfactor and the Heavy Quark Expansion in QCD: A Systematic Study,” *J. High Energy Phys.* **10**, 169.
- Gambino, Paolo, and Christoph Schwanda, 2014, “Inclusive semileptonic fits, heavy quark masses, and $|V_{cb}|$,” *Phys. Rev. D* **89**, 014022.
- Gambino, Paolo, and Nikolai Uraltsev, 2004, “Moments of semileptonic B decay distributions in the $1/m(b)$ expansion,” *Eur. Phys. J. C* **34**, 181–189.
- Gelhausen, Patrick, Alexander Khodjamirian, Alexei A. Pivovarov, and Denis Rosenthal, 2013, “Decay constants of heavy-light vector mesons from QCD sum rules,” *Phys. Rev. D* **88**, 014015.
- Glattauer, R., *et al.* (Belle Collaboration), 2016, “Measurement of the decay $B \rightarrow D\ell\nu_\ell$ in fully reconstructed events and determination of the Cabibbo-Kobayashi-Maskawa matrix element $|V_{cb}|$,” *Phys. Rev. D* **93**, 032006.
- Greub, C., M. Neubert, and B. D. Pecjak, 2010, “NNLO corrections to anti- $B \rightarrow X(u)\ell$ anti-nu(ℓ) and the determination of $|V_{ub}|$,” *Eur. Phys. J. C* **65**, 501–515.
- Gronau, Michael, and Jonathan L. Rosner, 2011, “Ratios of heavy hadron semileptonic decay rates,” *Phys. Rev. D* **83**, 034025.
- Gulez, Emel, Alan Gray, Matthew Wingate, Christine T. H. Davies, G. Peter Lepage, and Junko Shigemitsu (HPQCD Collaboration), 2006, “ B Meson Semileptonic Form Factors from Unquenched Lattice QCD,” *Phys. Rev. D* **73**, 074502.
- Ha, H., *et al.* (Belle Collaboration), 2011, “Measurement of the decay $B^0 \rightarrow \pi^-\ell^+\nu$ and determination of $|V_{ub}|$,” *Phys. Rev. D* **83**, 071101.
- Hagiwara, Kaoru, *et al.* (Particle Data Group), 2002, “Review of particle physics. Particle Data Group,” *Phys. Rev. D* **66**, 010001.
- Hamer, P., *et al.* (Belle Collaboration), 2015, “Search for $B^0 \rightarrow \pi^-\tau^+\nu_\tau$ with hadronic tagging at Belle,” [arXiv:1509.06521](https://arxiv.org/abs/1509.06521).
- Heller, A., *et al.* (Belle Collaboration), 2015, “Search for $B^+ \rightarrow \ell^+\nu_\ell$ decays with hadronic tagging using the full Belle data sample,” *Phys. Rev. D* **91**, 112009.
- Hoang, Andre H., Zoltan Ligeti, and Aneesh V. Manohar, 1999, “ B decay and the Upsilon mass,” *Phys. Rev. Lett.* **82**, 277–280.
- Hokuue, T., *et al.* (Belle Collaboration), 2007, “Measurements of branching fractions and q^2 distributions for $B \rightarrow \pi\ell\nu$ and $B \rightarrow \rho\ell\nu$

- decays with $B \rightarrow D^{(*)}\ell\nu$ decay tagging,” *Phys. Lett. B* **648**, 139–148.
- Huschle, M., *et al.* (Belle Collaboration), 2015, “Measurement of the branching ratio of $\bar{B} \rightarrow D^{(*)}\tau^-\bar{\nu}_\tau$ relative to $\bar{B} \rightarrow D^{(*)}\ell^-\bar{\nu}_\ell$ decays with hadronic tagging at Belle,” *Phys. Rev. D* **92**, 072014.
- Ikado, K., *et al.* (Belle Collaboration), 2006, “Evidence of the Purely Leptonic Decay $B^- \rightarrow \tau^- \text{ anti-}\nu(\tau)$,” *Phys. Rev. Lett.* **97**, 251802.
- Isgur, Nathan, D. Scora, B. Grinstein, and M. B. Wise, 1989, “Semileptonic B and D decays in the quark model,” *Phys. Rev. D* **39**, 799.
- Isgur, Nathan, and Mark B. Wise, 1989, “Weak Decays of Heavy Mesons in the Static Quark Approximation,” *Phys. Lett. B* **232**, 113.
- Isgur, Nathan, and Mark B. Wise, 1990, “Weak Transition Form Factors Between Heavy Mesons,” *Phys. Lett. B* **237**, 527.
- Ježabek, M., and Johann H. Kuhn, 1989, “Lepton Spectra from Heavy Quark Decay,” *Nucl. Phys.* **B320**, 20.
- Kakuno, H., *et al.* (Belle Collaboration), 2004, “Measurement of $|V_{ub}|$ using inclusive $B \rightarrow X(u)\ell \nu$ decays with a novel $X(u)$ reconstruction method,” *Phys. Rev. Lett.* **92**, 101801.
- Kang, Xian-Wei, Bastian Kubis, Christoph Hanhart, and Ulf-G. Meißner, 2014, “ $B_{\ell 4}$ decays and the extraction of $|V_{ub}|$,” *Phys. Rev. D* **89**, 053015.
- Khodjamirian, A., Th. Mannel, N. Offen, and Y.-M. Wang, 2011, “ $B \rightarrow \pi\ell\nu_\ell$ Width and $|V_{ub}|$ from QCD Light-Cone Sum Rules,” *Phys. Rev. D* **83**, 094031.
- Korner, J. G., and G. A. Schuler, 1990, “Exclusive Semileptonic Heavy Meson Decays Including Lepton Mass Effects,” *Z. Phys. C* **46**, 93.
- Kronenbitter, B., *et al.* (Belle Collaboration), 2015, “Measurement of the branching fraction of $B^+ \rightarrow \tau^+\nu_\tau$ decays with the semileptonic tagging method,” [arXiv:1503.05613](https://arxiv.org/abs/1503.05613).
- Lange, Bjorn O., Matthias Neubert, and Gil Paz, 2005, “Theory of charmless inclusive B decays and the extraction of $|V_{ub}|$,” *Phys. Rev. D* **72**, 073006.
- Lees, J. P., *et al.* (BABAR Collaboration), 2012a, “A Measurement of the Semileptonic Branching Fraction of the B_s Meson,” *Phys. Rev. D* **85**, 011101.
- Lees, J. P., *et al.* (BABAR Collaboration), 2012b, “Branching fraction and form-factor shape measurements of exclusive charmless semileptonic B decays, and determination of $|V_{ub}|$,” *Phys. Rev. D* **86**, 092004.
- Lees, J. P., *et al.* (BABAR Collaboration), 2012c, “Study of $\bar{B} \rightarrow X_u\ell\bar{\nu}$ decays in $B\bar{B}$ events tagged by a fully reconstructed B -meson decay and determination of $|V_{ub}|$,” *Phys. Rev. D* **86**, 032004.
- Lees, J. P., *et al.* (BABAR Collaboration), 2013a, “Branching fraction measurement of $B^+ \rightarrow \omega\ell^+\nu$ decays,” *Phys. Rev. D* **87**, 032004.
- Lees, J. P., *et al.* (BABAR Collaboration), 2013b, “Evidence of $B \rightarrow \tau\nu$ decays with hadronic B tags,” *Phys. Rev. D* **88**, 031102.
- Lees, J. P., *et al.* (BABAR Collaboration), 2013c, “Measurement of an Excess of $B \rightarrow D^{(*)}\tau \nu$ Decays and Implications for Charged Higgs Bosons,” *Phys. Rev. D* **88**, 072012.
- Lees, J. P., *et al.* (BABAR Collaboration), 2013d, “Measurement of the $B^+ \rightarrow \omega\ell^+\nu$ branching fraction with semileptonically tagged B mesons,” *Phys. Rev. D* **88**, 072006.
- Lees, J. P., *et al.* (BABAR Collaboration), 2015, “Measurement of the $D^0 \rightarrow \pi^- e^+\nu_e$ differential decay branching fraction as a function of q^2 and study of form factor parameterizations,” *Phys. Rev. D* **91**, 052022.
- Lees, J. P., *et al.* (BABAR Collaboration), 2016, “Observation of $\bar{B} \rightarrow D^{(*)}\pi^+\pi^-\ell^-\bar{\nu}$ Decays in e^+e^- Collisions at the $\Upsilon(4S)$ Resonance,” *Phys. Rev. Lett.* **116**, 041801.
- Leibovich, Adam K., Zoltan Ligeti, Iain W. Stewart, and Mark B. Wise, 1998, “Semileptonic B decays to excited charmed mesons,” *Phys. Rev. D* **57**, 308–330.
- Ligeti, Zoltan, Michael Luke, and Aneesh V. Manohar, 2010, “Constraining weak annihilation using semileptonic D decays,” *Phys. Rev. D* **82**, 033003.
- Ligeti, Zoltan, Iain W. Stewart, and Frank J. Tackmann, 2008, “Treating the b quark distribution function with reliable uncertainties,” *Phys. Rev. D* **78**, 114014.
- Limosani, A., *et al.* (Belle Collaboration), 2005, “Measurement of inclusive charmless semileptonic B-meson decays at the endpoint of the electron momentum spectrum,” *Phys. Lett. B* **621**, 28–40.
- Liventsev, D., *et al.* (Belle Collaboration), 2008, “Study of $B \rightarrow D^{**}\ell\nu$ with full reconstruction tagging,” *Phys. Rev. D* **77**, 091503.
- Luke, Michael E., 1990, “Effects of subleading operators in the heavy quark effective theory,” *Phys. Lett. B* **252**, 447–455.
- Mahmood, A. H., *et al.* (CLEO Collaboration), 2004, “Measurement of the B -meson inclusive semileptonic branching fraction and electron energy moments,” *Phys. Rev. D* **70**, 032003.
- Mannel, T., 2004, “Effective Field Theories in Flavor Physics,” *Springer Tracts Mod. Phys.* **203**, 1–175.
- Mannel, Thomas, 1994, “Operator product expansion for inclusive semileptonic decays in heavy quark effective field theory,” *Nucl. Phys.* **B413**, 396–412.
- Mannel, Thomas, and Matthias Neubert, 1994, “Resummation of nonperturbative corrections to the lepton spectrum in inclusive $B \rightarrow X$ lepton anti-neutrino decays,” *Phys. Rev. D* **50**, 2037–2047.
- Mannel, Thomas, Alexei A. Pivovarov, and Denis Rosenthal, 2014, “Inclusive semileptonic B decays from QCD with NLO accuracy for power suppressed terms,” [arXiv:1405.5072](https://arxiv.org/abs/1405.5072).
- Mannel, Thomas, Sascha Turczyk, and Nikolai Uraltsev, 2010, “Higher Order Power Corrections in Inclusive B Decays,” *J. High Energy Phys.* **11**, 109.
- Manohar, Aneesh V., and Mark B. Wise, 2000, “Heavy quark physics,” Cambridge Monogr. Part. Phys., Nucl. Phys., Cosmol. **10**, 1–191.
- Matyja, A., *et al.* (Belle Collaboration), 2007, “Observation of $B^0 \rightarrow D^{*-}\tau^+\nu(\tau)$ decay at Belle,” *Phys. Rev. Lett.* **99**, 191807.
- McNeile, C., C. T. H. Davies, E. Follana, K. Hornbostel, and G. P. Lepage, 2010, “High-Precision c and b Masses, and QCD Coupling from Current-Current Correlators in Lattice and Continuum QCD,” *Phys. Rev. D* **82**, 034512.
- Meißner, Ulf-G, and Wei Wang, 2014, “ $B_s \rightarrow K^{(*)}\ell\bar{\nu}$, Angular Analysis, S-wave Contributions and $|V_{ub}|$,” *J. High Energy Phys.* **01**, 107.
- Melnikov, Kirill, 2008, “ $\mathcal{O}(\alpha_s^2)$ corrections to semileptonic decay $b \rightarrow c\ell\bar{\nu}_\ell$,” *Phys. Lett. B* **666**, 336–339.
- Na, Heechang, Chris M. Bouchar, G. Peter Lepage, Chris Monahan, and Junko Shigemitsu (HPQCD Collaboration), 2015, “ $B \rightarrow D\ell\nu$ form factors at nonzero recoil and extraction of $|V_{cb}|$,” *Phys. Rev. D* **92**, 054510.
- Neubert, Matthias, 1994, “QCD based interpretation of the lepton spectrum in inclusive anti-B $\rightarrow X(u)$ lepton anti-neutrino decays,” *Phys. Rev. D* **49**, 3392–3398.
- Olive, K. A., *et al.* (Particle Data Group), 2014, “The Review of Particle Physics,” *Chin. Phys. C* **38**, 090001.

- Oswald, C., *et al.* (Belle Collaboration), 2013, “Measurement of the inclusive semileptonic branching fraction $\mathcal{B}(B_s^0 \rightarrow X^- \ell^+ \nu_\ell)$ at Belle,” *Phys. Rev. D* **87**, 072008 [**90**, 119901(E) (2014)].
- Oswald, Christian, and Todd K. Pedlar, 2013, “Results in B_s physics and bottomonium spectroscopy using the Belle $\Upsilon(5S)$ data,” *Mod. Phys. Lett. A* **28**, 1330036.
- Pak, Alexey, and Andrzej Czarnecki, 2008, “Heavy-to-heavy quark decays at NNLO,” *Phys. Rev. D* **78**, 114015.
- Quigg, Chris, 2013, “Gauge Theory of the Strong, Weak, and Electromagnetic Interactions” (Princeton University Press, Princeton, NJ), <http://chrisquigg.com/gauge-theories/>.
- Rosner, J. L., *et al.* (CLEO Collaboration), 2006, “Experimental limits on weak annihilation contributions to $b \rightarrow u \ell \nu$ decay,” *Phys. Rev. Lett.* **96**, 121801.
- Sato, Y., *et al.* (Belle Collaboration), 2016, “Measurement of the branching ratio of $\bar{B}^0 \rightarrow D^{*+} \tau^- \nu_\tau$ relative to $B^0 \rightarrow D^{*+} \ell \nu_\ell$ decays with a semileptonic tagging method,” [arXiv:1607.07923](https://arxiv.org/abs/1607.07923).
- Satoyama, N., *et al.* (Belle Collaboration), 2007, “A Search for the rare leptonic decays $B^+ \rightarrow \mu^+ \nu(\mu)$ and $B^+ \rightarrow e^+ \nu(\mu)$,” *Phys. Lett. B* **647**, 67–73.
- Schwanda, C., *et al.* (Belle Collaboration), 2007, “Moments of the Hadronic Invariant Mass Spectrum in $B \rightarrow X_c \ell \nu$ Decays at Belle,” *Phys. Rev. D* **75**, 032005.
- Scora, Daryl, and N. Isgur, 1995, “Semileptonic meson decays in the quark model: An update,” *Phys. Rev. D* **52**, 2783.
- Sentitemsu Imsong, I., Alexander Khodjamirian, Thomas Mannel, and Danny van Dyk, 2015, “Extrapolation and unitarity bounds for the $B \rightarrow \pi$ form factor,” *J. High Energy Phys.* **02**, 126.
- Shifman, Mikhail A., A. I. Vainshtein, and Valentin I. Zakharov, 1979, “QCD and Resonance Physics. Sum Rules,” *Nucl. Phys.* **B147**, 385–447.
- Shifman, Mikhail A., and M. B. Voloshin, 1988, “On Production of D and D^* Mesons in B Meson Decays,” *Sov. J. Nucl. Phys.* **47**, 511.
- Sibidanov, A., *et al.* (Belle Collaboration), 2013, “Study of Exclusive $B \rightarrow X_u \ell \nu$ Decays and Extraction of $|V_{ub}|$ using Full Reconstruction Tagging at the Belle Experiment,” *Phys. Rev. D* **88**, 032005.
- Sirlin, A., 1982, “Large $m(W)$, $m(Z)$ Behavior of the $O(\alpha)$ Corrections to Semileptonic Processes Mediated by W ,” *Nucl. Phys.* **B196**, 83.
- Uraltsev, Nikolai, 2001, “New exact heavy quark sum rules,” *Phys. Lett. B* **501**, 86–91.
- Uraltsev, Nikolai, 2004, “A ‘BPS’ expansion for B and D mesons,” *Phys. Lett. B* **585**, 253–262.
- Urquijo, P., *et al.* (Belle Collaboration), 2007, “Moments of the electron energy spectrum and partial branching fraction of $B \rightarrow X(c) e \nu$ decays at Belle,” *Phys. Rev. D* **75**, 032001.
- Urquijo, P., *et al.* (Belle Collaboration), 2010, “Measurement of $|V_{ub}|$ from Inclusive Charmless Semileptonic B Decays,” *Phys. Rev. Lett.* **104**, 021801.
- Voloshin, M. B., 2001, “Nonfactorization effects in heavy mesons and determination of $|V_{ub}|$ from inclusive semileptonic B decays,” *Phys. Lett. B* **515**, 74–80.
- Yook, Y., *et al.* (Belle Collaboration), 2015, “Search for $B^+ \rightarrow e^+ \nu$ and $B^+ \rightarrow \mu^+ \nu$ decays using hadronic tagging,” *Phys. Rev. D* **91**, 052016.